January 2019

# Hysteretic Behavior Of Thin-Walled Steel Tubular Columns Under Constant Axial Force And Cyclic Lateral Loading

Qusay A. Al-Kaseasbeh

# HYSTERETIC BEHAVIOR OF THIN-WALLED STEEL TUBULAR COLUMNS UNDER CONSTANT AXIAL FORCE AND CYCLIC LATERAL LOADING

by

Qusay Adel Al-Kaseasbeh

Bachelor of Civil Engineering, Mutah University, 2013

Mater of Science, North Dakota State University, 2016

A Dissertation

Submitted to the Graduate Faculty

of the

University of North Dakota

In partial fulfillment of the requirements

for the degree of

Doctor of Philosophy

Grand Forks, North Dakota

May
2019

This dissertation, submitted by Qusay Al-Kaseasbeh in partial fulfillment of the requirements for the Degree of Doctor of Philosophy in Civil Engineering from the University of North Dakota, has been read by the Faculty Advisory Committee under whom the work has been done, and is hereby approved.

Iraj H.P. Mamaghani, Chairperson

Daba Gedafa, Committee Member

Nabil Suleiman, Committee Member

Anjali Sandip, Committee Member

Surjoit Gupta, Member at Large

This dissertation is being submitted by the appointed advisory committee as having met all of the requirements of the Graduate School at the University of North Dakota and is hereby approved.

Dr. Chris Nelson, Associate Dean
School of Graduate Studies

5/3/19

Date

# PERMISSION

Title Hysteretic Behavior of Thin-Walled Steel Tubular Columns under Constant Axial Force and Cyclic Lateral Loading

Department Civil Engineering

Degree Doctor of Philosophy

In presenting this dissertation in partial fulfillment of the requirements for a graduate degree from the University of North Dakota, I agree that the library of this University shall make it freely available for inspection. I further agree that permission for extensive copying for scholarly purposes may be granted by the professor who supervised my dissertation work or, in his absence, by the Chairperson of the department or the dean of the Graduate School. It is understood that any copying or publication or other use of this dissertation or part thereof for financial gain shall not be allowed without my written permission. It is also understood that due recognition shall be given to me and to the University of North Dakota in any scholarly use which may be made of any material in my dissertation.

Qusay Al-Kaseasbeh
May 2019

**List of Figures** ..... **xvi**
**List of Tables** ..... **xvi**
**Nomenclature** ..... **xvii**
**Acknowledgments** ..... **xviii**
**List of Publications** ..... **xx**
**Abstract** ..... **xxii**
**Chapter 1 Introduction** ..... **24**
1.1 Thin-Walled Steel Tubular Columns ..... 24
1.2 Research Objectives ..... 28
1.3 Overview of Study Content ..... 30
**Chapter 2 Circular Columns under Unidirectional Cyclic Lateral Loading** ..... **33**
2.1 Introduction ..... 33
2.2 Numerical Model ..... 33
2.2.1 Unidirectional Cyclic Loading Program ..... 36
2.3 Proposed Thin-Walled Steel Tubular Column with Graded Thickness ..... 37
2.4 Results and Discussion ..... 38
2.4.1 Comparison of Numerical and Experimental Results ..... 38
2.4.1.1 Buckling Mode of C1 Column ..... 40
2.5 Hysteresis Behavior of C and GC Columns ..... 41
2.6 Parametric Study ..... 42
2.6.1 Effect of Radius-to-Thickness Ratio Parameter ($R_t$) ..... 44
2.6.2 Effect of Slenderness Ratio Parameter ($\lambda$) ..... 44
2.6.3 Effect of Axial Load ($P/P_y$) ..... 47
2.6.4 Effect of Number of Loading Cycles ($N$) ..... 47
2.7 Strength and Ductility Evaluation of C and GC Columns ..... 48
2.8 Summary ..... 52
**Chapter 3 Stiffened Square Box Columns under Unidirectional Cyclic Lateral Loading** ..... **54**
3.1 Introduction ..... 54
3.2 Numerical Model ..... 55

3.2.1 Unidirectional Cyclic Loading Protocol ..... 57
3.3 Proposed Thin-Walled Steel Column with Graded Thickness ..... 58
3.4 Numerical Results and Discussion ..... 60
3.4.1 Comparison of Numerical and Experimental Results ..... 60
3.4.1.1 Buckling Mode of B1 Column ..... 61
3.4.2 Hysteresis Behavior of B and GB Columns ..... 62
3.5 Parametric Study ..... 63
3.5.1 Effect of Width-to-Thickness Ratio Parameter ($R_f$) ..... 64
3.5.2 Effect of Slenderness Ratio Parameter ($\lambda$) ..... 67
3.5.3 Effect of Axial Load ($P/P_y$) ..... 69
3.5.4 Effect of Number of Loading Cycles ($N$) ..... 69
3.6 Strength and Ductility Evaluation of B and GB Columns ..... 72
3.7 Summary ..... 74

**Chapter 4 Circular Columns under Bidirectional Cyclic Lateral Loading ..... 76**

4.1 Introduction ..... 76
4.2 Numerical Model ..... 76
4.2.1 Bidirectional Cyclic Loading Protocol ..... 78
4.3 Comparison of Numerical and Experimental Results ..... 79
4.4 Review of Proposed Thin-Walled Steel Column with Graded Thickness ..... 79
4.5 Hysteresis Behavior of BC and BGC Columns ..... 82
4.6 Loading Path Effect ..... 83
4.6.1.1 Buckling Deformations ..... 86
4.6.1.2 Energy Absorption Capacity ..... 86
4.7 Parametric Study ..... 88
4.7.1 Effect of Radius-to-Thickness Ratio Parameter ($R_t$) ..... 89
4.7.2 Effect of Slenderness Ratio Parameter ($\lambda$) ..... 89
4.7.3 Effect of Axial Load ($P/P_y$) ..... 91
4.7.4 Effect of Number of Loading Cycles ($N$) ..... 92
4.8 Strength and Ductility Evaluation of BC and BGC Columns ..... 93
4.9 Summary ..... 96

**Chapter 5 Stiffened Square Box Columns under Bidirectional Cyclic Lateral Loading..... 98**

5.1 Introduction..... 98

5.2 Numerical Model..... 98

5.2.1 Bidirectional Cyclic Loading Program..... 101

5.3 Numerical Model..... 101

5.4 Review of Proposed Thin-Walled Steel Column with Graded Thickness..... 103

5.5 Hysteretic Behavior of BB and Proposed BGB Columns..... 104

5.6 Loading Path Effect..... 108

5.6.1.1 Buckling Deformations..... 109

5.6.1.2 Energy Absorption Capacity..... 110

5.7 Parametric Study..... 111

5.7.1 Effect of Width-to-Thickness Ratio Parameter ($R_f$)..... 111

5.7.2 Effect of Slenderness Ratio Parameter ($\lambda$)..... 113

5.7.3 Effect of Axial Load ($P/P_y$)..... 113

5.7.4 Effect of Number of Loading Cycles ($N$)..... 115

5.8 Strength and Ductility Evaluation of BB and BGB Columns..... 115

5.9 Summary..... 119

**Chapter 6 Summary and Future Work..... 121**

**REFERENCES..... 124**

# LIST OF FIGURES

Fig. 1.1. In-service Steel Bridge Piers (Courtesy of Google). ..... 26
Fig. 1.2. Steel Bridge Piers (Kulkarni, 2012). ..... 27
Fig. 1.3. Organization of the Chapters. ..... 32
Fig. 2.1. C Column Model: (a) Column; (b) FE Meshing; (c) Cross Section; and (d) Loading Program. ..... 36
Fig. 2.2. GC Column Model: (a) Column, and (b) Graded-thickness Sections. ..... 39
Fig. 2.3. Hysteretic Behavior of Analysis and Experiment of the C1 column. ..... 40
Fig. 2.4. Buckling Deformation of Columns. ..... 41
Fig. 2.5. Comparison of Hysteretic Behavior: (a) C1 & GC1, (b) C4 & GC4, (c) C5 & GC5, and (d) C6 & GC6. ..... 43
Fig. 2.6. Effect of $R_t$ parameter: (a) C columns with $\lambda = 0.26$, (b) C columns with $\lambda = 0.5$, (c) GC columns with $\lambda = 0.26$, and (d) GC columns with $\lambda = 0.5$. ..... 45
Fig. 2.7. Effect of $\lambda$ parameter: (a) C columns with $R_t = 0.116$, (b) C columns with $R_t = 0.08$, (c) GC columns with $R_t = 0.116$, and (d) GC columns with $R_t = 0.08$. ..... 46
Fig. 2.8. Envelope Curves with Different Axial Load. ..... 48
Fig. 2.9. Effect of $N$ on Ductility Capacity. ..... 49
Fig. 2.10. Ultimate Strength of C and GC Columns. ..... 50
Fig. 2.11. Ductility of C and GC Columns: (a) $\delta_m/\delta_y$, and (b) $\delta_{0.9}/\delta_y$. ..... 52
Fig. 3.1. B Column Model: (a) Column; (b) FE Meshing; (c) Cross Section; and (d) Loading Program. ..... 58
Fig. 3.2. GB Column Model: (a) Column, and (b) Graded-thickness Sections. ..... 59
Fig. 3.3. Hysteretic Behavior of Analysis and Experiment of the B1 column. ..... 62
Fig. 3.4. Buckling Deformation of Columns. ..... 62
Fig. 3.5. Hysteretic Behavior: (a) B1 & GB1, (b) B2 & GB2, (c) B3 & GB3, (d) B4 & GB4, (e) B5 & GB5, (f) B6 & GB6, (g) B7 & GB7, (h) B8 & GB8, (i) B9 & GB9, and (h) B10 & GB10. ..... 65
Fig. 3.6. Effect of $R_f$ parameter: (a) B columns with $\lambda = 0.26$, (b) B columns with $\lambda = 0.3$, (c) GB columns with $\lambda = 0.26$, and (d) GB columns with $\lambda = 0.3$. ..... 67

Fig. 3.7. Effect of λ parameter: (a) B columns with $R_f$ = 0.36, (b) B columns with $R_f$ = 0.26, (c) GB columns with $R_f$ = 0.36, and (d) GB columns with $R_f$ = 0.26. ..... 68
Fig. 3.8. Envelope Curves with Different Axial Load. ..... 70
Fig. 3.9. Effect of *N* on Strength and Ductility. ..... 71
Fig. 3.10. Ultimate Strength of the B and GB Columns. ..... 74
Fig. 3.11. Ductility Formulae for B and GB Columns: (a) $\delta_m/\delta_y$, and (b) $\delta_{0.9}/\delta_y$. ..... 74
Fig. 4.1.Tested Column Model: (a) Column; (b) FE Meshing; (c) Cross Section; and (d) Loading Program. ..... 77
Fig. 4.2. Hysteretic Behavior of Analysis and Experiment of the Tested Column. ..... 80
Fig. 4.3. Buckling Deformation of Tested Column. ..... 80
Fig. 4.4. (a) BC Column, (b) FE Meshing, (c) BGC Column, and (b) Graded-thickness Sections. ..... 81
Fig. 4.5. Hysteretic Behavior in Z direction of: (a) BC1 & BGC1, (b) BC2 & BGC2, (c) BC3 & BGC3, (d) BC4 & BGC4, (e) BC5 & BGC5, and (f) BC9 & BGC9. ..... 84
Fig. 4.6. Buckling Deformation of BC1 and BGC1 Columns. ..... 85
Fig. 4.7. Hysteretic Behavior of Uniform and Graded-thickness Columns. ..... 87
Fig. 4.8. Loading Paths of Columns: (a) BC1 vs. C1 Columns, and (b) BGC1 vs. GC1 Columns. ..... 87
Fig. 4.9. Energy Absorption Capacity of Columns. ..... 88
Fig. 4.10. Effect of $R_t$ parameter: (a) BC columns with λ = 0.26, (b) BC columns with λ = 0.5, (c) BGC columns with λ = 0.26, and (d) BGC columns with λ = 0.5. ..... 90
Fig. 4.11. Effect of λ (a) BC columns with $R_t$ = 0.116, (b) BC columns with $R_t$ = 0.08 (c) BGC columns with $R_t$ = 0.116, and (d) BGC columns with $R_t$ = 0.08. ..... 91
Fig. 4.12. Effect of Axial Load on Strength and Ductility. ..... 92
Fig. 4.13. Effect of *N* on Ductility Capacity. ..... 93
Fig. 4.14. Ultimate Strength of the BC and BGC Columns. ..... 95
Fig. 4.15. Ductility of BC and BGC Columns: (a) $\delta_{zm}/\delta_y$, and (b) $\delta_{z0.9}/\delta_y$. ..... 96
Fig. 5.1. Tested Column Model: (a) Column; (b) FE Meshing; (c) Cross Section; and (d) Loading Program. ..... 100
Fig. 5.2. Hysteretic Behavior of the Tested Column. ..... 102
Fig. 5.3. Buckling Deformation of Tested Column. ..... 102

Fig. 5.4. (a) BB Column, (b) FE Meshing, (c) BGB Column, and (d) Graded-thickness Sections. ..... 104
Fig. 5.5. Comparison of Hysteretic Loops in Z direction of: (a) BB1 & BGB1, (b) BB2 & BGB2, (c) BB3 & BGB3, (d) BB4 & BGB4, (e) BB5 & BGB5, (f) BB6 & BGB6, (g) BB7 & BGB7, (g) BB8 & BGB8, (g) BB9 & BGB9, and (g) BB10 & BGB10..... 106
Fig. 5.6. Buckling Deformation of Columns. ..... 107
Fig. 5.7. Hysteretic Behavior of Uniform and Graded-thickness Columns..... 109
Fig. 5.8. Loading Paths of Columns: (a) BB1 vs. B1 Columns, and (b) BGB1 vs. BG1 Columns. ..... 110
Fig. 5.9. Energy Absorption Capacity of Columns..... 110
Fig. 5.10. Effect of $R_f$ parameter: (a) BB columns with $\lambda = 0.26$, (b) BB columns with $\lambda = 0.3$, (c) BGB columns with $\lambda = 0.26$, and (d) BGB columns with $\lambda = 0.3$. ..... 112
Fig. 5.11. Effect of $\lambda$ parameter: (a) BB columns with $R_f = 0.36$, (b) BB columns with $R_f = 0.26$ (c) BGB columns with $R_f = 0.36$, and (d) BGB columns with $R_f = 0.26$. ..... 114
Fig. 5.12. Effect of Axial Load on Hysteretic Behavior. ..... 114
Fig. 5.13. Effect of $N$ on Hysteretic Behavior. ..... 115
Fig. 5.14. Ultimate Strength of the BB and BGB Columns..... 118
Fig. 5.15. Ductility of BB and BGB Columns: (a) $\delta_{zm}/\delta_y$, and (b) $\delta_{z0.9}/\delta_y$. ..... 118

# LIST OF TABLES

Table 2.1. Material and Geometrical Properties of Analyzed C and GC columns. ..... 37
Table 2.2. Strength and Ductility Evaluation of C and GC Columns. ..... 50
Table 3.1. Material and Geometrical Properties of Analyzed B and GB Columns. ..... 61
Table 3.2. Strength and Ductility Evaluation of B and GB Columns. ..... 71
Table 4.1. Material and Geometrical Properties of Analyzed BC and BGC Columns. ..... 82
Table 4.2. Strength and Ductility Evaluation of BC and BGC Columns. ..... 94
Table 5.1. Material and Geometrical Properties of Analyzed BB and BGB Columns. ..... 105
Table 5.2. Strength and Ductility Evaluation of BB and BGB Columns. ..... 117

# NOMENCLATURE

| | |
|---|---|
| **FEM (FE)** | Finite Element Model (Finite Element) |
| **C Column** | Uniform Thin-walled Steel **C**ircular Column under Unidirectional Cyclic lateral Loading. |
| **GC Column** | **G**raded-thickness Thin-walled Steel Circular Column under Unidirectional Cyclic lateral Loading. |
| **BC Column** | Uniform Thin-walled Steel **C**ircular Column under **B**idirectional Cyclic lateral Loading. |
| **BGC Column** | **G**raded-thickness Thin-walled Steel **C**ircular Column under **B**idirectional Cyclic lateral Loading. |
| **B Column** | Uniform Thin-walled Steel Square **B**ox Column under Unidirectional Cyclic lateral Loading. |
| **GB Column** | **G**raded-thickness Thin-walled Steel Square **B**ox Column under Unidirectional Cyclic lateral Loading. |
| **BB Column** | Uniform Thin-walled Steel Square **B**ox Column under **B**idirectional Cyclic lateral Loading. |
| **BGB Column** | **G**raded-thickness Thin-walled Steel Square **B**ox Column under **B**idirectional Cyclic lateral Loading. |
| $H_y$ | Yield Lateral Load. |
| $H_{yo}$ | Yield Lateral Load under Zero Axial Load. |
| $\delta_y$ | Yield Lateral Displacement. |
| $\delta_{yo}$ | Yield Lateral Displacement under Zero Axial Load. |
| $\delta_m$ | Maximum Lateral Displacement. |
| $\delta_{90}$ | Lateral Displacement Corresponding to 90% of Maximum Lateral Load. |

## ACKNOWLEDGMENTS

First and foremost, I express my deepest gratitude to my academic and research advisor Dr. Iraj Mamaghani for his guidance and help throughout my research and for gladly offering his knowledge and experience when needed. I particularly admire his scientific way of thinking and providing new ideas and his extraordinary human qualities. Thanks for making me feel at ND, USA like at my second home. His trust and support were extremely encouraging and helpful. I would also like to express my special thanks and highest appreciation to my PhD committee; Dr. Daba Gedafa, Dr. Nabil Suleiman, Dr. Anjali Sandip, and Dr. Surjoit Gupta for their support and help.

Additionally, I would like to express my appreciation to University of North Dakota for allowing me to do research and giving me opportunities to participate in various conferences held in the USA. Also, I would like to thank my friends and colleagues from Civil Engineering department.

Finally, I would like to thank all my family members. A special mention to my parents Adel Al-Kaseasbeh and Sahar Aldalain. Despite the distance, you have always been presented to love and support me under any circumstances. Last, but not least, I wouldn't have made till here without endless care, love, and encouragement of my wife Dr. Ala Alemaryeen, and lots of love to my son, Hashem. I'm very thankful to have you both in my life!

*To my parents*

*Adel Al-Kaseasbeh and Sahar Aldalain*

*and my wife*

*Dr. Ala Alemaryeen*

*and my son*

*Hashem Al-Kaseasbeh*

# LIST OF PUBLICATIONS

**Journal Articles:**

[1] **Al-Kaseasbeh, Q.**, and Mamaghani, I. H. P. (2019). "Buckling strength and ductility evaluation of thin-walled steel stiffened square box columns with uniform and graded thickness under cyclic loading". *Engineering Structures*, *186*, 498–507.

[2] **Al-Kaseasbeh, Q.**, and Mamaghani, I. H. P. (2018). "Buckling Strength and Ductility Evaluation of Thin-Walled Steel Tubular Columns with Uniform and Graded Thickness under Cyclic Loading". *Journal of Bridge Engineering*, 24(1), 04018105.

[3] **Al-Kaseasbeh, Q.**, and Mamaghani, I. H. P. (2019). "Design and Cyclic Elastoplastic Analysis of Graded Thin-Walled Steel Tubular Columns with Enhanced Strength and Ductility". International Journal of Modern Engineering (IJME), 19(1), 30–36.

[4] **Al-Kaseasbeh, Q.**, and Mamaghani, I. H. P. (2019). "Thin-Walled Steel Tubular Circular Columns with Uniform and Graded Thickness under Bidirectional Cyclic Loading". *Thin-Walled Structures*, ($2^{nd}$ round of revision).

[5] **Al-Kaseasbeh, Q.**, and Mamaghani, I. H. P. (2019). "Thin-Walled Steel Stiffened Square Box Columns with Uniform and Graded Thickness under Bidirectional Cyclic Loading". *Engineering Structures*, (to be submitted).

[6] **Al-Kaseasbeh, Q.**, Lin, Z., Wang, Y., Azarmi, F., and Qi, X. (2018). "Electrochemical Characterization of Steel Bridge Welds under Simulated Durability Test". *Journal of Bridge Engineering*, *23*(10), 04018068.

[7] Lin, Z., Azarmi, F., **Al-Kaseasbeh, Q.**, Azimi, M., and Yan, F. (2015). "Advanced Ultrasonic Testing Technologies with Applications to Evaluation of Steel Bridge Welding - An Overview". *Applied Mechanics and Materials*, *727–728*, 785–789.

**Conference Proceedings:**

[1] **Al-Kaseasbeh, Q.**, and Mamaghani, I. H. P. (2019). "Thin-Walled Steel Tubular Columns with Uniform and Graded Thickness under Cyclic Loading". In *Interdependence Between Structural Engineering and Construction Management*. Chicago, Illinois.

[2] **Al-Kaseasbeh, Q.**, and Mamaghani, I. H. P. (2019). "Performance of Thin-Walled Steel Tubular Circular Columns with Graded Thickness under Bidirectional Cyclic Loading". *Structures Congress 2019*. Orlando, FL: American Society of Civil Engineers, P. 1-10.

[3] **Al-Kaseasbeh, Q.**, and Mamaghani, I. H. P. (2018). "Design and Cyclic Elastoplatic Analysis of Graded Thin-Walled Steel Tubular Columns with Enhanced Strength and Ductility". *In 6th IAJC International Conference.* Orlando, Florida. (**"Best Graduate Paper" Award**).

[4] **Al-Kaseasbeh, Q.**, and Mamaghani, I. H. P. (2018). "Buckling Strength and Ductility Evaluation of Thin-Walled Steel Tubular Columns Under Cyclic Loading". In *10th International Conference on Short and Medium Span Bridges*. Quebec City, Canada.

[5] Lin, Z., Yan, F., Azimi, M., Azarmi, F., and **Al-Kaseasbeh, Q.** (2015). "A Revisit of Fatigue Performance Based Welding Quality Criteria in Bridge Welding Provisions and Guidelines". *In 2015 International Industrial Informatics and Computer Engineering Conference* (pp. 2042–2046). Atlantis Press.

# ABSTRACT

Thin-walled steel tubular bridge piers (column refers to “bridge pier” in the subsequent text) with either circular and square box cross sections are becoming an increasingly attractive choice as cantilever bridge piers in severe earthquake regions due to their architectural, structural and constructional advantages. However, thin-walled steel tubular columns are vulnerable to local buckling, global buckling or interaction between both under extreme loading events such as strong earthquakes. This buckling results in a significant strength and ductility degradation, which eventually leads to an early and full collapse of the thin-walled steel tubular columns. The work presented in this dissertation investigates the inelastic structural behavior of uniform and newly proposed graded-thickness thin-walled steel tubular circular and square box columns under a constant axial force as a superstructure dead load and uni/ bidirectional cyclic lateral loading. First of all, the adopted finite element model (FEM) in ABAQUS/Standard version 6.14, which takes into account the effect of both material and geometric nonlinearities, is verified with the experimental results reported in the literature and employed for the analysis. Second, the newly proposed graded-thickness column, with size and volume of material equivalent to the BB column, is evaluated under a constant axial force and uni/bidirectional cyclic lateral loading. The proposed graded-thickness column is proved to have significant improvements in the overall hysteretic behavior compared to its counterpart conventional uniform column. Then, the deterioration of the circular bidirectional cyclic loading path over the unidirectional path is emphasized. Finally, a comprehensive parametric study is carried out to investigate the effect of key design parameters including: radius-to-thickness ratio parameter ($R_t$), width-to-thickness ratio parameter ($R_f$), column slenderness ratio parameter ($\lambda$), magnitude of axial load ($P/P_y$), and number of loading cycles ($N$) on the overall hysteretic behavior of uniform and graded-thickness columns under a constant axial

force and uni/bidirectional cyclic lateral loading. Subsequently, design formulae have been derived to predict the ultimate strength and ductility of both uniform and proposed graded-thickness columns.

# CHAPTER 1 Introduction

## 1.1 Thin-Walled Steel Tubular Columns

Thin-walled steel tubular bridge piers ("bridge pier" is called column in the subsequent text) either with circular or stiffened square box sections are employed in a variety of structural applications for their favorable architectural, structural and constructional advantages in urban earthquake-prone regions (Al-Kaseasbeh and Mamaghani, 2018, 2019; Bedair, 2015; Guo et al., 2013a; Tao et al., 2005; Ucak and Tsopelas, 2014). In severe seismic regions, the integrity of civil engineering structures is exposed to increased earthquake risk (Jaiswal et al., 2017; Mahin, 1998; Miller, 1998; Nakashima et al., 1998). In response to these risks, thin-walled steel columns with either circular or stiffened square box sections are becoming an attractive choice in modern buildings, elevated storage tanks, transmission towers, onshore, and offshore structures (Bedair, 2015; Tao et al., 2005; Ucak and Tsopelas, 2014). In addition, these columns are commonly used for elevated highway bridge piers (Goto et al., 2012), as shown in Fig. 1.1, and wind turbines (Guo et al., 2013b) in severe earthquake regions due to their structural efficiency, attractive aesthetic appearance, high earthquake resistance, and potential for concrete infilling (Yang et al., 2017a; Zhao et al., 2015). Compared to their counterparts of reinforced concrete, thin-walled steel tubular columns are more efficient due to their light weight, high strength, ductility, and ease and speed of construction, especially, when limited construction space is needed (Mamaghani, 1996; Yang et al., 2017b). However, thin-walled steel columns are vulnerable to local buckling, global buckling, or interaction between both under extreme loading events such as strong earthquakes (e.g., the Kobe earthquake (1995), the Sichuan earthquake (2008), and the East Japan earthquake (2011)) (Al-Kaseasbeh and Mamaghani, 2018, 2019; Aoki and Susantha, 2005a; Ge et al., 2000a;

Mamaghani et al., 1996a, 1997). Local buckling leads to a significant strength and ductility degradation, and early full collapse of these columns due to uni/multidirectional cyclic lateral loading (Al-Kaseasbeh and Mamaghani, 2018, 2019; Aoki and Susantha, 2005a; Bedair, 2015; Bruneau, 1998; Gao et al., 1998b; Ge et al., 2000a; Li et al., 2017; Mamaghani et al., 1996b, 1997, 1995, 1996a; Shen et al., 1995; Ucak and Tsopelas, 2014; Usami et al., 1995; Yang et al., 2017a). The excessive permanent lateral deformation and collapse of steel bridge piers due to inelastic behavior and severe local buckling was reported (Bruneau, 1998; Usami et al., 1995), as shown Fig. 1.2. According to these observations, the hysteretic behavior of thin-walled steel tubular circular and square box columns with uniform plate thickness have been extensively investigated in the past few decades. Many experimental and numerical analyses have been conducted to identify the factors that might improve the strength and ductile behavior of the thin-walled steel columns under constant axial force and cyclic lateral loading (Fukumoto et al., 2003; Ge et al., 2000b; Liu and Young, 2003; Mustafa et al., 2016; Usami et al., 2000b; Usami and Ge, 1998). Local buckling, global buckling, or the interaction between both are governing factors in the strength and ductility evaluation of thin-walled steel columns (AISC, 2010). Local buckling in thin-walled steel tubular columns may cause premature collapse and reduce the overall strength and ductility of thin-walled steel tubular columns (Mustafa et al., 2016). It has been confirmed that the radius-to-thickness ratio parameter ($R_t$), width-to-thickness ratio parameter ($R_f$), and slenderness ratio parameter ($\lambda$) are the main structural parameters affecting the strength and ductility of thin-walled steel columns. Moreover, the strength and ductility of these columns are improved by decreasing $R_t$, $R_f$ and $\lambda$ (Al-Kaseasbeh and Mamaghani, 2018, 2019; Gao et al., 1998a; Kwon et al., 2007; Mamaghani and Packer, 2002). In general, local buckling of the thin-walled

steel tubular columns is affected by the $R_t$ or $R_f$ parameter, while global buckling is controlled by the λ parameter (Goto et al., 1998; Mamaghani, 2008; Mamaghani and Packer, 2002).

Fig. 1.1. In-service Steel Bridge Piers (Courtesy of Google).

(a) Local Buckling

(b) Full Collapse.

Fig. 1.2. Steel Bridge Piers (Kulkarni, 2012).

In the reality, the earthquake ground motion is complex and 3D loading components acting simultaneously, as opposed to assumed unidirectional cyclic lateral loading pattern (Anderson and Mahin, 2004; Dang et al., 2017; Okazaki et al., 2003; Watanabe et al., 2011). Moreover, hysteretic behavior of thin-walled steel tubular columns under multidirectional cyclic lateral loading is expected to be more critical and severe than the same amplitude of unidirectional cyclic loading. Since then, the hysteretic behavior of thin-walled steel tubular columns under bidirectional cyclic lateral loading was investigated by a number of researchers (Aoki et al., 2007; Dang and Aoki, 2013a; Goto, Yoshiaki et al., 2009; Watanabe et al., 2011). The studies revealed that thin-walled steel tubular columns under bidirectional cyclic lateral loading surfer an extensive degradation in strength and ductility compared to unidirectional cyclic lateral loading, and should be incorporated in the seismic design practice (Dang and Aoki, 2013a; Goto et al., 2006; Onishi et al., 2005; Oyawa et al., 2004; Watanabe et al., 2011). Thin-walled steel bridge piers are key structural components

in bridge seismic design (Jiang et al., 2002). Along with the $R_f$ and $\lambda$; cross-sectional configuration, cyclic lateral loading pattern, and different factors must be practically considered in the seismic design of the thin-walled steel tubular columns (Goto et al., 2006). Recent developments in the manufacturing technology of high strength steel make thin-walled steel tubular columns are affordable and extremely attractive in civil engineering applications (Tao et al., 2005). Over the past few decades, several studies concluded that all retrofit schemes including longitudinal stiffeners, diaphragms, corner reinforcement, inner cruciform plates, corner plates, and concrete infill have improved the strength and ductility of the thin-walled steel tubular columns (Mamaghani, 2004, 2005; Susantha et al., 2005). Furthermore, setting the diaphragm along the longitudinal axis of the column delays the local buckling occurrence (Ge et al., 2000a). New thin-walled corrugated and cellular steel columns have been introduced by Ucak and Tsopelas (2006) (Ucak and Tsopelas, 2006). It was found that these new types of sections demonstrate superior performance in both strength and ductility properties, and post-buckling. Columns with tapered plates have been introduced to improve the ultimate strength and ductility of steel bridge piers as effective and economical techniques to improve the ductility (Susantha et al., 2005; Takaku et al., 2004).

### 1.2 Research Objectives

Up to date, researchers investigated thin-walled steel tubular columns either with circular or square box sections with uniform thickness under uni/multidirectional cyclic lateral loading. All these studies addressed that thin-walled steel columns suffer local buckling near the base in a range that is equal to the diameter or side width of the circular and square box columns, respectively (Al-Kaseasbeh and Mamaghani, 2018, 2019; Nishikawa et al., 1998a; Tang et al., 2016a; Usami, 1996; Wang et al., 2016). In order to overcome this deficiency and ensure an adequate strength and

ductile behavior of thin-walled steel columns, a graded-thickness thin-walled steel tubular column ,with size and volume of material equivalent to a uniform thin-walled steel tubular column, has been proposed and investigated by the authors under constant axial force and uni/bidirectional cyclic lateral loading (Al-Kaseasbeh and Mamaghani, 2018, 2019). In evaluating the proposed graded-thickness column, its strength and ductility improvement under uni/bidirectional cyclic lateral loading is obvious as the proposed graded-thickness column inhibit the local buckling near the base of the column. Moreover, the proposed graded-thickness column delays the local buckling occurrence and absorbs more energy under severe earthquakes. To the best of the authors' knowledge, no literature (except the publications out of this study) has been reported on thin-walled steel tubular columns with graded thickness. Therefore, investigation is needed to understand the behavior of such structures along with the development of the manufacturing of steel structures.

This study aims to establish the utility of newly proposed graded-thickness thin-walled steel tubular column in an attempt to improve the overall hysteretic behavior of conventional uniform thin-walled steel tubular columns. The newly proposed graded-thickness column is evaluated in regard to its strength, ductility, energy absorption, and post-buckling under constant axial force and uni/bidirectional cyclic lateral loading. In order to achieve this goal, four tested thin-walled steel tubular circular and square box columns with uniform thickness, reported literature (Aoki et al., 2007; Dang et al., 2017; Goto et al., 2006; Nishikawa et al., 1998a), were numerically analyzed under constant axial force and uni/bidirectional cyclic lateral loading to validate the accuracy of the adopted Finite element Model (FEM) in ABAQUS/Standard version 6.14 (Hibbit et al., 2014a). Then, the newly proposed graded-thickness columns with size and volume of material equivalent

to the uniform columns is introduced and investigated under constant axial force from the superstructure and uni/bidirectional cyclic lateral loading.

The study results indicate the proposed graded-thickness columns are advantageous in achieving significant improvements in the ultimate strength, ductility, energy absorption, and post-buckling compared to their counterpart BB columns, emphasizing the effect of the plate thickness and sectional configuration in the proposed graded-thickness columns. The achieved improvements in the overall behavior of the proposed columns is due to their ability to inhibit and/or eliminate the local buckling near the base of the column, where the local buckling usually occurs. Furthermore, a comparison study concluded that the hysteretic behavior of thin-walled steel tubular columns is more severe and critical under bidirectional cyclic lateral loading compared to unidirectional cyclic lateral loading. As a part of this research work, a comprehensive parametric study is carried out to provide insight into the effects of key design parameters including: radius-to-thickness ratio parameter ($R_t$), the width-to-thickness ratio parameter ($R_f$), the column slenderness ratio parameter ($\lambda$), the magnitude of the axial load ($P/P_y$), and the number of loading cycles ($N$) on overall hysteretic behavior of thin-walled steel tubular columns under uni/bidirectional cyclic lateral loading. Finally, a series of design formulae is given to predict the strength and ductility of the uniform and graded-thickness thin-walled steel tubular columns. The proposed formulae are expected to be useful guidelines in the practical design and steel fabrication.

### 1.3 Overview of Study Content

As shown in Fig. 1.3, this dissertation consists of six chapters. The present chapter gives a general introduction about thin-walled steel tubular columns and the need of the proposed graded-thickness columns. Chapter 2 and Chapter 3 deal, respectively, with the hysteretic behavior of thin-

walled steel tubular circular and square box columns with uniform and graded-thickness under a constant axial force and unidirectional cyclic later loading.

In Chapter 4, the hysteretic behavior of thin-walled steel tubular circular columns with uniform and graded-thickness under circular bidirectional cyclic later loading is investigated in detail. The effect of cyclic loading pattern on the overall hysteretic behavior is evaluated compared to unidirectional cyclic lateral loading (see Chapter 2). Hysteretic behavior of thin-walled steel square box columns with uniform and graded-thickness under circular bidirectional cyclic lateral loading is carried out in Chapter 5. The bidirectional loading effect is also compared to unidirectional loading pattern (see Chapter 3). Finally, the conclusions and future work are summarized in Chapter 6.

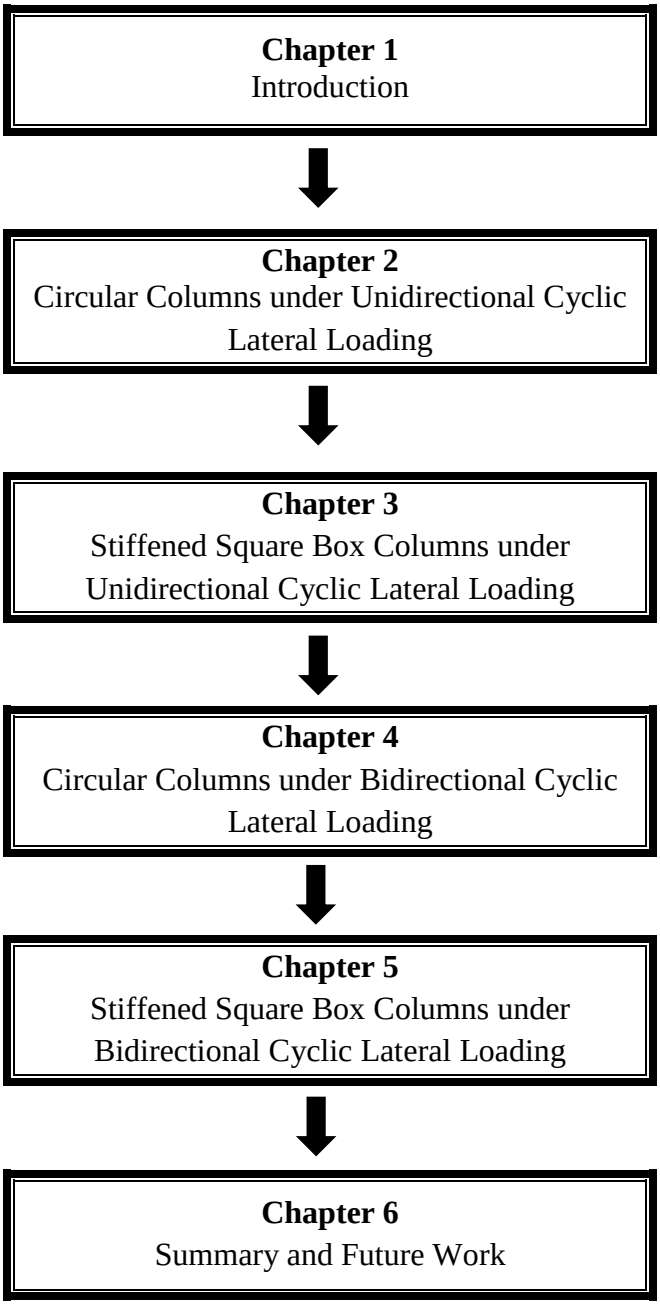


Fig. 1.3. Organization of the Chapters.

# CHAPTER 2 Circular Columns under Unidirectional Cyclic Lateral Loading

## 2.1 Introduction

This chapter aims to establish the utility of newly proposed graded-thickness circular sections (GC) in improving the ultimate strength, ductility, and post-buckling of conventional uniform thin-walled steel tubular columns (C). To achieve this goal, a uniform circular column (C1) tested by Nishikawa et al., 1998 (Nishikawa et al., 1998b) has been numerically analyzed under constant axial force and unidirectional cyclic lateral loading. The accuracy of the adopted FEM has been verified through the comparison between the FE analysis and the experimental results. Then, a graded-thickness circular column (GC) with size and volume of material equivalent to a uniform circular column (C) is introduced. This study proves that the proposed GC column shows significant improvements in strength, ductility, and post-buckling compared to its counterpart C column. The main reason for the improved behavior of GC columns is their ability to eliminate buckling near the base of the column (section A-A, see Fig. 2.1 and Fig. 2.2) where the buckling most likely occurs. In the section 2.6, a parametric study is carried out to investigate effects of the radius-to-thickness ratio parameter ($R_t$), the column slenderness ratio parameter ($\lambda$), the magnitude of the axial load ($P/P_y$), and the number of loading cycles ($N$) on the strength and ductility of both C and GC columns. Finally, design formulae are provided to predict the strength and ductility of C and GC columns. The proposed formulae are expected to be useful in the practical design of such columns.

## 2.2 Numerical Model

A series of FE analyses on the hysteretic behavior of thin-walled steel tubular circular columns are carried out using the commercially available finite-element software Abaqus/Standard version

6.14 (Hibbit et al., 2014a). The FEM takes into consideration both material and geometric non-linearities. The linear kinematic hardening model, von Mises yield surface, and associated plastic flow rule for material nonlinearity available in Abaqus were adopted in the analysis. This model is used to simulate the inelastic behavior of materials that are subjected to cyclic loading (Hibbit et al., 2014a). The accuracy of the employed FEM is validated in comparison with the experimental data available in the literature (Nishikawa et al., 1998b). The most important parameters considered in the design of thin-walled steel tubular circular columns are the radius-to-thickness ratio parameter ($R_t$) and the column slenderness ratio parameter ($\lambda$) (Mamaghani and Packer, 2002). $R_t$ is concerned with the local buckling of thin-walled columns, while $\lambda$ controls global stability (Mamaghani, 2008; Mamaghani and Packer, 2002). For the tested column (C1), these parameters are defined as follows (Chen, W. F. and Duan, 2014; Mamaghani, 1996):

$$R_t = \frac{D}{2t}\frac{\sigma_y}{E}\sqrt{3\left(1-\nu^2\right)} \tag{2.1}$$

$$\lambda = \frac{2h}{r}\frac{1}{\pi}\sqrt{\frac{\sigma_y}{E}} \tag{2.2}$$

Where $h$ = column height = 3403 mm; $r$ = radius of gyration of cross section = 315 mm; $\sigma_y$ = yield stress= 289.6 MPa; $E$ = Young's modulus = 206 GPa; $\nu$ = Poisson's ratio = 0.3; $D$ = Diameter of circular cross-section = 900 mm; and $t$ = plate thickness = 9 mm. The previously defined parameters are reported in the literature (Nishikawa et al., 1998b). Under the test, the column is subjected to a constant axial force ($P$) and unidirectional cyclic lateral displacement at the top of the column. In thin-walled steel tubular circular columns, excessive deformation tends to develop in a local part and consequently the redistribution of stress becomes unexpected. The test results indicate that local buckling occurs near the column base in a range that is equal to the diameter of the cross section ($D$) (Nishikawa et al., 1998a; Usami, 1996). For this purpose, as shown in Fig.

2.1, the two-node beam element (B31) is employed for the upper part of the column, whereas reduced integration four-node conventional shell elements (S4R), which accurately consider the localized deformation, are used for the lower part of the column. All used elements are available in the Abaqus/standard library (Hibbit et al., 2014a). The interface between the shell (S4R) and beam (B31) elements is modeled using multi-point constraint (MPC). The analyzed cantilever column is fixed at the base and subjected to a constant axial force ($P$) and unidirectional cyclic lateral displacement at its top. To reduce the computational time, the bottom half of the lower part (equal to the cross-section diameter, $D$) is divided into 26 shell elements, while the remaining height ($D$) is only divided into 14 shell elements along the column axis. Forty elements for both segments are used in the circumferential direction. The upper part of the column (height of $h$-$2D$) is divided into beam elements with the size of 90. The above stated mesh sizes are determined by trial-and-error. It is found that such mesh density gives accurate results. The default value of five integration points over the thickness is used. The displacement convergence criterion is selected in the analysis and the convergence tolerance is taken as $10^{-5}$. More details of elastoplastic large displacement analyses are reported in (Mamaghani et al., 1995; Shen et al., 1995). The initial geometrical imperfection and residual stresses are not considered in the current analysis as they were not quantified in the tested columns (Goto et al., 1998; Nishikawa et al., 1996, 1998b). Moreover, both of them have insignificant influence on the overall cyclic behavior after the first half-cycle (Banno et al., 1998; Mamaghani et al., 1996b, 1996a). Table 2.1 shows the geometrical properties of the analyzed C and GC columns. It is assumed that all the analyzed columns are made of the same carbon steel SS400 (JIS, 2012) (equivalent to ASTM A36 (ASTM, 2014)) as the tested column (C1).

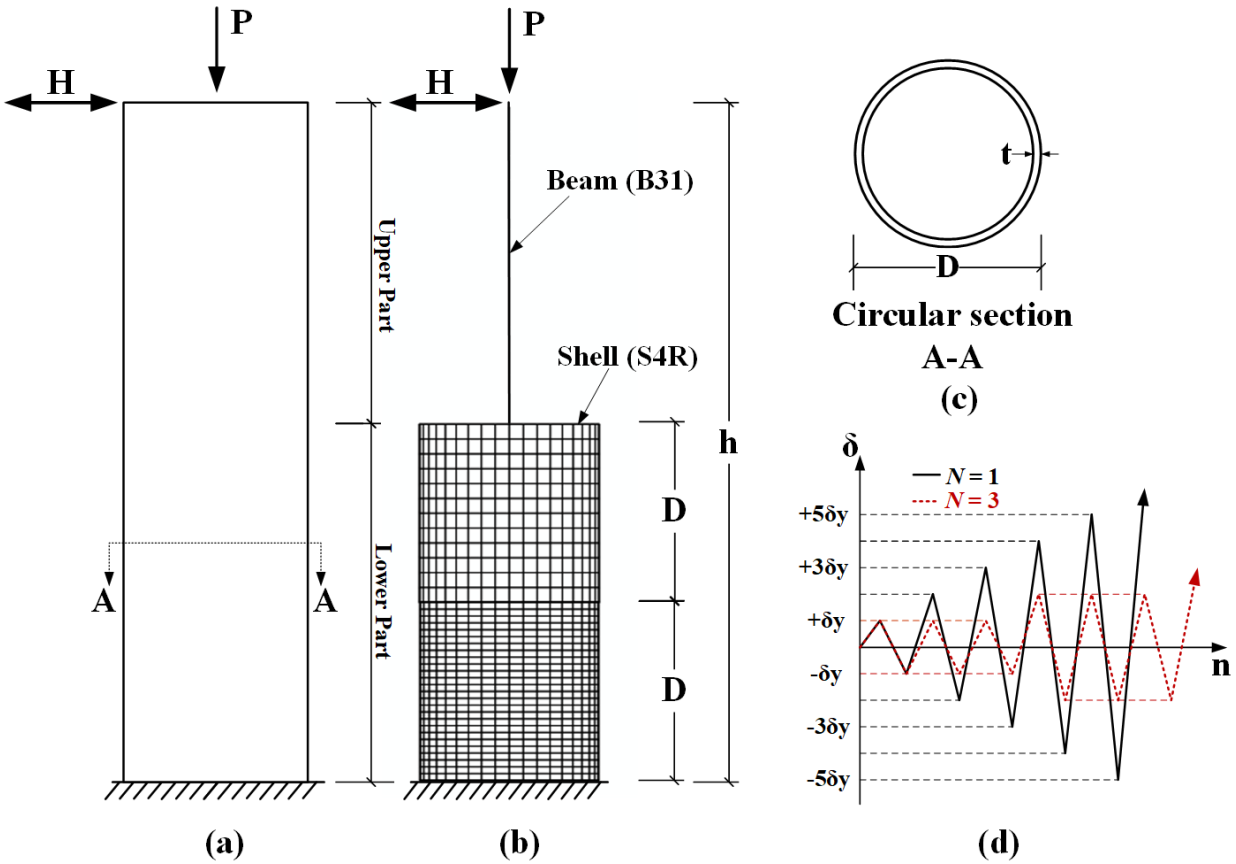


Fig. 2.1. C Column Model: (a) Column; (b) FE Meshing; (c) Cross Section; and (d) Loading Program.

### 2.2.1 Unidirectional Cyclic Loading Program

The schematic presentation of the displacement-controlled unidirectional cyclic loading is illustrated in Fig. 2.1d, adopted as a lateral loading program. The solid line denotes one-cycle loading ($N$ = 1), while the dashed line stands for three-cycle loading ($N$ = 3). Throughout the loading history, the unidirectional cyclic loading is quasi-statically applied to the top of the column with a constant axial force ($P$). The amplitude of the cyclic displacement is increased step by step as a multiple of the yield displacement ($\delta_y$) which is defined by Eq. (2.3):

$$\delta_y = \frac{H_y h^3}{3EI} \tag{2.3}$$

Where $H_y = (\sigma_y - P/A)\, Z/h$ = lateral yield load and $A$, $h$, $EI$, and $Z$ = cross-sectional area, the height, the bending stiffness, and the section modulus, respectively, of the column (Goto, Y et al., 2010).

The values of the yield displacement and lateral yield load for all analyzed columns are listed in Table 2.2.

Table 2.1. Material and Geometrical Properties of Analyzed C and GC columns.

| C Columns | | | | | | GC Columns | | | | | | | | |
|---|---|---|---|---|---|---|---|---|---|---|---|---|---|---|
| **Column** | ***h(mm)*** | ***t(mm)*** | $R_t$ | $\lambda$ | $P/P_y$ | **Column** | ***h(mm)*** | ***t (mm)*** | | | $R_t$ | $\lambda$ | $P/P_y$ |
| | | | | | | | | $t_1$ | $t_2$ | $t_3$ | | | |
| **C1 -tested** | 3403 | 9.00 | 0.116 | 0.26 | 0.124 | **GC1** | 3403 | 11.25 | 9.00 | 7.75 | 0.116 | 0.26 | 0.124 |
| **C2** | 3403 | 10.45 | 0.100 | 0.26 | 0.124 | **GC2** | 3403 | 13.00 | 10.45 | 9.00 | 0.100 | 0.26 | 0.124 |
| **C3** | 3403 | 13.00 | 0.080 | 0.26 | 0.124 | **GC3** | 3403 | 16.25 | 13.00 | 11.20 | 0.080 | 0.26 | 0.124 |
| **C10** | 3403 | 17.40 | 0.060 | 0.26 | 0.124 | **GC10** | 3403 | 21.75 | 17.40 | 15.00 | 0.060 | 0.26 | 0.124 |
| **C11** | 3403 | 26.00 | 0.040 | 0.26 | 0.124 | **GC11** | 3403 | 32.65 | 26.00 | 22.50 | 0.040 | 0.26 | 0.124 |
| **C4** | 3960 | 9.00 | 0.116 | 0.30 | 0.124 | **GC4** | 3960 | 11.25 | 9.00 | 8.00 | 0.116 | 0.30 | 0.124 |
| **C5** | 3960 | 10.45 | 0.100 | 0.30 | 0.124 | **GC5** | 3960 | 13.00 | 10.45 | 9.36 | 0.100 | 0.30 | 0.124 |
| **C6** | 3960 | 13.00 | 0.080 | 0.30 | 0.124 | **GC6** | 3960 | 16.25 | 13.00 | 11.65 | 0.080 | 0.30 | 0.124 |
| **C6-10** | 3960 | 13.00 | 0.080 | 0.30 | 0.100 | **GC6-10** | 3960 | 16.25 | 13.00 | 11.65 | 0.080 | 0.30 | 0.100 |
| **C6-15** | 3960 | 13.00 | 0.080 | 0.30 | 0.150 | **GC6-15** | 3960 | 16.25 | 13.00 | 11.65 | 0.080 | 0.30 | 0.150 |
| **C6-20** | 3960 | 13.00 | 0.080 | 0.30 | 0.200 | **GC6-20** | 3960 | 16.25 | 13.00 | 11.65 | 0.080 | 0.30 | 0.200 |
| **C6-30** | 3960 | 13.00 | 0.080 | 0.30 | 0.300 | **GC6-30** | 3960 | 16.25 | 13.00 | 11.65 | 0.080 | 0.30 | 0.300 |
| **C12** | 3960 | 17.40 | 0.060 | 0.30 | 0.124 | **GC12** | 3960 | 21.75 | 17.40 | 15.60 | 0.060 | 0.30 | 0.124 |
| **C13** | 3960 | 26.00 | 0.040 | 0.30 | 0.124 | **GC13** | 3960 | 32.65 | 26.00 | 23.40 | 0.040 | 0.30 | 0.124 |
| **C7** | 6600 | 9.00 | 0.116 | 0.50 | 0.124 | **GC7** | 6600 | 11.25 | 9.00 | 8.60 | 0.116 | 0.50 | 0.124 |
| **C8** | 6600 | 10.45 | 0.100 | 0.50 | 0.124 | **GC8** | 6600 | 13.00 | 10.45 | 9.96 | 0.100 | 0.50 | 0.124 |
| **C9** | 6600 | 13.00 | 0.080 | 0.50 | 0.124 | **GC9** | 6600 | 16.25 | 13.00 | 12.40 | 0.080 | 0.50 | 0.124 |
| **C14** | 6600 | 17.40 | 0.060 | 0.50 | 0.124 | **GC14** | 6600 | 21.75 | 17.40 | 16.60 | 0.060 | 0.50 | 0.124 |
| **C15** | 6600 | 26.00 | 0.040 | 0.50 | 0.124 | **GC15** | 6600 | 32.65 | 26.00 | 24.90 | 0.040 | 0.50 | 0.124 |

For all columns: Diameter *(D)* = 900 mm, $\sigma_y$ = 289.6 MPa, E = 206 GPa, and, $\nu$ = 0.3.
All columns are loaded with one-cycle at each displacement ($N$ = 1), except C1 and GC1 loaded with $N$ = 1 and 3.
$P_y = \sigma_y * A$, $A = \pi/4 * (D^2 - D_i^2)$, $D_i = D - 2t$, $t$ = thickness for the C column.

## 2.3 Proposed Thin-Walled Steel Tubular Column with Graded Thickness

C columns are experiencing premature buckling (i.e., local buckling, global buckling, or the interaction between both), near the base of the column, under combined axial force and cyclic lateral loading (Usami, 1996). This buckling makes these members unable to fully utilize their strength and ductility capacities. To overcome these shortcomings, thin-walled steel tubular columns with graded thickness (called "graded-thickness" column and denoted as GC) are used as

alternatives to the conventional thin-walled steel circular columns (C). The column height and diameter are kept the same for both C and GC columns. The GC column is divided into three segments of constant cross sections along its longitudinal axis. The first and second segments have the same height that is equal to the diameter ($D$) of the circular section from the base. The third segment has a height of ($h$-$2D$). As shown in Fig. 2.2, a thicker cross section ($t_1$=1.25$t$) is used along the first segment, and the original thickness ($t_2$= $t$; thickness of the C column) is kept for the second segment. Finally, the remaining material volume is distributed on the third segment with $t_3$. The above configurations of the GC column are chosen based on which achieve better behavior. Table 2.1 shows the material and geometrical properties of the C and GC columns. As can be seen, the geometrical properties (except the plate thickness) are the same for both types of columns.

### 2.4 Results and Discussion

The computed results were obtained using the commercially available finite-element software Abaqus/Standard version 6.14 (Hibbit et al., 2014a). Moreover, the accuracy of the employed FEM has been validated in comparison with the experimental results of the cyclic loading test from the literature (Nishikawa et al., 1998b).

#### 2.4.1 Comparison of Numerical and Experimental Results

The normalized lateral load vs. lateral displacement curves of the FE analyses, determined from the one-cycle lateral loading ($N$ = 1), (see Fig. 2.1d), are shown in Fig. 2.3. In these figures, $H_y$ and $\delta_y$ denote the lateral yield load and yield displacement, respectively. Initially, the hysteresis loops from FE analyses are compared to the experimental results available in the literature

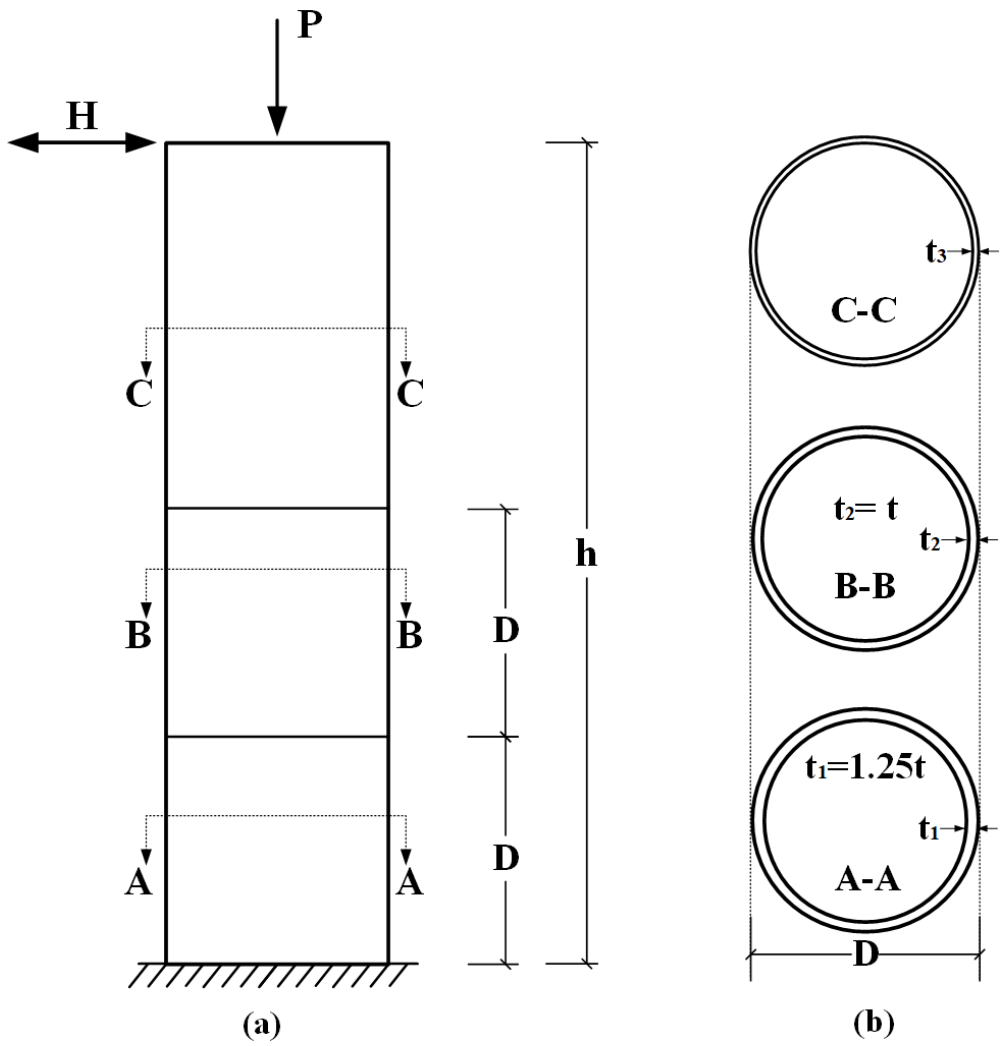


Fig. 2.2. GC Column Model: (a) Column, and (b) Graded-thickness Sections.

(Nishikawa et al., 1998b). As seen from Fig. 2.3, the comparison of lateral load vs. lateral displacement curves of the C1 column shows a relatively good agreement with the experimental results. The predicted ultimate strength of the C1 column (i.e., $H_{max}/H_y$ = 1.403) obtained from the analysis differs only by 3% from the experimental results (i.e., $H_{max}/H_y$ = 1.445). This indicates that FE analysis, using the kinematic hardening material model, describes with a reasonable accuracy the structural behavior with considering the local buckling of thin-walled steel tubular columns with circular sections. However, the columns' stiffness with reversal loading at large

lateral displacements is slightly overestimated. The reason is that the kinematic hardening model does not accurately consider the Bauschinger effect (Goto et al., 1998; Mamaghani et al., 1995; Shen et al., 1995). Similar findings have been reported in other studies (Goto et al., 1998; Ucak and Tsopelas, 2006).

#### 2.4.1.1 Buckling Mode of C1 Column

As shown in Fig. 2.4, the deformed shape of the C1 column (Fig. 2.4b) at the end of the FE analysis was compared to the deformed shape at the end of the experiment (Fig. 2.4a) (Goto et al., 1998). Similar to the experimental observations, the column bulged outward near the base and formed an elephant foot bulge buckling mode. The deformed shape was captured relatively well in the analysis.

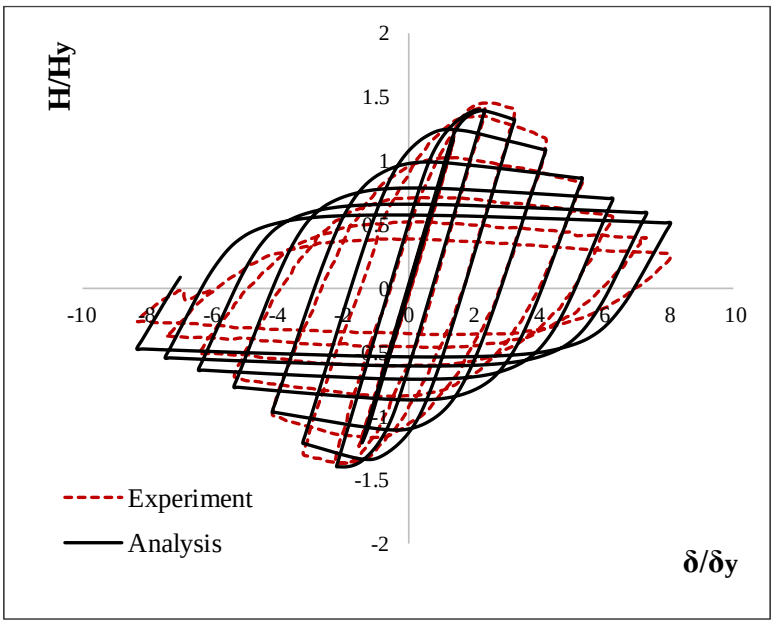


Fig. 2.3. Hysteretic Behavior of Analysis and Experiment of the C1 column.

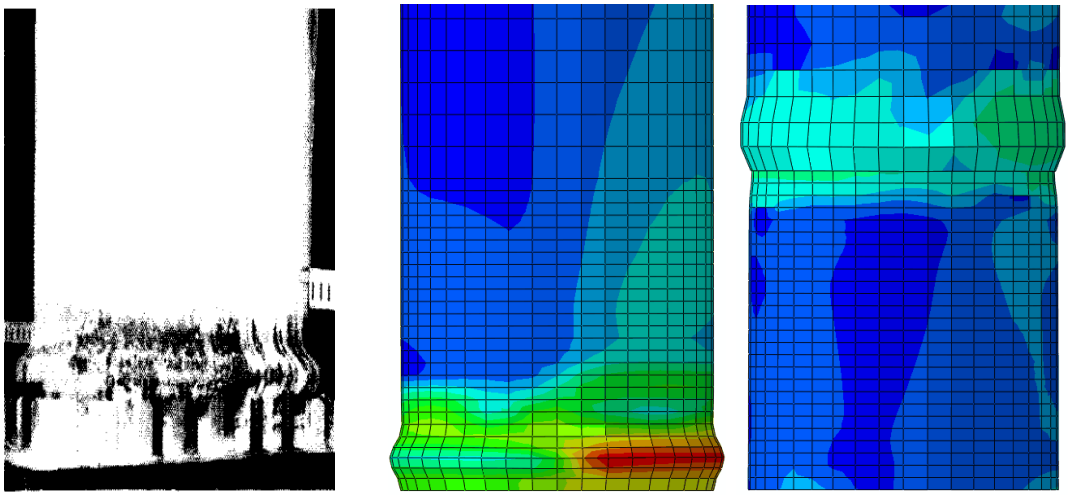

(a) Experiment (Goto et al., 1998) (b) C1 Column (c) GC1 Column

Fig. 2.4. Buckling Deformation of Columns.

## 2.5 Hysteresis Behavior of C and GC Columns

Based on the results in Fig. 2.3, the comparison between the numerical and experimental results indicates that the FEM can predict the structural non-linear behavior with reasonable accuracy. The results obtained from the FE analysis differ only by 3% from the test results. Using the same validated FEM, a comparison study has been performed between the hysteretic behavior of the C and GC columns under the same axial force and unidirectional cyclic lateral loading, as shown in Fig. 2.5. A significant increase in both ultimate strength and ductility was observed when the GC columns were used with the same size and volume of the materials as in the counterpart C columns. Moreover, the post-buckling of the GC columns was improved as compared to their C column counterparts. For example, in the C1 column (see Fig. 2.5a), the buckling initiates when the displacement is between $2\delta_y$ and $3\delta_y$. A strength drop of 17.6% of the ultimate strength (observed at $\delta = +2.16\delta_y$) occurs at $\delta = +4\delta_y$. As the displacement increases, the column strength decreases

in a rapid pattern to 38% of its ultimate strength at $\delta = +8\delta_y$. On the other hand, the GC1 column shows a maximum load capacity at $\delta = +3\delta_y$. Only an 8.4% strength drop of the ultimate strength took place at $\delta = +4\delta_y$, which gives an indication that the local buckling started between $3\delta_y$ and $4\delta_y$. As the displacement amplitude was increased, more strength deterioration was observed. The residual strength of the GC1 column was 51.6% of its ultimate strength at $\delta = +8\delta_y$. It is worth mentioning that the strength significantly dropped at $\delta = -4\delta_y$, and $\delta = -8\delta_y$ for both columns. A similar trend was observed for all the analyzed columns, as shown in Fig. 2.5b, c, and d. Fig. 2.4 shows the final deformed shape of the GC column compared to the C column at $\delta = +8\delta_y$. The GC columns show a delay in the buckling occurrence. Moreover, the buckled shape of the C columns occurred near the base of the column as expected, while buckling shifted upward from the base in the case of the GC columns, as shown in Fig. 2.4c.

### 2.6 Parametric Study

The validated FEM was then employed to carry out an extensive parametric study to find out the effects of different parameters on the overall hysteretic behavior of the C and GC columns. A total of 40 columns including one tested column (C1 column) are analyzed using the commercially available finite-element software Abaqus/standard version 6.14 (Hibbit et al., 2014a). The studied parameters that are commonly used in the design and that affect the overall behavior of the thin-walled steel tubular columns are: the radius-to-thickness ratio parameter ($R_t$) with a range of (0.04 – 0.116), the column slenderness ratio parameter ($\lambda$) varying from 0.26 to 0.5, the axial load ratio ($P/P_y$), where five different ratios ($0.1P_y$, $0.124P_y$, $0.15P_y$, $0.20P_y$, and, $0.3P_y$) are applied on C6 and GC6 columns, and the number of loading cycles at each displacement amplitude ($N$). To examine the effect of loading cycle numbers ($N$), all the columns are analyzed under one-cycle of

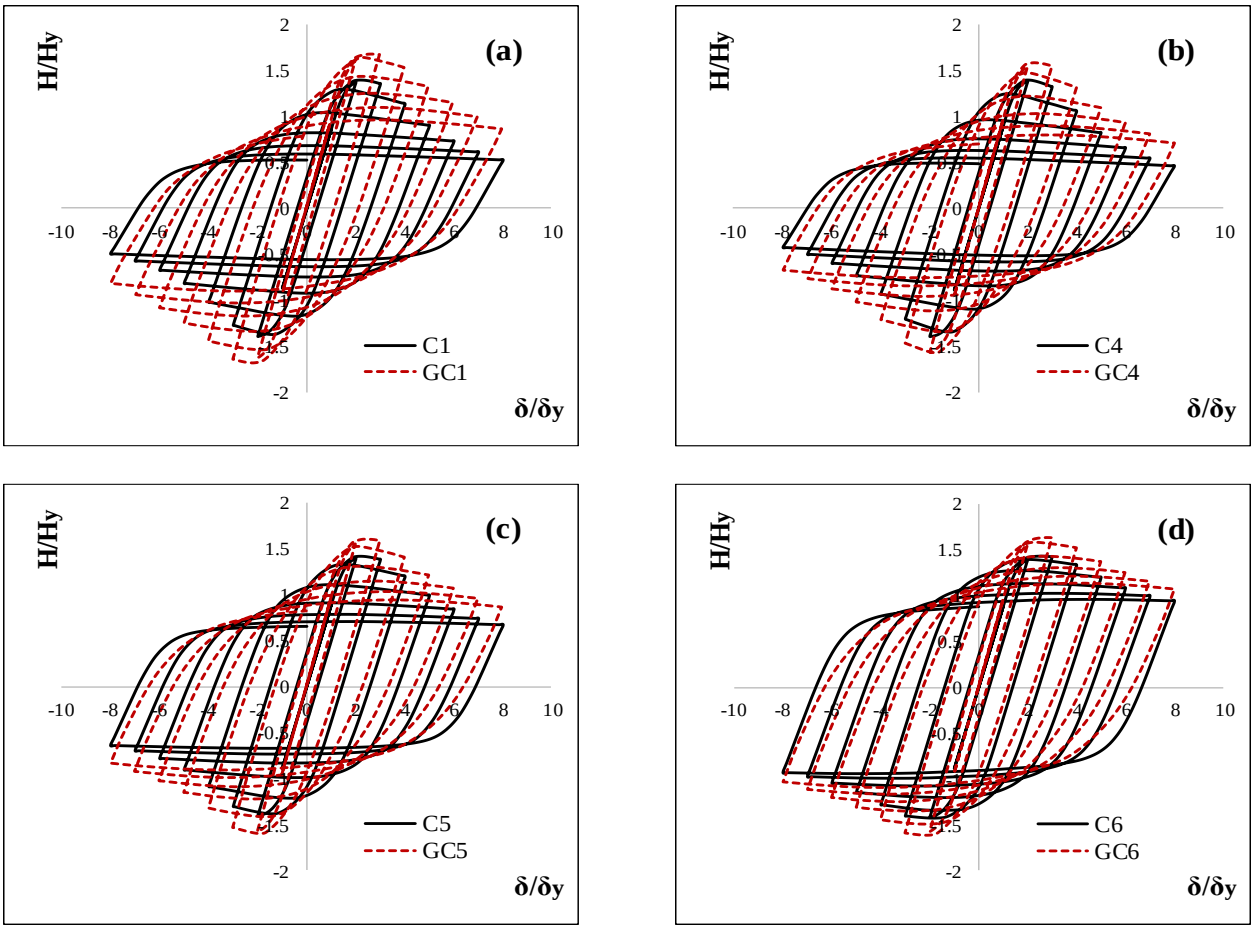


Fig. 2.5. Comparison of Hysteretic Behavior: (a) C1 & GC1, (b) C4 & GC4, (c) C5 & GC5, and (d) C6 & GC6.

displacement (*N = 1*), except the C1 and GC1 columns, which have been analyzed under one (*N = 1*), and three (*N = 3*) displacement cycles. The ranges of the studied parameters are selected as they are commonly adopted by the researchers (Usami et al., 2000b, 2000a). Also, in the practical design, $0.03 \leq R_t \leq 0.08$ and $0.2 \leq \lambda \leq 0.4$ are generally used for bridge piers with circular cross sections under $P/P_y \leq 0.2$ (Chen, W. F. and Duan, 2014). The columns listed in Table 2.1 are assumed to be made of carbon steel SS400 (JIS, 2012) (equivalent to ASTM A36 (ASTM, 2014)).

### 2.6.1 Effect of Radius-to-Thickness Ratio Parameter ($R_t$)

The effect of the radius-to-thickness ratio parameter ($R_t$) on the strength and ductility of the column is studied. The increase in $R_t$ might be either due to an increase in the radius of the column or a decrease in the thickness. In this study, all columns are analyzed by keeping the diameter constant and changing the thickness. Fig. 2.6 shows the lateral load vs. lateral displacement envelope curves of both the C and GC columns. With the decrease of $R_t$, higher ultimate strength and ductility in both C and GC columns is obtained. For example, as $R_t$ in the C columns decreases from 0.116 (C1 column) to 0.04 (C11 column) with $\lambda = 0.26$ (see Fig. 2.6a), the normalized ultimate strength is increased by 10%. In addition, the normalized maximum displacement corresponding to the ultimate strength is increased by 132% (i.e., $\delta_m/\delta_y$ shifted from (2.16 to 5). Similarly, decreasing $R_t$ in the GC columns from 0.116 (in GC1column) to 0.04 (GC11 column) with $\lambda = 0.26$ (see Fig. 2.6c), improves the ultimate strength by 9%. Also, the normalized maximum displacement corresponding to the ultimate strength is increased by 85% (i.e. $\delta_m/\delta_y$ shifted from 2.71 to 5). Furthermore, columns with smaller $R_t$ experience higher ductility than those with larger $R_t$. By looking at Fig. 2.6, it should be noted that the improvement of the ultimate strength becomes less when $\lambda$ gets larger (see Fig. 2.6b and d), as discussed in the following section.

### 2.6.2 Effect of Slenderness Ratio Parameter ($\lambda$)

The effect of the slenderness ratio parameter ($\lambda$) on the strength and ductility of the column is examined, as presented in Fig. 2.7. Ultimate strength and ductility are improved as $\lambda$ values get smaller in both C and GC Columns.

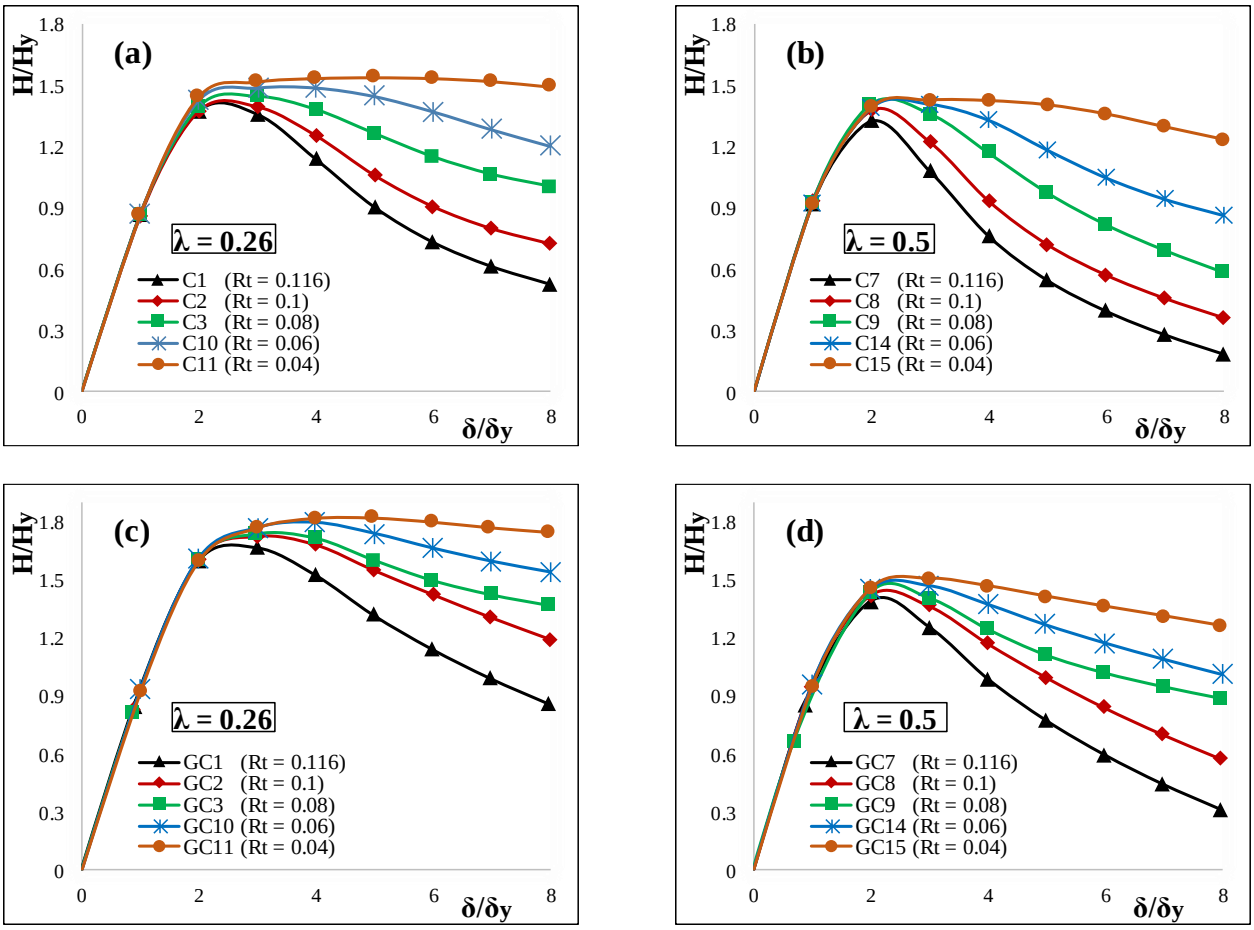


Fig. 2.6. Effect of $R_t$ parameter: (a) C columns with λ = 0.26, (b) C columns with λ = 0.5, (c) GC columns with λ = 0.26, and (d) GC columns with λ = 0.5.

As an example, the normalized ultimate strength and the normalized maximum displacement corresponding to the ultimate strength are improved by 7.25% and 103%, respectively, when λ decreases from 0.5 in the case of the C15 column to 0.26 in the C11 column (see Table 2.2). ). A similar trend is observed in the case of GC columns, where the normalized ultimate strength and the normalized maximum displacement are increased by 21% and 72%, respectively.

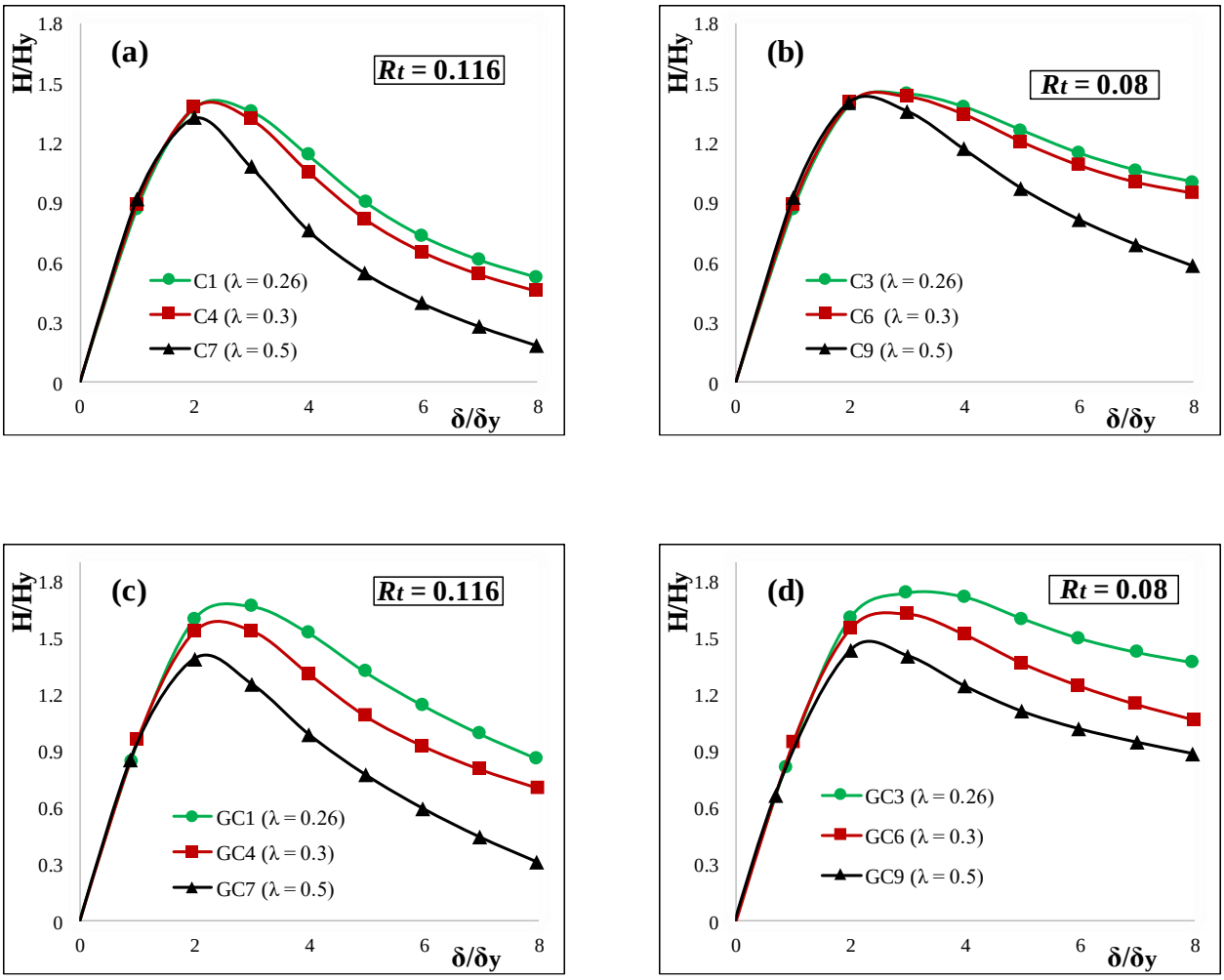


Fig. 2.7. Effect of λ parameter: (a) C columns with $R_t$ = 0.116, (b) C columns with $R_t$ = 0.08, (c) GC columns with $R_t$ = 0.116, and (d) GC columns with $R_t$ = 0.08.

Moreover, when λ is higher, the area surrounded by the envelope curve decreases and the slope becomes steeper after the ultimate strength point, especially, in the case of λ = 0.5. In other words, the strength after the peak point drops in a rapid pattern in average of 42% and 32% for C7 and GC7 columns, respectively, in case of λ = 0.5. In contrast, in the case of λ = 0.26, where less strength drops, the drop is 20% and 14% for C1 and GC1 columns, respectively. The reason is attributed to the *P-Δ* effect in the case of the long columns (Gao et al., 1998a).

### 2.6.3 Effect of Axial Load ($P/P_y$)

The effect of the axial load ratio on the ultimate strength and ductility of the C and GC columns is investigated. Five of C columns (C6-10, C6-12.4, C6-15, C6-20, and C6-30) and five of the GC columns (GC6-10, GC6-12.4, GC6-15, GC6-20, and GC6-30) are analyzed under different axial loads, where the number after the hyphen indicates the applied axial load ratio (i.e., $P/P_y$ = 0.1, 0.124, 0.15, 0.2, and 0.3, respectively). The envelope curves of the normalized lateral load ($H/H_{y0}$) vs. lateral displacement ($\delta/\delta_{y0}$) are shown in Fig. 2.8. $H_{y0}$ and $\delta_{y0}$ represents the lateral yield load and yield displacement under zero axial load, respectively. For both C6 and GC6 columns with higher axial load, the maximum strength is reduced. For instance, the maximum strength is decreased by 15% and 23% in C6 and GC6 columns, respectively, when $P/P_y$ increases from 0.1 to 0.3. Furthermore, the post-buckling curve slope becomes steeper, which dissipate less energy as observed in the cases of C6-30 and GC6-30 columns. When $P/P_y$ = 0.3, the slope of C6-30 and GC6-30 columns decreases by 53% and 70%, respectively, in each loading step, while the slope decreases by 9.7% and 7.4% in the cases of C6-10 and GC6-10 columns, respectively. The main reason is believed to be due to the $P$-$\Delta$ effect in the case of large axial loads as found in (Gao et al., 1998a).

### 2.6.4 Effect of Number of Loading Cycles ($N$)

Fig. 2.9 shows the comparison of the envelope curves of the C (Fig. 2.9a) and GC (Fig. 2.9b) columns in the cases of one ($N$ = 1) and three ($N$ = 3) loading cycles at each lateral displacement level. It is noted that when the displacement is greater than $3\delta_y$, the strength decreases in a rapid pattern in the case of $N$ = 3 compared to the case of $N$ = 1 for both C and GC columns. Furthermore, the slope of the post-buckling curve in the case of $N$ = 3 is steeper than that for $N$ = 1 when the

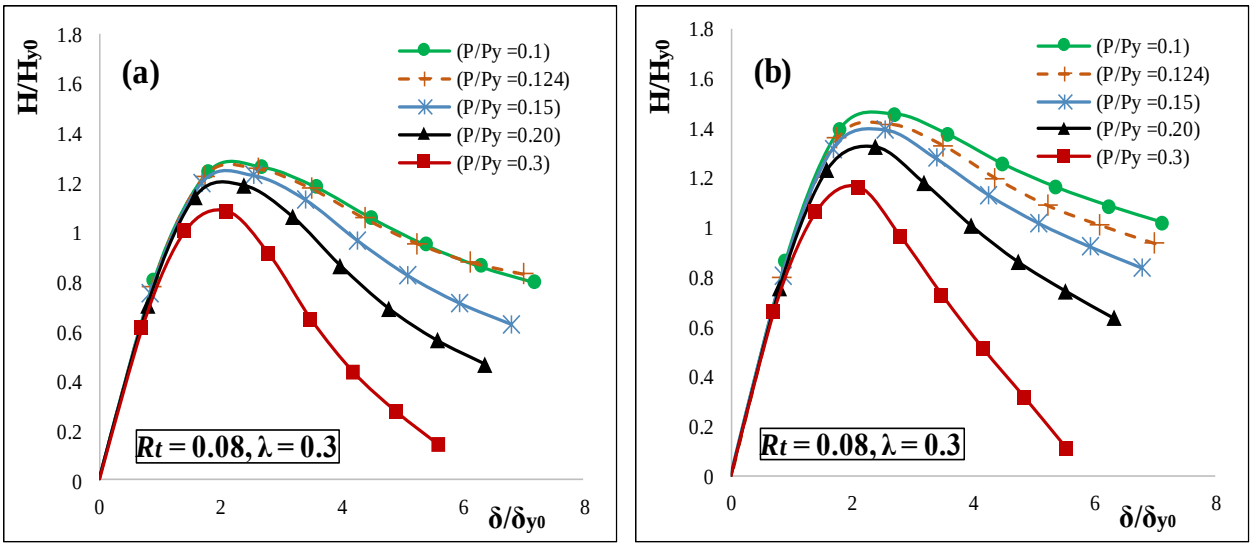


(a) C6 Column (b) GC6 Column

Fig. 2.8. Envelope Curves with Different Axial Load.

lateral displacement is greater than $3\delta_y$. For example, C1 and GC1 columns slopes decrease by 21% and 15% in the case of $N$ = 1, respectively. In comparison, C1 and GC1 columns slopes decrease by 26% and 18.5% in the case of $N$ = 3, respectively. On the other hand, no remarkable effect is observed when the lateral displacement is less than $3\delta_y$, which might be due to small plastic deformation.

### 2.7 Strength and Ductility Evaluation of C and GC Columns

Table 2.2 summarizes the computed ultimate strength values from the lateral load vs. lateral displacement responses of the analyzed columns. For both C and GC columns, the $H_{max}/H_y$ vs. $(1+P/P_y)$ $R_t$ λ relationship is plotted taking into account the axial load ($P/P_y$) effect as shown in Fig. 2.10. The proposed formulae that fit the computed ultimate strength of the analyzed C and GC columns are as follows:

$$\frac{H_{max}}{H_y} = \frac{1.13}{\left[(1+\frac{P}{P_y}).R_t\lambda\right]^{0.07}} \quad \text{C Columns} \quad 0.01 \le R_t\,\lambda \le 0.06 \qquad (2.4)$$

$$\frac{H_{max}}{H_y} = \frac{0.973}{\left[(1+\frac{P}{P_y}).R_t\lambda\right]^{0.14}} \quad \text{GC Columns} \quad 0.01 \le R_t\,\lambda \le 0.06 \qquad (2.5)$$

Based on Fig. 2.10, the ultimate strength is improved if $R_t$ decreases under constant λ. Similarly, the ultimate strength increases if λ decreases with constant $R_t$. The failure of thin-walled steel tubular columns is considered to have occurred when the displacement equals either $\delta_m$ or $\delta_{0.9}$. $\delta_m$ is the displacement corresponding to the ultimate strength, where $\delta_{0.9}$ is defined as the displacement point where the strength drops to 90% of its ultimate value after the peak (Mamaghani, 1996; Mamaghani et al., 2015; Usami, 1996). The $\delta_m/\delta_y$ and $\delta_{0.9}/\delta_y$ are key parameters used to evaluate the ductility performance for both C and GC columns. However, the $\delta_{0.9}/\delta_y$ parameter considers the cyclic characteristics and fully utilizes the strength of the steel at large plastic displacements. Moreover, the strength of thin-walled steel tubular circular columns decreases significantly after the peak value due to the influence of local buckling. Therefore, it is more reasonable to use the $\delta_{0.9}/\delta_y$ parameter to evaluate the ductility (Gao et al., 1998a; Mamaghani et al., 2015; Usami et al., 2000b).

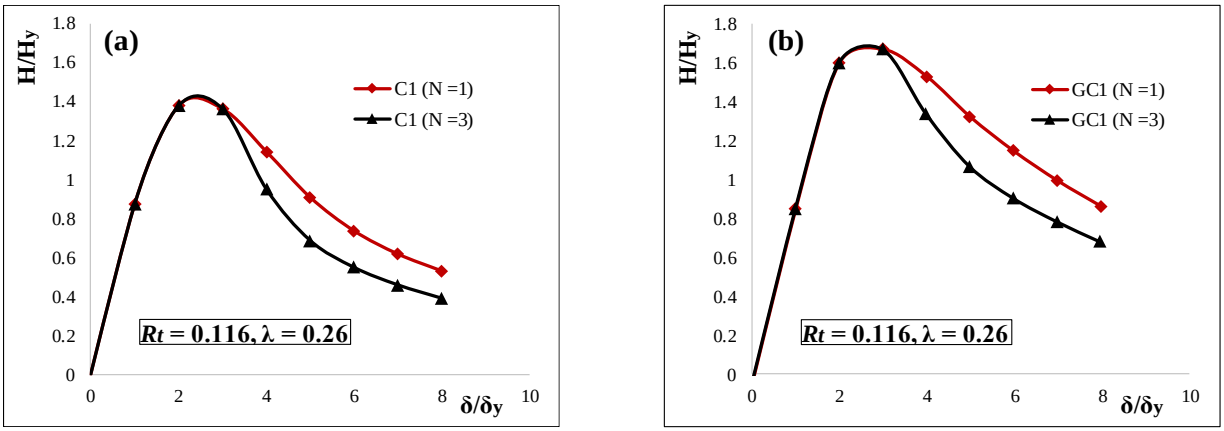


(a) C1 Column (b) GC1 Column

Fig. 2.9. Effect of *N* on Ductility Capacity.

Table 2.2. Strength and Ductility Evaluation of C and GC Columns.

| C Columns | | | | | | GC Columns | | | | | |
|---|---|---|---|---|---|---|---|---|---|---|---|
| **Column** | $H_y$ **(KN)** | $\delta_y$ **(mm)** | $H_{max}/H_y$ | $\delta_m/\delta_y$ | $\delta_{0.9}/\delta_y$ | **Column** | $H_y$ **(KN)** | $\delta_y$ **(mm)** | $H_{max}/H_y$ | $\delta_m/\delta_y$ | $\delta_{0.9}/\delta_y$ |
| **C1 -tested** | 414.2 | 10.6 | 1.403 | 2.16 | 3.45 | **GC1** | 414.2 | 10.6 | 1.675 | 2.71 | 4.10 |
| **C2** | 478.7 | 10.6 | 1.409 | 2.40 | 3.90 | **GC2** | 478.7 | 10.6 | 1.728 | 3.00 | 4.97 |
| **C3** | 593.2 | 10.6 | 1.448 | 2.82 | 4.68 | **GC3** | 593.2 | 10.6 | 1.746 | 2.83 | 5.3 |
| **C10** | 779.5 | 10.6 | 1.495 | 3.00 | 6.34 | **GC10** | 779.5 | 10.6 | 1.799 | 3.82 | 6.68 |
| **C11** | 1135.5 | 10.6 | 1.54 | 5.00 | > $8\delta_y$ | **GC11** | 1135.5 | 10.6 | 1.825 | 5.00 | > $8\delta_y$ |
| **C4** | 355.9 | 14.3 | 1.395 | 1.98 | 3.25 | **GC4** | 355.9 | 14.3 | 1.578 | 2.28 | 3.52 |
| **C5** | 411.4 | 14.3 | 1.417 | 2.16 | 3.58 | **GC5** | 411.4 | 14.3 | 1.601 | 2.43 | 3.78 |
| **C6** | 509.8 | 14.3 | 1.439 | 2.52 | 4.35 | **GC6** | 509.8 | 14.3 | 1.632 | 2.78 | 4.33 |
| **C6-10** | 523.7 | 14.3 | 1.408 | 2.52 | 4.31 | **GC6-10** | 523.7 | 14.3 | 1.619 | 2.84 | 4.51 |
| **C6-15** | 494.6 | 14.3 | 1.457 | 2.34 | 4.11 | **GC6-15** | 494.6 | 14.3 | 1.645 | 2.76 | 4.14 |
| **C6-20** | 465.5 | 14.3 | 1.501 | 2.28 | 3.87 | **GC6-20** | 465.5 | 14.3 | 1.666 | 2.61 | 3.88 |
| **C6-30** | 407.3 | 14.3 | 1.575 | 2.22 | 3.52 | **GC6-30** | 407.3 | 14.3 | 1.689 | 2.34 | 3.48 |
| **C12** | 669.8 | 14.3 | 1.467 | 3.00 | 5.63 | **GC12** | 669.8 | 14.3 | 1.704 | 3.00 | 6.02 |
| **C13** | 975.8 | 14.3 | 1.501 | 5.00 | > $8\delta_y$ | **GC13** | 975.8 | 14.3 | 1.738 | 4.00 | > $8\delta_y$ |
| **C7** | 213.6 | 39.7 | 1.334 | 1.88 | 2.52 | **GC7** | 213.6 | 39.7 | 1.405 | 1.88 | 2.94 |
| **C8** | 246.8 | 39.7 | 1.381 | 2.00 | 2.88 | **GC8** | 246.8 | 39.7 | 1.445 | 2.00 | 3.35 |
| **C9** | 305.9 | 39.7 | 1.408 | 1.98 | 3.49 | **GC9** | 305.9 | 39.7 | 1.460 | 2.08 | 3.57 |
| **C14** | 401.9 | 39.7 | 1.418 | 2.34 | 4.38 | **GC14** | 401.9 | 39.7 | 1.489 | 2.33 | 4.38 |
| **C15** | 585.5 | 39.7 | 1.436 | 2.46 | 7.12 | **GC15** | 585.5 | 39.7 | 1.508 | 2.91 | 6.12 |

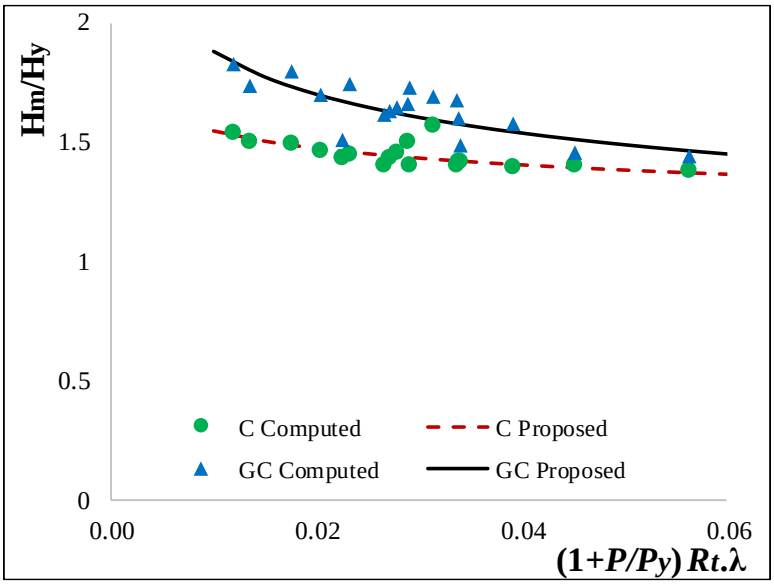


Fig. 2.10. Ultimate Strength of C and GC Columns.

Table 2.2 shows an increasing trend of strength and ductility in both the C and GC columns as the $R_t$ and λ decrease. All $\delta_m/\delta_y$ and $\delta_{0.9}/\delta_y$ values of both the C and GC columns are plotted vs. integrated $R_t$, λ and/or $P/P_y$, as shown in Fig. 2.11. The $\delta_{0.9}/\delta_y$ values of C11, C13, GC11, and GC12 columns are not obtainable in the analysis as the post-buckling strength does not drop to 90% of the ultimate strength as the lateral displacement increases. The proposed formulae that fit the computed $\delta_m/\delta_y$ and $\delta_{0.9}/\delta_y$ values of the analyzed columns are as follows:

$$\frac{\delta_m}{\delta_y} = \frac{0.326}{(R_t\lambda)^{0.55}} \tag{2.6}$$

$$\frac{\delta_{0.9}}{\delta_y} = \frac{0.3}{\left[(1+\frac{P}{P_y}).R_t\lambda^{0.5}\right]^{0.88}} \quad \text{C Columns} \quad 0.01 \le R_t\,\lambda \le 0.06 \tag{2.7}$$

$$\frac{\delta_m}{\delta_y} = \frac{0.375}{(R_t\lambda)^{0.54}} \tag{2.8}$$

$$\frac{\delta_{0.9}}{\delta_y} = \frac{0.48}{\left[(1+\frac{P}{P_y}).R_t\lambda^{0.5}\right]^{0.75}} \quad \text{GC Columns} \quad 0.01 \le R_t\,\lambda \le 0.06 \tag{2.9}$$

As can be seen from Fig. 2.8, the axial load magnitude has a significant effect on the post-buckling of the C and GC columns. Therefore, the axial load effect is considered in the fitting of the equation of the ductility parameter $\delta_{0.9}/\delta_y$ as it appears in Eqs. (2.7) and (2.9). In contrast, the axial load has an insignificant effect on the maximum displacement of the C and GC columns. Thus, axial load influence is not included in the equation fitting of $\delta_m/\delta_y$ parameter, as shown in Eqs. (2.6) and (2.8).

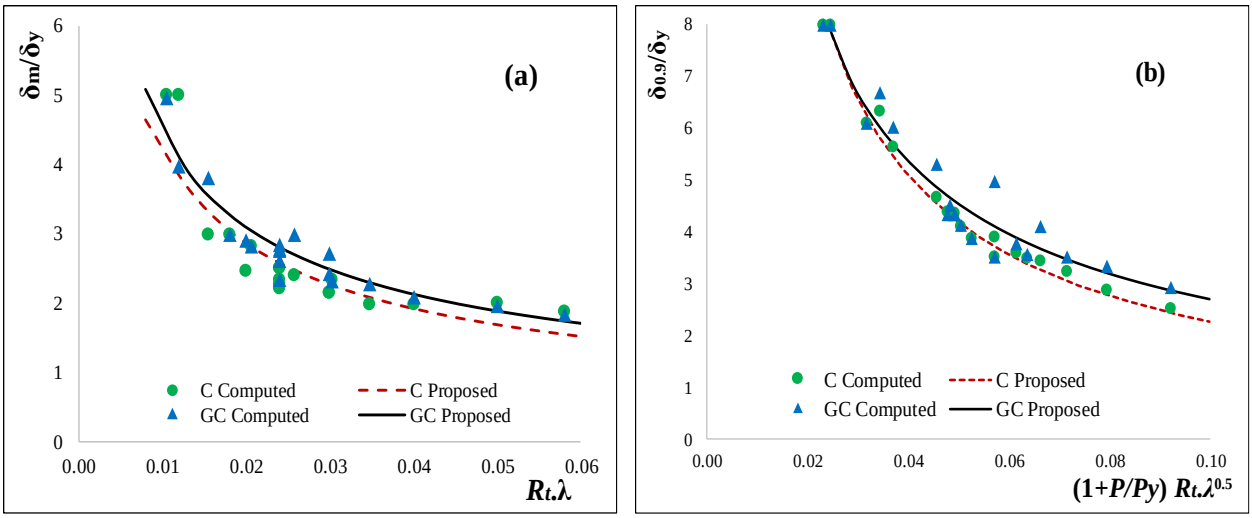


Fig. 2.11. Ductility of C and GC Columns: (a) $\delta_m/\delta_y$, and (b) $\delta_{0.9}/\delta_y$.

## 2.8 Summary

In this chapter, the cyclic behavior of thin-walled steel tubular circular columns with uniform (C) and graded-thickness (GC) was investigated through FE numerical modeling. GC columns were introduced to improve the behavior of C columns. The effect of the radius-to-thickness ratio parameter ($R_t$), the column slenderness ratio parameter (λ), the axial load ratio($P/P_y$), and the number of cycles of loading ($N$) were investigated. Based on this study, some important conclusions are summarized as follows:

- A satisfactory agreement between the analysis and experimental results confirms the ability of the FEM to capture the column behavior taking into account the local buckling of thin-walled steel tubular columns under combined constant axial force and unidirectional cyclic lateral displacement. The predicted ultimate strength of the C1 column obtained from the FEM differs only by 3% from the experimental results.
- Graded-thickness columns (GC) were introduced to improve the behavior of uniform thin-walled steel tubular circular columns (C), which resulted in significant improvements in

the strength, ductility, and post-buckling. Generally, an improvement of 21% and 16% in the ultimate strength was achieved using GC columns compared to C columns when $\lambda$ = 0.26 and 0.3, respectively. In the case of $\lambda$ = 0.5, the ultimate strength was improved by only 5% as GC columns compared to C columns.

- An extensive parametric study indicates that with the decrease of $R_t$ and $\lambda$, an increase was obtained in ultimate strength, ductility, and post-buckling. Also, the ultimate strength of the C and GC columns decreased when the axial load was increased. This effect was more significant as the displacement increased beyond $3\delta_y$. Moreover, a significant strength deterioration occurred when loading cycles number ($N$) at each displacement level increased.
- Finally, proposed formulae to predict the ultimate strength and ductility of C and GC columns are provided. The proposed formulae are expected to be useful in the practical design.

# CHAPTER 3 Stiffened Square Box Columns under Unidirectional Cyclic Lateral Loading

## 3.1 Introduction

This chapter aims to propose a newly graded-thickness thin-walled steel stiffened square box columns (GB) in an attempt to improve the ultimate strength, ductility, energy absorption, and post-buckling of a uniform thin-walled steel stiffened square box columns (B). To achieve this goal, a uniform thin-walled steel stiffened square box column (B1) has been numerically analyzed under a constant axial force ($P$) and unidirectional cyclic lateral loading. The accuracy of the adopted FEM has been verified based on the experimental results in the literature (Nishikawa et al., 1998b). Then, a GB column with size and volume of material equivalent to a B column is introduced. The study results indicate that the proposed GB column shows significant improvements in ultimate strength, ductility, energy absorption, and post-buckling compared to its counterpart B column emphasizing the effect of the plate thickness and sectional configuration in the GB columns. The main reason for the improved behavior of the GB columns is their ability to eliminate the buckling near the base of the column (section A-A, see Fig. 3.1 and Fig. 3.2) where the buckling most likely occurs. In the section 3.5, a parametric study is carried out to assess the effects of key design parameters on the strength, ductility, and energy dissipation of both B and GB columns. These key parameters include the width-to-thickness ratio parameter ($R_f$), the column slenderness ratio parameter ($\lambda$), the magnitude of the axial load ($P/P_y$), and the number of loading cycles ($N$). Finally, a series of design formulae is given to predict the strength and ductility of the B and GB columns. The proposed formulae are expected to be useful guidelines in the practical design and steel fabrication.

### 3.2 Numerical Model

A series of FE analyses on the cyclic behavior of thin-walled steel stiffened square box columns are carried out using a commercial finite element software, Abaqus/Standard version 6.14 (Hibbit et al., 2014a). The FEM considers both material and geometric nonlinearities. The linear kinematic hardening material model with the von Mises yield criterion and associated plastic flow rule, is used in this study. This model is used to simulate the inelastic behavior of materials that are subjected to cyclic loading. More details about this model are reported in (Chaboche, 1986; Hassan et al., 2018a; Mamaghani et al., 1995; Shen et al., 1995). The accuracy of the employed FEM is validated in comparison with the experimental results available in the literature (Nishikawa et al., 1998b). The strength and ductility of thin-walled steel stiffened square box columns are affected by $R_f$ and λ (Frangopol and Saydam, 2014; Mamaghani and Packer, 2002). $R_f$ controls the local buckling of the plate, while λ has a considerable effect on the global stability of the column (Aoki and Susantha, 2005a; Mamaghani, 2008; Mamaghani and Packer, 2002). For the tested column (B1 column), definitions of $R_f$ and λ parameters are given as follows (Aoki and Susantha, 2005b; Frangopol and Saydam, 2014):

$$R_f = \frac{D}{t}\sqrt{\frac{\sigma_y}{E}\frac{12\left(1-\nu^2\right)}{\pi^2 k_R}} \quad , k_R = 4n^2 \tag{3.1}$$

$$\lambda = \frac{2h}{r}\frac{1}{\pi}\sqrt{\frac{\sigma_y}{E}} \tag{3.2}$$

Where $h$ = column height = 3403 mm; $r$ = radius of gyration of cross section = 356 mm; $\sigma_y$ = yield stress= 378.6 MPa; $E$ = Young's modulus = 206 GPa; $\nu$ = Poisson's ratio = 0.3; $D$ = plate width = 900 mm; and $t$ = plate thickness = 9 mm, $k_R$ = buckling coefficient of the subpanel, $n$ = the number

of subpanels for each plate. The tested column data are reported in the literature (Nishikawa et al., 1998b). During the experiment, the cantilever column is fixed at the base and subjected to constant axial force ($P$) and quasi-static unidirectional cyclic lateral displacement at its top. In thin-walled steel stiffened square box columns, the experimental results indicate that local buckling occurs near the column base in a range that is equal to the side width ($D$) (Nishikawa et al., 1998a; Tang et al., 2016b; Usami, 1996). For this purpose, as shown in Fig. 3.1, subpanels, longitudinal stiffeners, and diaphragms are modeled by the four-node shell elements with reduced integration, S4R. These elements consider accurately the local buckling for the lower part of the column ($2D$). The beam-column element (B31) is employed for the upper part of the column ($h$-$2D$). All used elements are available in the Abaqus library (Hibbit et al., 2014a). The interface between the S4R and B31 elements has been modeled using the multi-point constraint (MPC). For computational efficiency, the bottom half of the lower part (equal to the side width of the square box section, $D$) is divided into 30 S4R elements, while the remaining height ($D$) is only divided into 18 S4R elements. Each subpanel between the stiffeners has six columns of S4R elements. Three columns of S4R elements are assigned in the longitudinal stiffeners. The upper part of the column (height of $h$-$2D$) is divided into B31 elements with the size of 90 mm. The mesh sizes stated above are decided by trial-and-error. It is found that such mesh density provides accurate results but does not significantly increase the computational time. In S4R elements, the default value of five integration points over the thickness is used. The displacement convergence criterion is selected in the analysis and the convergence tolerance is taken as $10^{-5}$. The initial geometrical imperfection and residual stresses are not considered in the current analysis as they were not quantified in the tested columns (Goto et al., 1998; Nishikawa et al., 1996, 1998b). Moreover, both initial geometrical imperfection and residual stresses due to welding of the flange and web plates have insignificant influence on

the overall cyclic behavior after the first half-cycle (Ucak and Tsopelas, 2012). Banno et al. (1998) (Banno et al., 1998) and Mamaghani et al. (1996) (Mamaghani et al., 1996a, 1996b) have found that effects of initial geometrical imperfection and residual stresses will reduce the initial stiffness and strength under monotonic loading but have insignificant effect on the overall hysteretic response of thin-walled structures under cyclic loading. Different studies concluded that the residual stresses effect on the overall cyclic behavior can be neglected (Hassan et al., 2018b). Table 3.1 lists the material and geometrical properties of the analyzed B and BG columns.

### 3.2.1 Unidirectional Cyclic Loading Protocol

The unidirectional displacement-controlled cyclic loading protocol is employed in this study, as shown in Fig. 3.1d. The solid line signifies one-cycle loading ($N = 1$), while the dashed line refers to three-cycle loading ($N = 3$). Throughout the loading history, a quasi-static cyclic lateral loading is applied to the top of the column accompanied by constant axial force ($P$). The amplitude of the cyclic displacement is increased step by step as a multiple of the yield displacement ($\delta_y$) which is defined by Eq. (3.3):

$$\delta_y = \frac{H_y h^3}{3EI} \tag{3.3}$$

$$H_y = \left(\sigma_y - \frac{P}{A}\right)\frac{S}{h} \tag{3.4}$$

where Eq. (3.4) is to calculate the lateral yield load and $A$, $h$, $E$, $I$, and $S$ = cross-sectional area, the height, the young's modulus, moment of inertia of the cross section, and the elastic section modulus of the column, respectively (see Table 3.1) (Banno et al., 1998; Nishikawa et al., 1998b).

The yield displacements and lateral yield loads for all analyzed B and BG columns are listed in Table 3.2.

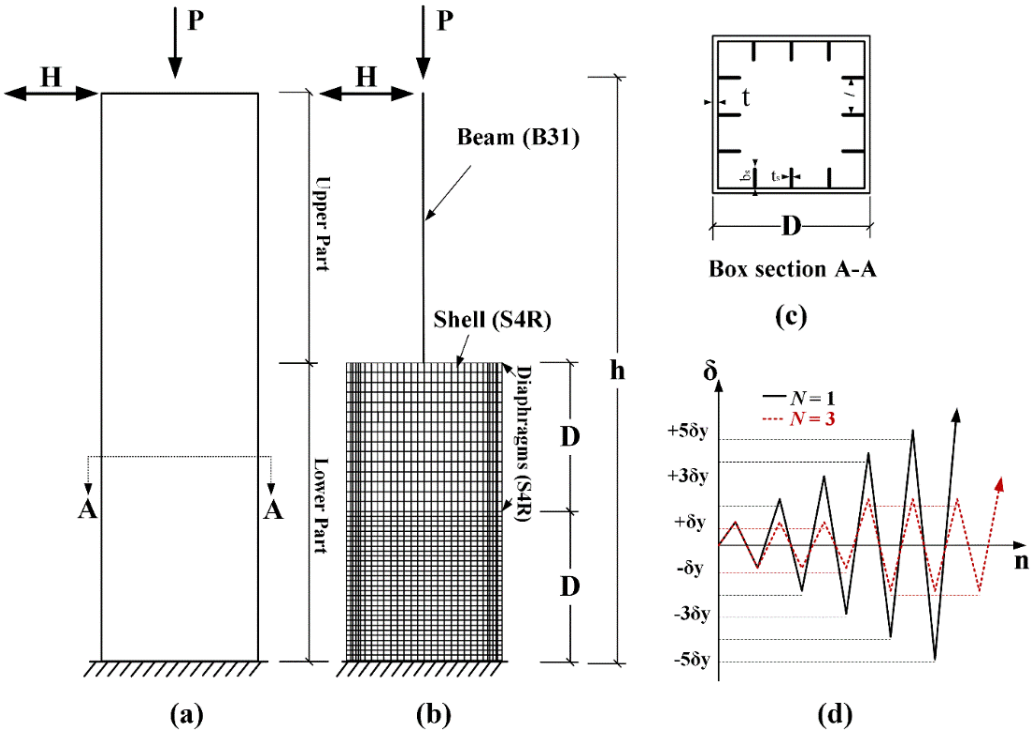


Fig. 3.1. B Column Model: (a) Column; (b) FE Meshing; (c) Cross Section; and (d) Loading Program.

### 3.3 Proposed Thin-Walled Steel Column with Graded Thickness

Under combined axial force and unidirectional cyclic lateral loading, B columns experience premature buckling, whether in terms of local buckling or overall buckling near the base of the column in a range that is equal to the side width of the square box section (*D*) (Nishikawa et al., 1998a; Tang et al., 2016b; Usami, 1996). This buckling detracts from B columns' strength and ductility capacities. To overcome these limitations, thin-walled steel stiffened square box columns with graded thickness (denoted as GB in the subsequent text) are proposed as

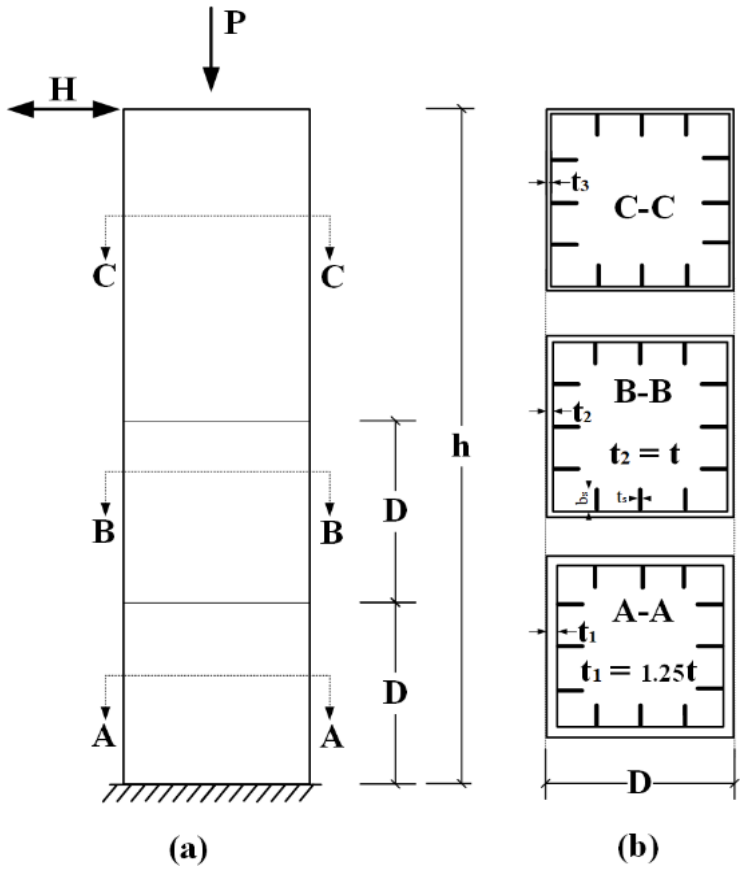


Fig. 3.2. GB Column Model: (a) Column, and (b) Graded-thickness Sections.

alternatives for the uniform thin-walled steel stiffened square box columns (B). The height and sides of the column are kept the same for both B and GB columns. The GB column is divided into three segments of constant cross sections along its longitudinal axis. The height of the first and second segments is equal to the sides of the square box section ($D$). The third segment has a height of ($h$-$2D$). As shown in Fig. 3.2, a thicker cross section ($t_1$=1.25$t$) is used along the first segment, and the original thickness ($t_2$= $t$; thickness of B column) is retained for the second segment. Finally, the remaining material volume is distributed on the third segment with $t_3$. The above configurations of the GB column are chosen based on which achieves favorable behavior by eliminating local buckling near the base of the column. Table 3.1 shows the material and

geometrical properties of the B and GB columns. As noted, the same material and geometrical properties (except for the plate thickness), element type, mesh size, boundary conditions, and loading protocol are used for both B and GB columns.

### 3.4 Numerical Results and Discussion

In this section, the computed lateral load vs. lateral displacement hysteresis curve of the tested column (B1 column), obtained using a commercial finite element software, Abaqus/standards version 6.14 (Hibbit et al., 2014a) is presented. The accuracy of the employed FEM has been substantiated using the experimental results that were obtained by the Public Works Research Institute (PWRI) of Japan (Nishikawa et al., 1998b).

#### 3.4.1 Comparison of Numerical and Experimental Results

Fig. 3.3 compares the normalized lateral load vs. lateral displacement hysteresis curves of the B1 column obtained from the FE analysis and experiment (Nishikawa et al., 1998b), under the one-unidirectional cycle lateral displacement history (see Fig. 3.1d). The solid line denotes the numerical results, while the dashed line stands for the experimental results. In this figure, $H_y$ and $\delta_y$ denote the lateral yield load and yield displacement, respectively. As seen in Fig. 3.3, the comparison shows a relatively good match with the experimental results. The FEM predicts the ultimate strength of the B1 column with less than 5% error (FEM: $H_{max}/H_y$ = 1.33, Experiment: $H_{max}/H_y$ = 1.40). This indicates that FE analysis, using the kinematic hardening material model, could reasonably capture the structural behavior of thin-walled steel stiffened square box columns with regard to local buckling.

Table 3.1. Material and Geometrical Properties of Analyzed B and GB Columns.

| B Columns | | | | | | GB Columns | | | | | | | | |
|---|---|---|---|---|---|---|---|---|---|---|---|---|---|---|
| Column | $h$(mm) | $t$(mm) | $R_f$ | $\lambda$ | $P/P_y$ | Column | $h$(mm) | $t$ (mm) | | | $R_f$ | $\lambda$ | $P/P_y$ |
| | | | | | | | | $t_1$ | $t_2$ | $t_3$ | | | |
| **B1 -tested** | 3403 | 9.00 | 0.56 | 0.26 | 0.122 | **GB1** | 3403 | 11.25 | 9.00 | 7.75 | 0.56 | 0.26 | 0.122 |
| **B2** | 3403 | 11.00 | 0.46 | 0.26 | 0.122 | **GB2** | 3403 | 13.75 | 11.00 | 9.46 | 0.46 | 0.26 | 0.122 |
| **B3** | 3403 | 14.00 | 0.36 | 0.26 | 0.122 | **GB3** | 3403 | 17.50 | 14.00 | 12.00 | 0.36 | 0.26 | 0.122 |
| **B4** | 3403 | 16.90 | 0.30 | 0.26 | 0.122 | **GB4** | 3403 | 21.14 | 16.90 | 14.55 | 0.30 | 0.26 | 0.122 |
| **B5** | 3403 | 19.50 | 0.26 | 0.26 | 0.122 | **GB5** | 3403 | 24.40 | 19.50 | 16.80 | 0.26 | 0.26 | 0.122 |
| **B5-10** | 3403 | 19.50 | 0.26 | 0.26 | 0.100 | **GB5-10** | 3403 | 24.40 | 19.50 | 16.80 | 0.26 | 0.26 | 0.100 |
| **B5-15** | 3403 | 19.50 | 0.26 | 0.26 | 0.150 | **GB5-15** | 3403 | 24.40 | 19.50 | 16.80 | 0.26 | 0.26 | 0.150 |
| **B5-20** | 3403 | 19.50 | 0.26 | 0.26 | 0.200 | **GB5-20** | 3403 | 24.40 | 19.50 | 16.80 | 0.26 | 0.26 | 0.200 |
| **B5-30** | 3403 | 19.50 | 0.26 | 0.26 | 0.300 | **GB5-30** | 3403 | 24.40 | 19.50 | 16.80 | 0.26 | 0.26 | 0.300 |
| **B6** | 3920 | 9.00 | 0.56 | 0.30 | 0.122 | **GB6** | 3920 | 11.25 | 9.00 | 8.00 | 0.56 | 0.30 | 0.122 |
| **B7** | 3920 | 11.00 | 0.46 | 0.30 | 0.122 | **GB7** | 3920 | 13.00 | 11.00 | 9.36 | 0.46 | 0.30 | 0.122 |
| **B8** | 3920 | 14.00 | 0.36 | 0.30 | 0.122 | **GB8** | 3920 | 16.25 | 14.00 | 11.65 | 0.36 | 0.30 | 0.122 |
| **B9** | 3920 | 16.90 | 0.30 | 0.30 | 0.122 | **GB9** | 3920 | 21.14 | 16.90 | 15.13 | 0.30 | 0.30 | 0.122 |
| **B10** | 3920 | 19.50 | 0.26 | 0.30 | 0.122 | **GB10** | 3920 | 16.25 | 19.50 | 11.65 | 0.26 | 0.30 | 0.122 |
| **B11** | 6530 | 9.00 | 0.56 | 0.50 | 0.122 | **GB11** | 6530 | 11.25 | 9.00 | 8.60 | 0.56 | 0.50 | 0.122 |
| **B12** | 6530 | 11.00 | 0.46 | 0.50 | 0.122 | **GB12** | 6530 | 13.00 | 11.00 | 9.96 | 0.46 | 0.50 | 0.122 |
| **B13** | 6530 | 14.00 | 0.36 | 0.50 | 0.122 | **GB13** | 6530 | 16.25 | 14.00 | 12.40 | 0.36 | 0.50 | 0.122 |
| **B14** | 6530 | 16.90 | 0.30 | 0.50 | 0.122 | **GB14** | 6530 | 21.14 | 16.90 | 16.11 | 0.30 | 0.50 | 0.122 |
| **B15** | 6530 | 19.50 | 0.26 | 0.50 | 0.122 | **GB15** | 6530 | 21.75 | 19.50 | 16.60 | 0.26 | 0.50 | 0.122 |

For all columns: Sides *(D)* = 900 mm, $t_s / b_s / l$ = *6/ 80/ 225 mm*. $\sigma_y$ = 378.6 MPa, $E$ = 206 GPa, and, $\nu$ = 0.3.
All columns are loaded with one-cycle at each displacement ($N$ = 1), except B3 and GB3 loaded with $N$ = 1 and 3.
$P_y = \sigma_y * A$, $A = (D^2 - D_i^2)$, $D_i = D - 2t$, $t$ = thickness for the B column.
$I$ = moment of inertia = $(D^4 - D_i^4)/12$ (Include the stiffeners), $S$ = elastic section modulus = $(D^4 - D_i^4)/6\ D$.

### 3.4.1.1 Buckling Mode of B1 Column

At the end of the FE analysis, the buckling shape of the column B1 (Fig. 3.4b) is captured and compared to the buckling shape from the experiment (Fig. 3.4a) (Chen, W. F. and Duan, 2014). In the experiment, the flange suffered from inward local buckling while the web buckled outward above the base of the column. This buckling mode is due to the fact that right angle between the web and flange keeps unchanged due to rigid connection between them (Mamaghani, 1996). The buckling shape is predicted relatively well by the adopted FEM. However, the outward buckling

of the web in the analysis is not as prominent as in the experiment. Similar findings have been reported in other studies (Goto et al., 1998; Shen et al., 1995; Ucak and Tsopelas, 2006).

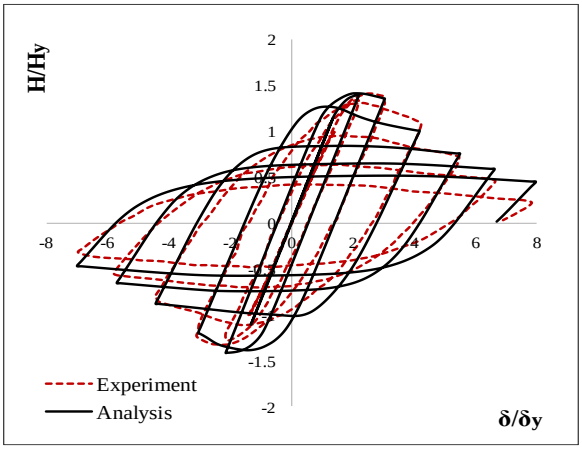


Fig. 3.3. Hysteretic Behavior of Analysis and Experiment of the B1 column.

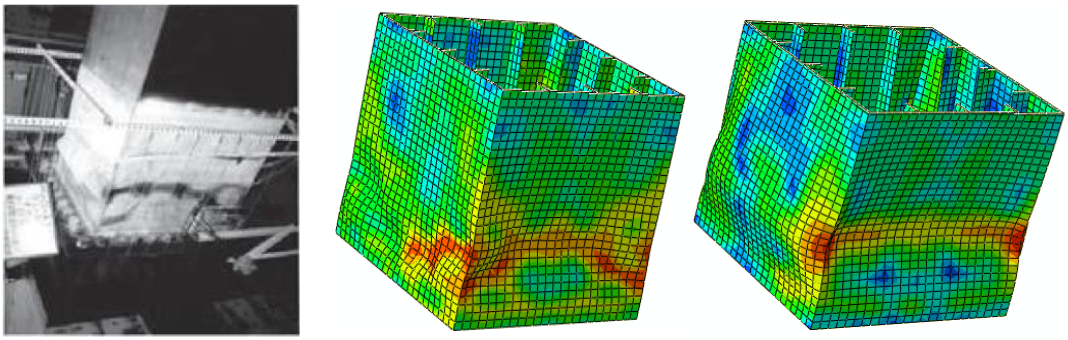

(a) Experiment (Frangopol and Saydam, 2014) (b) B1 Column (c) GB1 Column

Fig. 3.4. Buckling Deformation of Columns.

### 3.4.2 Hysteresis Behavior of B and GB Columns

To investigate the differences between the hysteretic behavior of B and GB columns under the same axial force and unidirectional cyclic lateral loading, a numerical study is conducted using the

validated FEM. The normalized lateral load vs. lateral displacement hysteresis curves of the B and GB columns are shown in Fig. 3.5. In this figure, a significant increase in both ultimate strength and ductility is noticed when the GB columns are used. Moreover, the post-buckling of the GB columns is improved as compared to their B column counterparts. For example, in the GB1 column (see Fig. 3.5a) with $R_f$ of 0.56 and λ of 0.26, the normalized ultimate strength (i.e., $H_{max}/H_y$) is 1.65 and the corresponding normalized maximum displacement (i.e., $\delta_m/\delta_y$) occurs at 3 which are greater than the B1 column by 24% and 32%, respectively. In the case of the B1 column, the buckling starts when the displacement is between $2\delta_y$ and $3\delta_y$. A drop of 36% of the ultimate strength (i.e., $H_{max}/H_y$ = 1.33 observed at $\delta = +2.28\delta_y$) occurs at $\delta = +4\delta_y$. As the displacement increases, the column strength decreases at a fast rate to 14% of its maximum strength by the end of the analysis. By contrast, the GB1 column shows its $H_{max}/H_y$ at $\delta = +3\delta_y$, which indicates that the local buckling occurs between $3\delta_y$ and $4\delta_y$. Only a 9% drop of the $H_{max}/H_y$ takes place at $\delta = +4\delta_y$, while the residual strength of the GB1 column is 25% of its $H_{max}/H_y$ at $\delta = +8\delta_y$. This comparison shows the superiority of the GB columns and implies that the local buckling is delayed in the GB columns as compared to the B columns. A similar trend is apparent in all the other analyzed B and GB columns, as shown in Fig. 3.5(b-j). The buckled shape of the GB1 column (see Fig. 3.4c) is compared to the column B1 (see Fig. 3.4b) at the end of the analysis. The GB1 column suffers less severe local buckling in the flange and the web as compared to its counterpart B1 column. A similar buckling is observed for all the other analyzed B and GB columns.

### 3.5 Parametric Study

Based on the validated FEM, a comprehensive parametric study is carried out to provide insight into the effect of key design parameters on the strength, ductility, and energy absorption capacity

of the B and GB columns. A total of 40 columns, including one tested column (B1 column), are analyzed. The main studied parameters that are commonly considered in the practical design and that affect the overall behavior of the thin-walled steel stiffened square box columns are: the width-to-thickness ratio parameter ($R_f$) with a range of (0.26 – 0.56), the column slenderness ratio parameter ($\lambda$) varying from 0.26 to 0.5, the axial load ratio ($P/P_y$), where five different ratios (i.e. $P/P_y$ = 0.1, 0.122, 0.15, 0.20, and, 0.3) are applied on the B5 and GB5 columns, and the number of loading cycles at each displacement amplitude ($N$). To study the effect of the loading cycle numbers ($N$), all the columns are analyzed under one-cycle displacement ($N$ = 1), except the B3 and GB3 columns, which have been analyzed under one ($N$ = 1), and three ($N$ = 3) displacement cycles. The ranges of the studied parameters are selected as they are commonly used by the researchers (Ucak and Tsopelas, 2006; Usami et al., 2000b). Additionally, in the practical design, $0.3 \leq R_f \leq 0.5$ and $0.2 \leq \lambda \leq 0.5$ are generally used for bridge piers with square box cross sections (Chen, W. F. and Duan, 2014). For thin-walled steel stiffened square box columns, diaphragms are usually installed at an interval smaller than the pier width ($D$), $\alpha = a/D \leq 1.0$, where $a$ is the distance between diaphragms (Chen, W. F. and Duan, 2014). There is no limitation in $n$. However, $n$ = 4-6 is usually used. The columns listed in Table 3.1 assumed to be made of carbon steel SM490 (JIS, 2012) (equivalent to ASTM A242 (ASTM, 2018)) as the tested column (B1).

### 3.5.1 Effect of Width-to-Thickness Ratio Parameter ($R_f$)

The effect of the width-to-thickness ratio parameter ($R_f$) on the strength and ductility of the B and GB columns is studied. The increase in $R_f$ might be either due to an increase in the sides of the column or a decrease in the thickness. In this chapter, all columns are analyzed by keeping the sides of the column constant and changing the thickness. Fig. 3.6 shows the envelope curves for different values of $R_f$ for both B and GB columns. The results indicate that by decreasing $R_f$ and

keeping all other parameters unchanged, the ultimate strength and ductility of both B and GB columns are increased. For example, the B10 column has slightly higher energy absorption and ductility capacity than that of the B6 column, although, the improvements to the $H_{max}/H_y$ and $\delta_m/\delta_y$

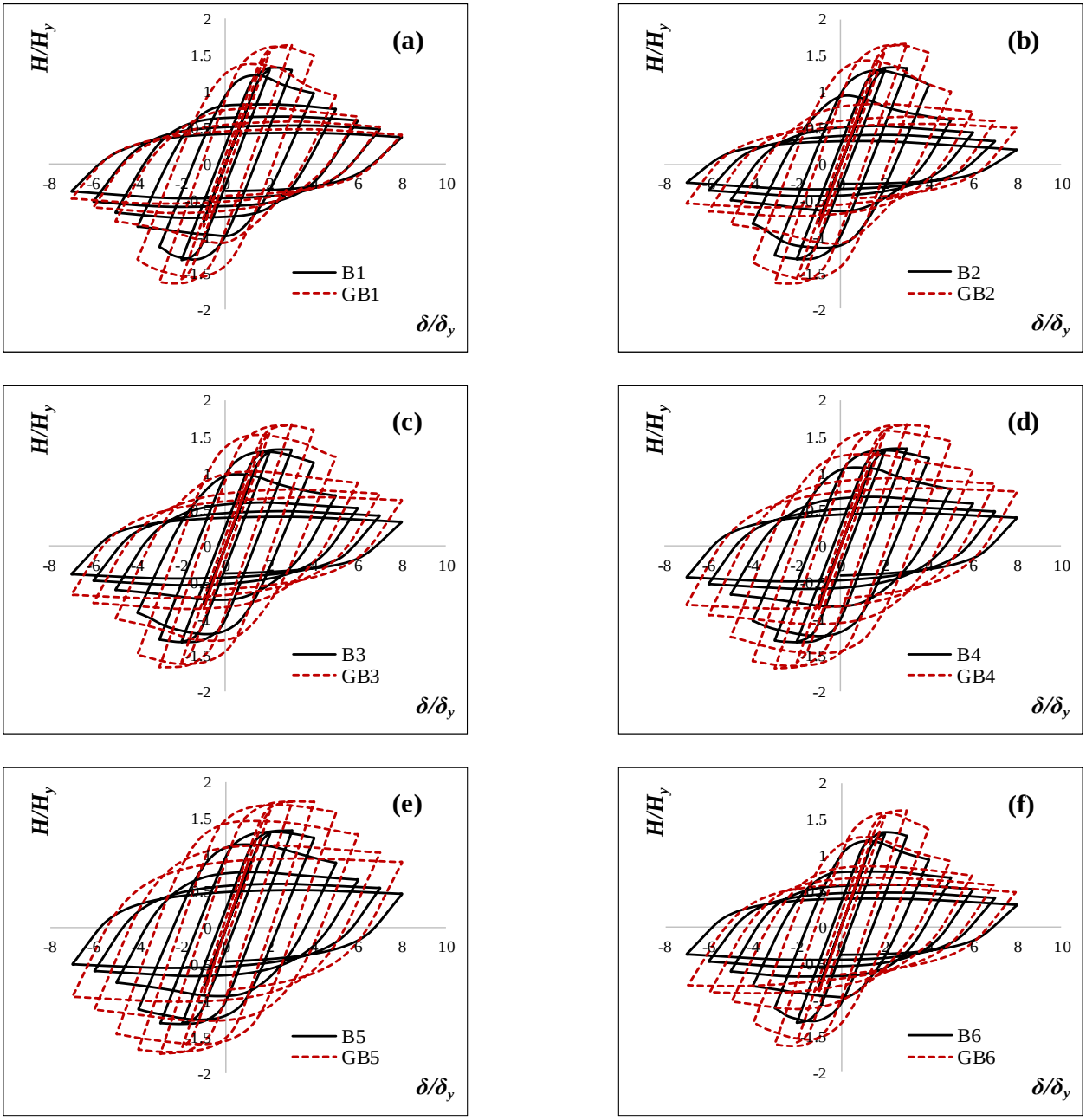


Fig. 3.5. Hysteretic Behavior: (a) B1 & GB1, (b) B2 & GB2, (c) B3 & GB3, (d) B4 & GB4, (e) B5 & GB5, (f) B6 & GB6, (g) B7 & GB7, (h) B8 & GB8, (i) B9 & GB9, and (h) B10 & GB10.

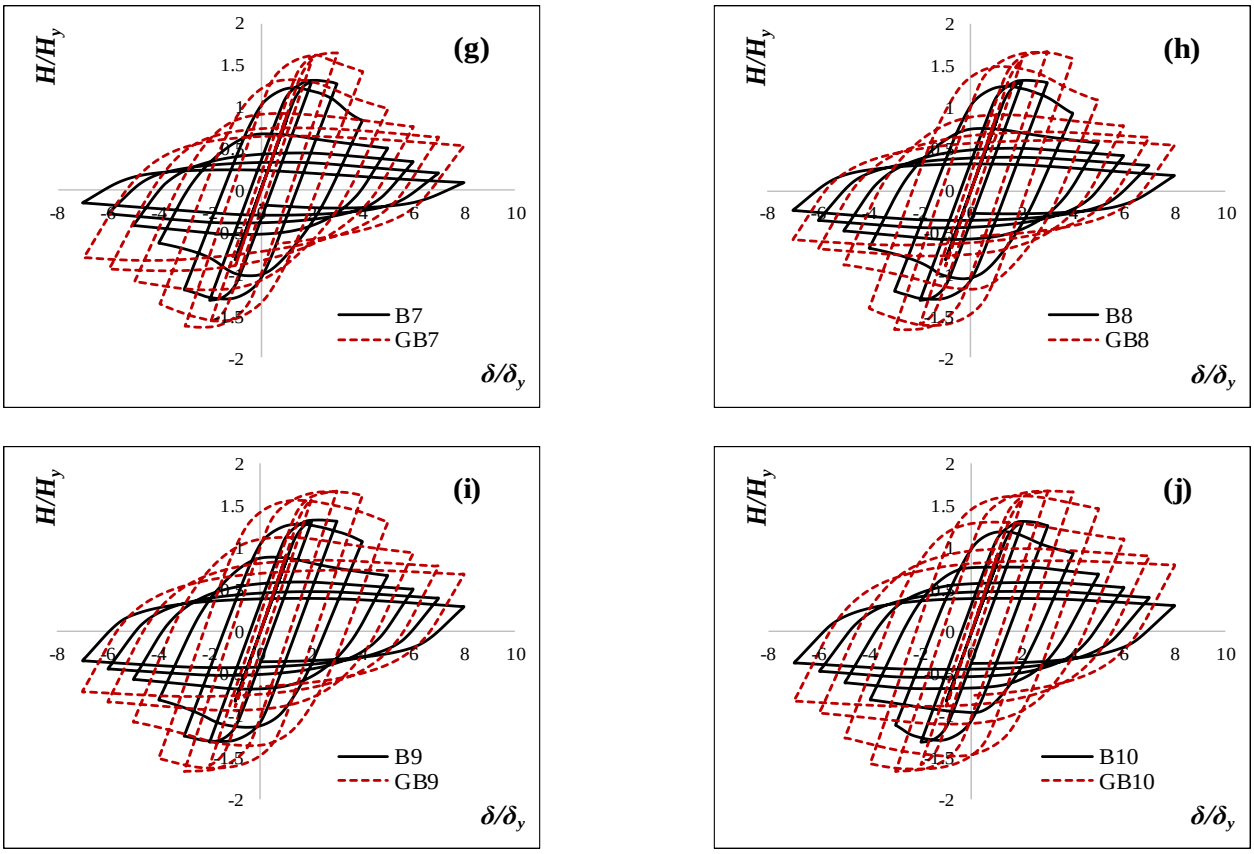


Fig. 4.5. Continued.

are not substantial when $R_f$ decreases from 0.56 to 0.26 (see Fig. 3.6b). A similar trend is noticed in the cases of the GB10 and GB6 columns, as shown in Fig. 3.6d. In addition, the slope of the post-buckling curve becomes less steep as $R_f$ decreases. After the peak, the strength drops twice as fast as the GB1 column (at an average of 40%) and B1 column (at an average of 48%) compared to the GB5 column (at an average of 18%) and B5 column (at an average of 24%). In other words, columns with smaller $R_f$ values absorb more energy and experience higher ductility than those with larger $R_f$ values.

### 3.5.2 Effect of Slenderness Ratio Parameter (λ)

The effect of the slenderness ratio parameter (λ) on the strength and ductility of the B and GB columns is shown in Fig. 3.7. Both ultimate strength and ductility are increased as λ gets smaller in both B and GB columns. For example, when λ decreases from 0.5 in the B15 column to 0.26 in the B5 column, the $H_{max}/H_y$ and $\delta_m/\delta_y$ are increased by 6.25% and 72%, respectively (see Fig. 3.7b). In the case of GB columns, a similar tendency is apparent when λ decreases from 0.5 in the case of the GB15 column to 0.26 in the GB5 column (see Fig. 3.7d).

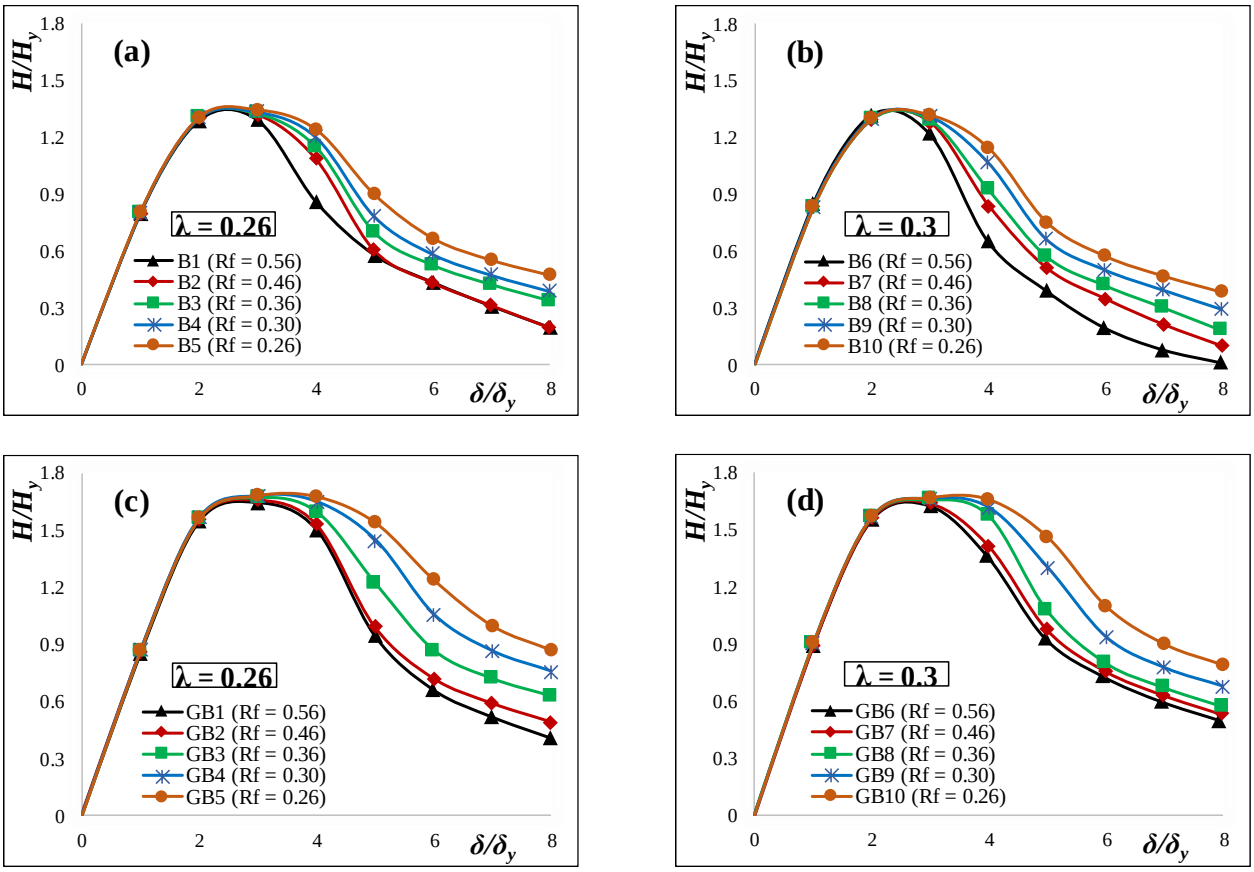


Fig. 3.6. Effect of $R_f$ parameter: (a) B columns with λ = 0.26, (b) B columns with λ = 0.3, (c) GB columns with λ = 0.26, and (d) GB columns with λ = 0.3.

The $H_{max}/H_y$ and $\delta_m/\delta_y$ are increased by 16% and 67%, respectively. In addition, the area surrounded by the envelope curve decreases, and the slope of the post-buckling curve becomes steeper after the peak as λ gets higher, especially, in the case of λ = 0.5. In other words, the strength drops at a very fast rate in average of 166% and 120% for the B13 and GB13 columns, respectively, after the peak. In the case of λ = 0.5 both columns have zero-strength capacity at about $\delta = +6\delta_y$ as noticed in Fig. 3.7. On the other hand, in the case of λ = 0.26, less of a strength drop occurs. The strength of the B3 and GB3 columns drops at an average of 33% and 22%, respectively. The reason is attributed to the *P-Δ* effect in the case of the long columns (Gao et al., 1998a).

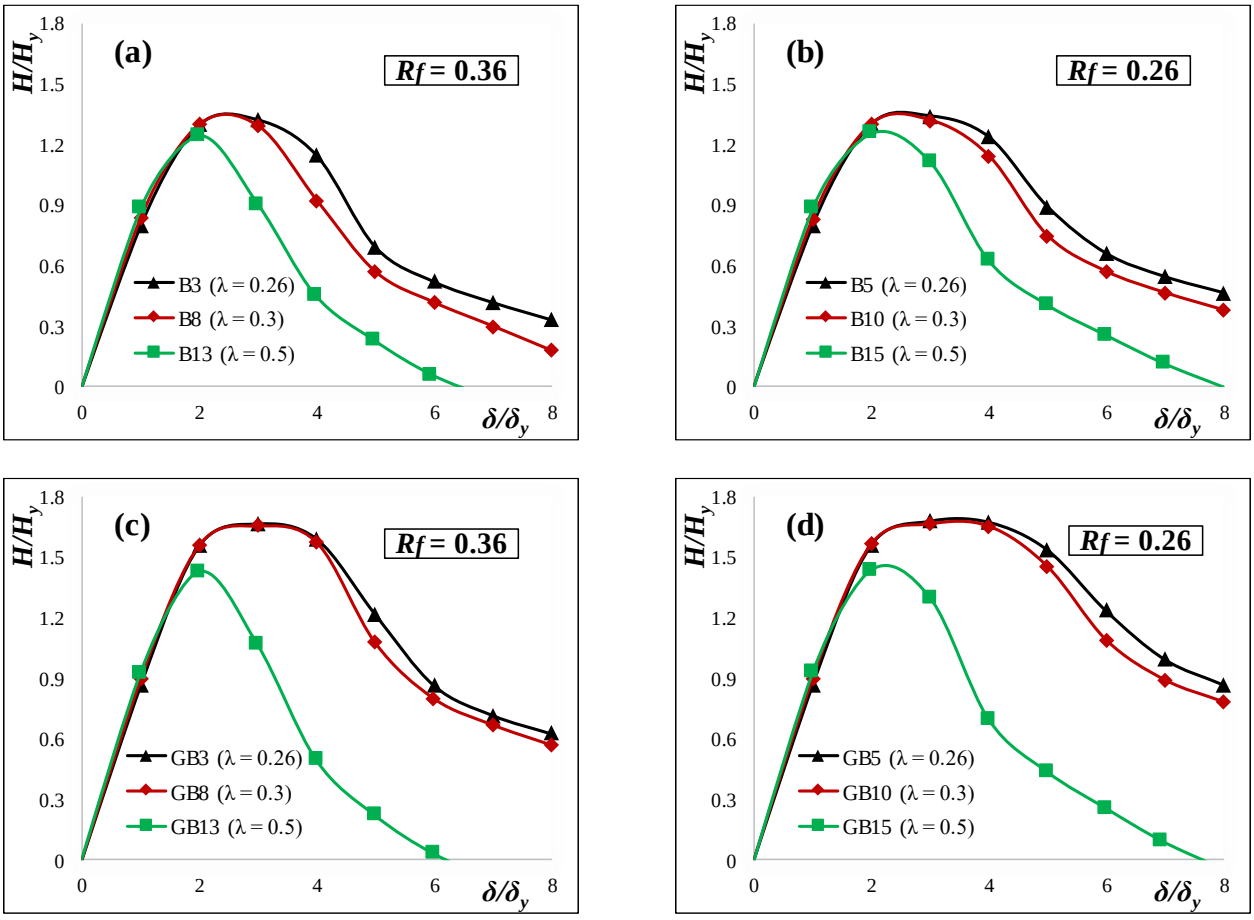


Fig. 3.7. Effect of λ parameter: (a) B columns with $R_f$ = 0.36, (b) B columns with $R_f$ = 0.26, (c) GB columns with $R_f$ = 0.36, and (d) GB columns with $R_f$ = 0.26.

### 3.5.3 Effect of Axial Load ($P/P_y$)

The effect of the axial load on the ultimate strength and ductility of the B and GB columns is investigated. Five of the B5 columns (B5-10, B5-12.2, B5-15, B5-20, and B5-30) and five of the GB5 columns (GB5-10, GB5-12.2, GB5-15, GB5-20, and GB5-30) are analyzed under different axial loads, where the number after the hyphen refers to the applied axial load ratio (i.e., $P/P_y$ = 0.1, 0.122, 0.15, 0.2, and 0.3, respectively). The envelope curves of the lateral load ($H/H_{y0}$) vs. lateral displacement ($\delta/\delta_{y0}$) are normalized by $H_{y0}$ and $\delta_{y0}$ to highlight the influence of the axial load, as shown in Fig. 3.8. $H_{y0}$ and $\delta_{y0}$ denote the lateral yield load and the yield displacement under zero axial load, respectively. As the axial load increases, the $H_{max}/H_{y0}$ decreases due to the $P$-$\Delta$ effect in the case of large axial loads (Gao et al., 1998a; Usami et al., 2000b). For example, the $H_{max}/H_{y0}$ is decreased by 14.5% and 8.6% in the cases of the B5 and GB5 columns, respectively, when $P/P_y$ increases from 10% to 30%. Moreover, in the cases of B5-30 and GB5-30 columns, the slope of the post-buckling curve becomes steeper, when the columns absorb less energy under the cyclic load. When $P/P_y$ = 0.3, the post-buckling slope of the B5-30 and GB5-30 columns decreases at an average of 76% and 47%, respectively, in each loading step. The slope of the B5-10 and GB5-10 columns decreases by 20% and 12%, respectively. In Fig. 3.8a, it should be noted that the B5-30 column reaches a zero-strength capacity level around $\delta = +5\delta_{y0}$, while the GB5-30 column can sustain more lateral load at the same displacement level.

### 3.5.4 Effect of Number of Loading Cycles ($N$)

Fig. 3.9 shows the comparison of the computed envelope curves of the B3 (Fig. 3.9a) and GB3 (Fig. 3.9b) columns in the cases of one ($N$ = 1) and three ($N$ = 3) loading cycles at each lateral displacement amplitude.

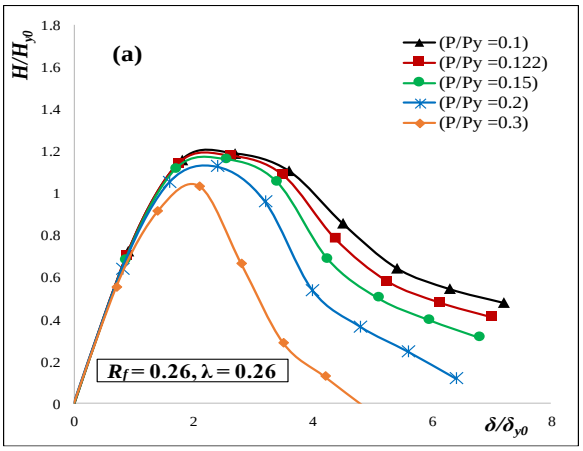


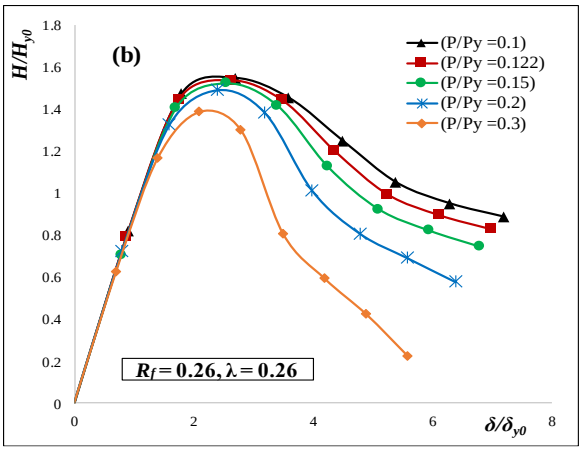


(a) B5 Column (b) GB5 Column

Fig. 3.8. Envelope Curves with Different Axial Load.

In the B3 column, it is noted that when the displacement is greater than $2\delta_y$, larger damage is observed, and the strength decreases rapidly in the case of $N = 3$ as compared to $N = 1$. By contrast, the strength starts to decrease at a fast rate approximately at $3\delta_y$ in the case of the GB3 column. The slope of the post-buckling curve is steeper in the case of $N = 3$ than that for $N = 1$ when the lateral displacement is greater than $2\delta_y$ (B3 column) and $3\delta_y$ (GB3 column). It should be emphasized that the deterioration in the GB3 column is considerably less than the B3 column under $N = 3$. For example, B3 and GB3 slopes decrease, respectively, at an average of 27% and 19% in the case of $N = 1$, while, the slopes decrease at average of 123% and 25% in the case of $N = 3$. On the other hand, no remarkable effect is noticed when $\delta$ is less than $2\delta_y$ (B3 column) and $3\delta_y$ (GB3 column) which might be due to small plastic deformation.

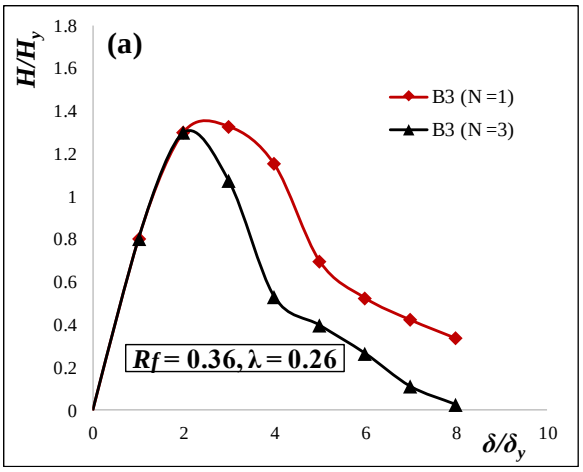


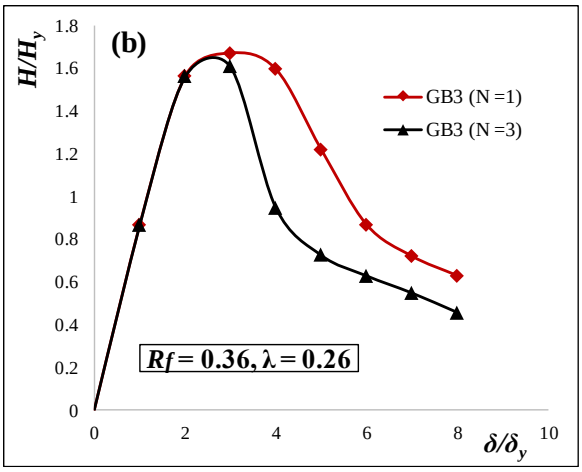


(a) B3 Column (b) GB3 Column

Fig. 3.9. Effect of *N* on Strength and Ductility.

Table 3.2. Strength and Ductility Evaluation of B and GB Columns.

| B Columns | | | | | | GB Columns | | | | | |
|---|---|---|---|---|---|---|---|---|---|---|---|
| **Column** | $H_y$ **(KN)** | $\delta_y$ **(mm)** | $H_{max}/H_y$ | $\delta_m/\delta_y$ | $\delta_{0.9}/\delta_y$ | **Column** | $H_y$ **(KN)** | $\delta_y$ **(mm)** | $H_{max}/H_y$ | $\delta_m/\delta_y$ | $\delta_{0.9}/\delta_y$ |
| **B1 -tested** | 1039 | 13.80 | 1.328 | 2.28 | 3.30 | **GB1** | 1039 | 13.80 | 1.644 | 3.00 | 4.04 |
| **B2** | 1240 | 13.80 | 1.331 | 2.34 | 3.51 | **GB2** | 1240 | 13.80 | 1.655 | 3.00 | 4.07 |
| **B3** | 1529 | 13.80 | 1.332 | 2.40 | 3.72 | **GB3** | 1529 | 13.80 | 1.669 | 3.00 | 4.25 |
| **B4** | 1804 | 13.8 | 1.338 | 2.64 | 3.98 | **GB4** | 1804 | 13.8 | 1.678 | 3.00 | 4.67 |
| **B5** | 2044 | 13.80 | 1.342 | 2.88 | 4.09 | **GB5** | 2044 | 13.80 | 1.683 | 3.20 | 5.08 |
| **B5-10** | 2095 | 14.19 | 1.319 | 2.88 | 4.14 | **GB5-10** | 2095 | 14.19 | 1.653 | 3.00 | 5.13 |
| **B5-15** | 1979 | 13.40 | 1.369 | 2.70 | 4.02 | **GB5-15** | 1979 | 13.40 | 1.726 | 3.20 | 5.02 |
| **B5-20** | 1862 | 12.61 | 1.411 | 2.58 | 3.67 | **GB5-20** | 1862 | 12.61 | 1.808 | 3.36 | 4.87 |
| **B5-30** | 1630 | 11.00 | 1.482 | 2.58 | 3.27 | **GB5-30** | 1630 | 11.00 | 1.958 | 3.28 | 4.42 |
| **B6** | 906 | 18.37 | 1.315 | 2.04 | 3.20 | **GB6** | 906 | 18.37 | 1.627 | 2.82 | 3.59 |
| **B7** | 1076 | 18.37 | 1.319 | 2.16 | 3.24 | **GB7** | 1076 | 18.37 | 1.639 | 2.82 | 3.72 |
| **B8** | 1327 | 18.37 | 1.321 | 2.22 | 3.28 | **GB8** | 1327 | 18.37 | 1.657 | 3.00 | 4.17 |
| **B9** | 1566 | 18.37 | 1.324 | 2.28 | 3.44 | **GB9** | 1566 | 18.37 | 1.663 | 3.00 | 4.37 |
| **B10** | 1774 | 18.37 | 1.327 | 2.46 | 3.71 | **GB10** | 1774 | 18.37 | 1.669 | 3.04 | 4.77 |
| **B11** | 544 | 50.97 | 1.240 | 1.58 | 2.26 | **GB11** | 544 | 50.97 | 1.436 | 1.86 | 2.44 |
| **B12** | 646 | 50.97 | 1.243 | 1.60 | 2.29 | **GB12** | 646 | 50.97 | 1.441 | 1.88 | 2.42 |
| **B13** | 797 | 50.97 | 1.248 | 1.62 | 2.35 | **GB13** | 797 | 50.97 | 1.444 | 1.9 | 2.36 |
| **B14** | 940 | 50.97 | 1.256 | 1.62 | 2.59 | **GB14** | 940 | 50.97 | 1.455 | 1.92 | 2.89 |
| **B15** | 1065 | 50.97 | 1.263 | 1.68 | 2.86 | **GB15** | 1065 | 50.97 | 1.456 | 1.92 | 2.91 |

### 3.6 Strength and Ductility Evaluation of B and GB Columns

Table 3.2 shows the computed ultimate strength from the lateral load vs. lateral displacement curves of the analyzed columns. For both B and GB columns, the $H_{max}/H_y$ vs. $(1+P/P_y)\ R_f\ \lambda$ relationship is plotted taking into account the axial load ($P/P_y$) effect as shown in Fig. 3.10. The proposed formulae that fit the computed ultimate strength of the analyzed B and GB columns are as follows:

$$\frac{H_{\max}}{H_y} = \frac{1.126}{\left[(1+\frac{P}{P_y})R_f\lambda\right]^{0.076}} \qquad \text{B Columns} \qquad (3.5)$$

$$\frac{H_{\max}}{H_y} = \frac{1.185}{\left[(1+\frac{P}{P_y})R_f\lambda\right]^{0.15}} \qquad \text{GB Columns} \qquad (3.6)$$

Based on Fig. 3.10, the ultimate strength is improved if $R_f$ decreases under constant λ. Similarly, the ultimate strength increases if λ decreases with constant $R_f$. The failure of thin-walled steel columns is considered to have occurred when the displacement equals either $\delta_m$ or $\delta_{0.9}$. $\delta_m$ is the displacement corresponding to the ultimate strength, where $\delta_{0.9}$ is defined as the displacement point where the strength drops to 90% of its ultimate value after the peak (Mamaghani et al., 2015, 1995; Shen et al., 1995; Usami, 1996). The $\delta_m/\delta_y$ and $\delta_{0.9}/\delta_y$ are key parameters used to evaluate the ductility performance for both B and GB columns. However, the $\delta_{0.9}/\delta_y$ parameter considers the cyclic characteristics and fully utilizes the strength of the steel at large plastic displacements. Moreover, the strength of thin-walled steel columns decreases significantly after the peak due to the influence of local buckling. Therefore, it is more reasonable to use the $\delta_{0.9}/\delta_y$ parameter to evaluate ductility (Gao et al., 1998a; Mamaghani et al., 2015; Usami et al., 2000b). Table 3.2

shows an increasing trend of the strength and ductility in both the B and GB columns as the $R_f$ and λ decrease. All $\delta_m/\delta_y$ and $\delta_{0.9}/\delta_y$ values of both B and GB columns are plotted vs. integrated $R_f$, λ and/or $P/P_y$, as shown in Fig. 3.11. The proposed formulae that fit the computed $\delta_m/\delta_y$ and $\delta_{0.9}/\delta_y$ values of the analyzed columns are as follows:

$$\frac{\delta_m}{\delta_y} = \frac{0.842}{(R_f \lambda)^{0.43}} \quad (3.7)$$

$$\frac{\delta_{0.9}}{\delta_y} = \frac{1.402}{\left[(1+\frac{P}{P_y})R_f \lambda\right]^{0.4}} \quad (3.8)$$

B Columns

$$\frac{\delta_m}{\delta_y} = \frac{1.031}{(R_f \lambda)^{0.425}} \quad (3.9)$$

$$\frac{\delta_{0.9}}{\delta_y} = \frac{1.144}{\left[(1+\frac{P}{P_y})R_f \lambda\right]^{0.575}} \quad (3.10)$$

GB Columns

As can be seen from Fig. 3.8, the axial load magnitude has a significant effect on the post-buckling of the B and GB columns. Therefore, the axial load influence is considered in the fitting of the ductility parameter $\delta_{0.9}/\delta_y$ as it appears in Eqs. (3.8) and (3.10). In contrast, the axial load has an insignificant effect on the maximum displacement of the B and GB columns. Thus, axial load influence is not included in the fitting of the $\delta_m/\delta_y$ parameter, as shown in Eqs. (3.7) and (3.9). The applicable restrictions of these formulae are: $0.26 \le R_f \le 0.56$, $0.26 \le \lambda \le 0.5$, $P/P_y \le 0.3$.

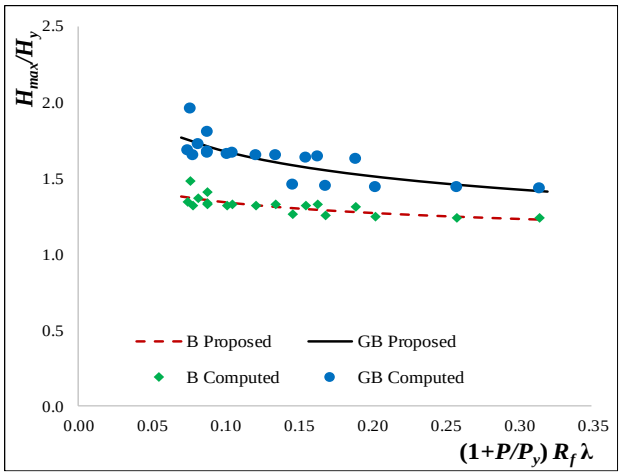


Fig. 3.10. Ultimate Strength of the B and GB Columns.

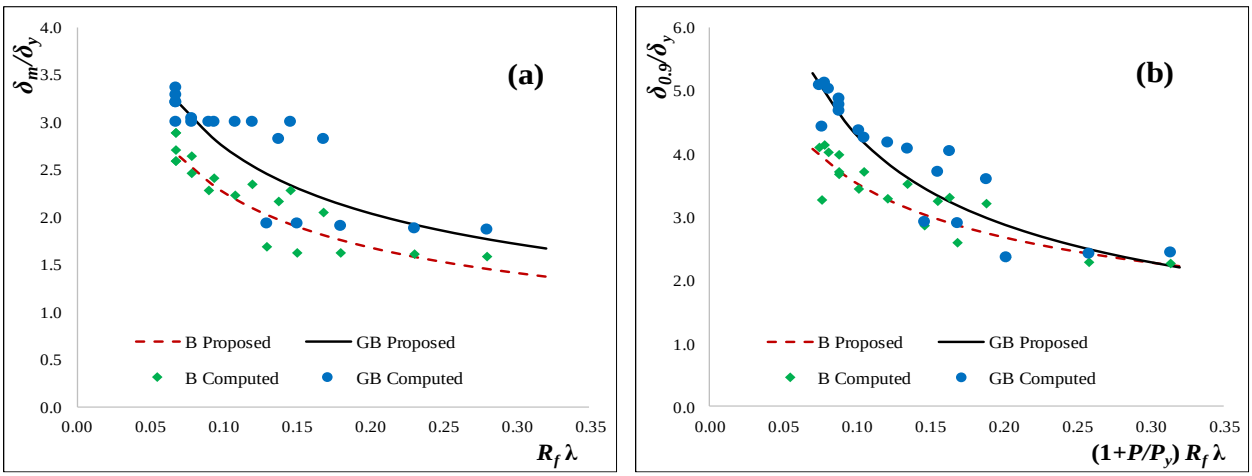


Fig. 3.11. Ductility Formulae for B and GB Columns: (a) $\delta_m/\delta_y$, and (b) $\delta_{0.9}/\delta_y$.

## 3.7 Summary

In this chapter, the cyclic behavior of thin-walled stiffened square box steel columns with uniform (B) and graded-thickness (GB) was investigated through FE analysis. GB columns were introduced to improve the behavior of B columns. The effect of the key design parameters, including the width-to-thickness ratio parameter ($R_f$), the slenderness ratio parameter (λ), the axial load

ratio($P/P_y$), and the number of cycles of loading ($N$) were studied. Based on this study, some important conclusions have been drawn, as follows:

- A satisfactory match between the analysis and experimental results confirms the ability of the FEM to capture the column behavior taking into account the local buckling of thin-walled stiffened square box steel columns under a constant axial force and unidirectional cyclic lateral displacement. The predicted ultimate strength of the B1 column obtained from the FEM differs with less than 5% error from the experimental results.
- Graded-thickness columns (GB) were introduced to improve the behavior of uniform thin-walled steel columns (B), which resulted in significant improvements in their strength, ductility, and post-buckling. Generally, an improvement of 25% in the ultimate strength was achieved using GB columns compared to B columns when $\lambda = 0.26$ and 0.3. In the case of $\lambda = 0.5$, the ultimate strength was improved by 16% in the GB columns as compared B columns.
- A comprehensive parametric study indicates that with the decrease of $R_f$ and $\lambda$, an increase was obtained in both ultimate strength and ductility capacities. Also, the ultimate strength decreased when the axial load was increased. This effect was more significant as the displacement increased beyond $3\delta_y$. Moreover, a significant strength deterioration occurred when loading cycles number ($N$) at each displacement level increased.
- Finally, a series of proposed formulae to predict the ultimate strength and ductility of the B and GB columns was provided. The proposed formulae are expected to be useful for the practical design of the thin-walled steel stiffened square box columns.

# CHAPTER 4 Circular Columns under Bidirectional Cyclic Lateral Loading

## 4.1 Introduction

This chapter aims to evaluate the hysteretic behavior of uniform (BC) and proposed graded-thickness (BGC) thin-walled steel tubular circular columns under a constant axial force and bidirectional cyclic lateral loading. To achieve this goal, a uniform thin-walled steel tubular circular column has been numerically analyzed under a constant axial force and circular bidirectional cyclic lateral loading. The accuracy of the adopted FEM has been substantiated based on the experimental results in the literature (Goto et al., 2006). Then, the proposed BGC column with size and volume of material equivalent to a BC column is investigated. The study results indicate that BGC columns show significant improvements in ultimate strength, ductility, and post-buckling compared to their counterpart BC columns, emphasizing the effect of the plate thickness and sectional configuration of the proposed BGC columns. The main reason for the improved overall hysteretic behavior of the BGC columns is their ability to mitigate and/or eliminate the local buckling that commonly occurs near the base of the column.

## 4.2 Numerical Model

FE analysis is carried out using the finite-element software ABAQUS/Standard version 6.14 where material and geometric nonlinearities are considered (Hibbit et al., 2014a). The accuracy of the employed FEM is validated in comparison with the experimental results (test PT3.5-1) available in the literature (Goto et al., 2006). $R_t$ and $\lambda$ are key design parameters in the practical design of thin-walled steel tubular circular columns, where $R_t$ affects the local buckling and $\lambda$ controls the global buckling (Al-Kaseasbeh and Mamaghani, 2018). $R_t$ and $\lambda$ of the column are defined as follows:

$$R_t = \frac{D}{2t}\frac{\sigma_y}{E}\sqrt{3(1-\nu^2)} \tag{4.1}$$

$$\lambda = \frac{2h}{r}\frac{1}{\pi}\sqrt{\frac{\sigma_y}{E}} \tag{4.2}$$

where $h$ = column height, $D$ = column diameter, $t$ = plate thickness, $r$ = radius of gyration of cross section, $\sigma_y$ = yield stress, $E$ = Young's modulus, and $\nu$ = Poisson's ratio. For the tested column (test PT3.5-1), $h$ = 1460 mm, $D$ = 258.2 mm, $t$ =3.5 mm, $r$ = 90 mm, $\sigma_y$ = 350 MPa, $E$ = 206 GPa, and $\nu$ = 0.3 (Goto et al., 2006). The analyzed cantilever column is assumed to be fixed at the base and subjected to a constant axial load ($P$) and circular bidirectional cyclic lateral displacement at the top, as shown in Fig. 4.1. The two-node beam element (B31) is employed for the upper part of the column, whereas the reduced integration four-node shell elements (S4R), which accurately consider the local buckling, are used for the lower part of the column.

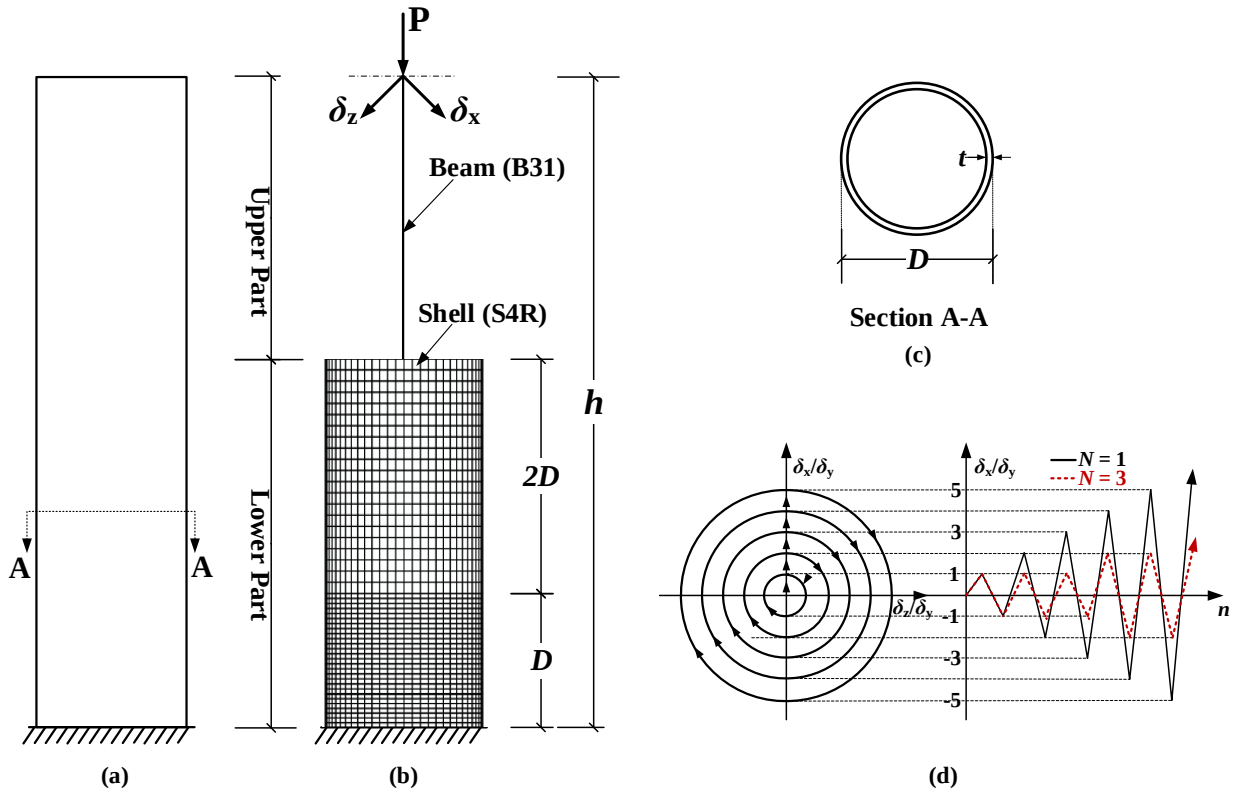


Fig. 4.1.Tested Column Model: (a) Column; (b) FE Meshing; (c) Cross Section; and (d) Loading Program.

All used elements are available in the Abaqus/Standard library. The interface between S4R and B31 elements is modeled using multi-point constraint (MPC). For computational efficiency, the bottom portion of the lower part (equal to the cross-section diameter, *D*), where the local buckling usually occurs, is divided into 27 S4R elements. The remaining height of the lower part (2*D*) is divided only in 21 S4R elements. 40 S4R elements are used in the circumferential direction in the lower part of the column. The upper part of the column (height of *h*-2*D*) is divided into B31 elements with size of 90 mm. The above-stated mesh sizes are determined by trial and error and found to give more efficient and reasonable results.

### 4.2.1 Bidirectional Cyclic Loading Protocol

Among different bidirectional loading paths, the displacement-controlled circular cyclic lateral loading is adopted as the most critical and severe loading program, illustrated in Fig. 4.1d (Goto et al., 2006; Ucak and Tsopelas, 2014). The adopted loading is quasi-statically applied to the top of the column with a constant axial load (*P*). The amplitude of the cyclic displacement is increased as a multiple of the yield displacement ($\delta_y$) which is defined by:

$$\delta_y = \frac{H_y h^3}{3EI} \tag{4.3}$$

$$H_y = \left( \sigma_y - \frac{P}{A} \right) \frac{S}{h} \tag{4.4}$$

where *A*, *I*, and *S* , respectively, are the cross-sectional area, moment of inertia, and elastic section modulus of the column (Al-Kaseasbeh and Mamaghani, 2018; Goto et al., 2006).

### 4.3 Comparison of Numerical and Experimental Results

The comparison of lateral load vs. lateral displacement hysteresis curves of the tested column, in both lateral X and Z directions obtained from the analysis are compared to the experimental results in the literature (Goto et al., 2006) and presented in Fig. 4.2.The solid line signifies the analysis results, while the dashed line denotes the experimental results. $H_y$ and $\delta_y$ are the lateral yield load and the yield displacement, respectively. In both X and Z directions, a relatively good agreement with the experimental results is noticed. The FEM predicts the ultimate strength of the column with 1.5% error in X direction (FEM: $H_{xmax}/H_y$ = 1.33, Experiment: $H_{xmax}/H_y$ = 1.35, see Fig. 4.2a) and 4% in Z direction (FEM: $H_{zmax}/H_y$ = 1.25, Experiment: $H_{zmax}/H_y$ = 1.30, see Fig. 4.2b). As the comparison results revealed, the FEM, using the kinematic hardening material model, is able to capture the structural behavior of thin-walled steel tubular circular columns with reasonable accuracy considering the local buckling under a constant axial load and circular bidirectional cyclic lateral loading. In terms of buckling, the buckling shape of the tested column (Goto et al., 2006) (see Fig. 4.3a) is compared to the FE buckling shape at the end of the analysis (see Fig. 4.3b). In both the experiment and FE analysis, the column bulged outward near the base and formed an elephant-foot-bulge buckling mode. As a result, the buckling shape is captured relatively well by the adopted FEM.

### 4.4 Review of Proposed Thin-Walled Steel Column with Graded Thickness

Authors have recently proposed and investigated the overall behavior of the graded-thickness thin-walled steel tubular circular column (called “graded-thickness” column and denoted as BGC in this study) to eliminate and delay the local buckling under constant axial load and unidirectional cyclic lateral loading (Al-Kaseasbeh and Mamaghani, 2018).

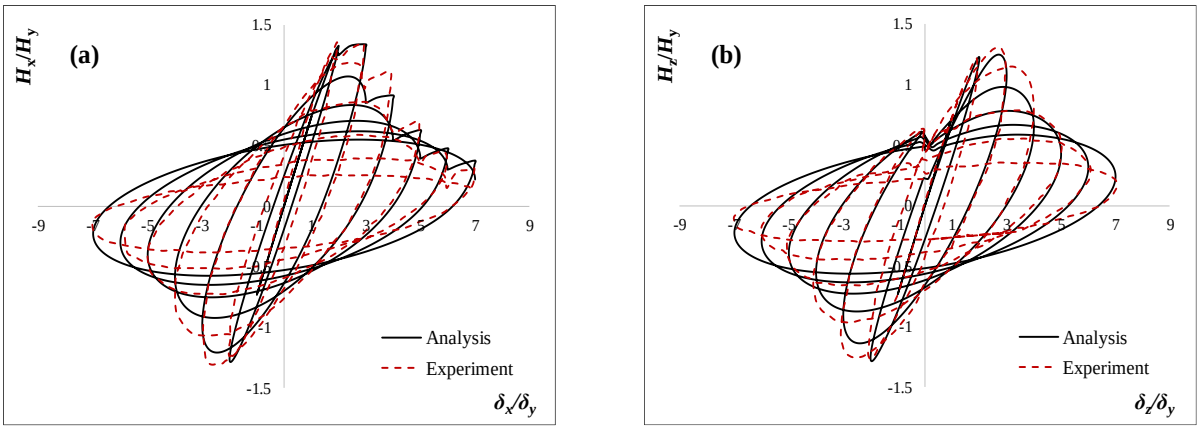


Fig. 4.2. Hysteretic Behavior of Analysis and Experiment of the Tested Column.

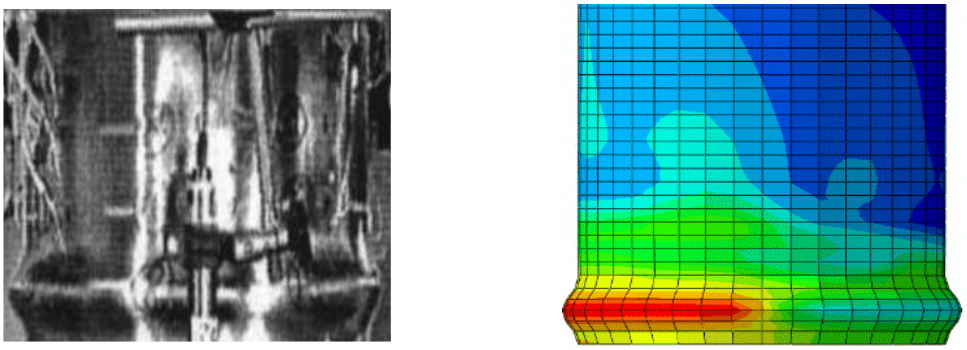

(a) Experiment (Goto et al., 2006)

(b) FE Analysis

Fig. 4.3. Buckling Deformation of Tested Column.

The proposed BGC column has a size and volume of material equivalent to a uniform column (denoted as BC). The BGC column has three segments of constant cross sections along its height. The first and second segments have the same height, a height that is equal to the diameter of BC column. The third segment has a height of ($h$-2$D$) where $h$ and $D$ are kept the same for both BC and BGC columns as shown in Fig. 4.4c. In the proposed BGC column (see Fig. 4.4d), the first and second segments have a thickness of 1.25$t$, and $t$, respectively, where $t$ is the thickness of the BC column. Finally, the thickness of the third segment, $t_3$, is calculated by equating the volume of material in both BC and BGC columns. The above configuration of the BGC column was chosen

based on failure pattern from the available test results in the literature (Usami, 1996). The material and geometrical properties of the BC and BGC columns are listed in Table 4.1. The same geometrical properties (except the plate thickness) are used for both type of BC and BGC columns, which are assumed to be made of the same carbon steel ASTM A36 (ASTM, 2014).

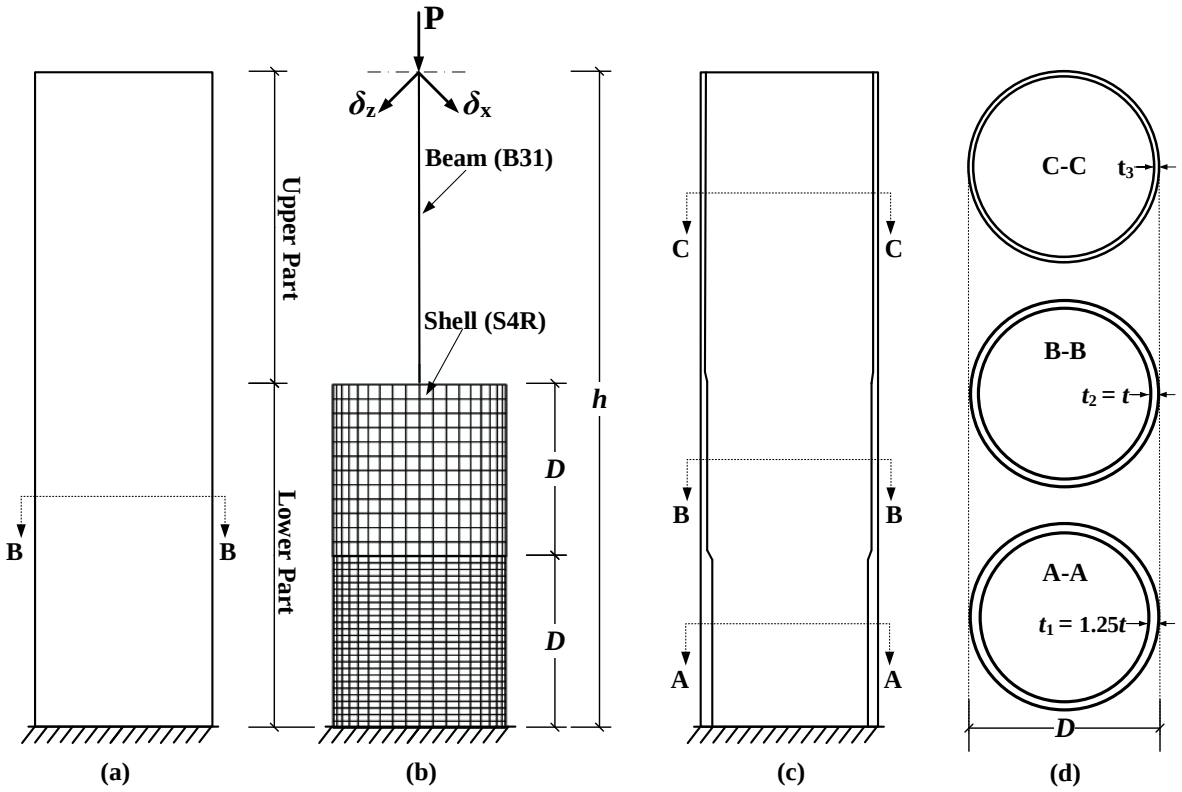


Fig. 4.4. (a) BC Column, (b) FE Meshing, (c) BGC Column, and (b) Graded-thickness Sections.

As shown in Fig. 4.4b, the same FEM details of the tested column, except the FE meshing, are used for both BC and BGC columns. For computational efficiency, the bottom half of the lower part (equal to the cross-section diameter, *D*) is divided into 26 S4R elements, while the remaining height (*D*) is only divided into 14 elements. In the circumferential direction of the lower part of the column, 40 S4R elements are used. The upper part of the column (height of *h*-2*D*) is divided into B31 elements with size of 90 mm.

Table 4.1. Material and Geometrical Properties of Analyzed BC and BGC Columns.

| BC Columns | | | | | | BGC Columns | | | | | | | | |
|---|---|---|---|---|---|---|---|---|---|---|---|---|---|---|
| Column | $h$(mm) | $t$(mm) | $R_t$ | $\lambda$ | $P/P_y$ | Column | $h$(mm) | $t$ (mm) | | | $R_t$ | $\lambda$ | $P/P_y$ |
| | | | | | | | | $t_1$ | $t_2$ | $t_3$ | | | |
| **BC1** | 3403 | 9.00 | 0.116 | 0.26 | 0.124 | **BGC1** | 3403 | 11.25 | 9.00 | 7.75 | 0.116 | 0.26 | 0.124 |
| **BC2** | 3403 | 10.45 | 0.100 | 0.26 | 0.124 | **BGC2** | 3403 | 13.00 | 10.45 | 9.00 | 0.100 | 0.26 | 0.124 |
| **BC3** | 3403 | 13.00 | 0.080 | 0.26 | 0.124 | **BGC3** | 3403 | 16.25 | 13.00 | 11.20 | 0.080 | 0.26 | 0.124 |
| **BC10** | 3403 | 17.40 | 0.060 | 0.26 | 0.124 | **BGC10** | 3403 | 21.75 | 17.40 | 15.00 | 0.060 | 0.26 | 0.124 |
| **BC11** | 3403 | 26.00 | 0.040 | 0.26 | 0.124 | **BGC11** | 3403 | 32.65 | 26.00 | 22.50 | 0.040 | 0.26 | 0.124 |
| **BC4** | 3960 | 9.00 | 0.116 | 0.30 | 0.124 | **BGC4** | 3960 | 11.25 | 9.00 | 8.00 | 0.116 | 0.30 | 0.124 |
| **BC5** | 3960 | 10.45 | 0.100 | 0.30 | 0.124 | **BGC5** | 3960 | 13.00 | 10.45 | 9.36 | 0.100 | 0.30 | 0.124 |
| **BC6** | 3960 | 13.00 | 0.080 | 0.30 | 0.124 | **BGC6** | 3960 | 16.25 | 13.00 | 11.65 | 0.080 | 0.30 | 0.124 |
| **BC6-10** | 3960 | 13.00 | 0.080 | 0.30 | 0.100 | **BGC6-10** | 3960 | 16.25 | 13.00 | 11.65 | 0.080 | 0.30 | 0.100 |
| **BC6-15** | 3960 | 13.00 | 0.080 | 0.30 | 0.150 | **BGC6-15** | 3960 | 16.25 | 13.00 | 11.65 | 0.080 | 0.30 | 0.150 |
| **BC6-20** | 3960 | 13.00 | 0.080 | 0.30 | 0.200 | **BGC6-20** | 3960 | 16.25 | 13.00 | 11.65 | 0.080 | 0.30 | 0.200 |
| **BC6-30** | 3960 | 13.00 | 0.080 | 0.30 | 0.300 | **BGC6-30** | 3960 | 16.25 | 13.00 | 11.65 | 0.080 | 0.30 | 0.300 |
| **BC12** | 3960 | 17.40 | 0.060 | 0.30 | 0.124 | **BGC12** | 3960 | 21.75 | 17.40 | 15.60 | 0.060 | 0.30 | 0.124 |
| **BC13** | 3960 | 26.00 | 0.040 | 0.30 | 0.124 | **BGC13** | 3960 | 32.65 | 26.00 | 23.40 | 0.040 | 0.30 | 0.124 |
| **BC7** | 6600 | 9.00 | 0.116 | 0.50 | 0.124 | **BGC7** | 6600 | 11.25 | 9.00 | 8.60 | 0.116 | 0.50 | 0.124 |
| **BC8** | 6600 | 10.45 | 0.100 | 0.50 | 0.124 | **BGC8** | 6600 | 13.00 | 10.45 | 9.96 | 0.100 | 0.50 | 0.124 |
| **BC9** | 6600 | 13.00 | 0.080 | 0.50 | 0.124 | **BGC9** | 6600 | 16.25 | 13.00 | 12.40 | 0.080 | 0.50 | 0.124 |
| **BC14** | 6600 | 17.40 | 0.060 | 0.50 | 0.124 | **BGC14** | 6600 | 21.75 | 17.40 | 16.60 | 0.060 | 0.50 | 0.124 |
| **BC15** | 6600 | 26.00 | 0.040 | 0.50 | 0.124 | BGC15 | 6600 | 32.65 | 26.00 | 24.90 | 0.040 | 0.50 | 0.124 |

For all columns: Diameter *(D)* = 900 mm, $\sigma_y$ = 289.6 MPa, $E$ = 206 GPa, and, $v$ = 0.3.
All columns are loaded with one-cycle at each displacement ($N$ = 1), except BC1 and BGC1 loaded with $N$ = 1 and 3. $P_y = \sigma_y * A$, $A = \pi/4 * (D^2 - D_i^2)$, $D_i = D - 2t$, $t$ = thickness for the BC column.

## 4.5 Hysteresis Behavior of BC and BGC Columns

To investigate the hysteretic behavior of BC and BGC columns under a constant axial load and circular bidirectional cyclic lateral loading, a numerical study was conducted using the validated FEM. In the bidirectional circular cyclic lateral loading, the applied displacement is equal in both lateral X and Z directions. Consequently, the response is similar for circular cross-section in both X and Z directions (e.g., see the results in Fig. 4.2a and b). In this chapter, the results in the Z direction are presented in the further analysis. The normalized lateral load vs. lateral displacement

hysteresis loops of both BC and BGC columns are shown in Fig. 4.5. The results in this figure reveal significant improvements in both strength and ductility when the proposed BGC columns are used. Moreover, the post-buckling of the BGC columns is improved compared to their BC column counterparts. For example, the normalized ultimate strength of BGC1 column (i.e., $H_{zmax}/H_y$ = 1.45) is 15% greater than the BC1 column ($H_{zmax}/H_y$ = 1.26) as shown in Fig. 4.5a. For both BC1 and BGC1 columns, the buckling initiates as the normalized maximum displacement approaching $2\delta_y$ (i.e. $\delta_{zm}/\delta_y$ = 2). However, the buckling initiates at the same time for both BC1 and BGC1 columns, the strength deterioration happens at a rapid rate in the case of the BC1 column compared to BGC1 column. In other words, the $H_{zmax}/H_y$ of BC1 column drops by 52% at $\delta_{zm}/\delta_y$ = 4, while the $H_{zmax}/H_y$ decreases by 38% in the BGC1 column. These results indicate the superior behavior of the proposed BGC columns over the BC columns. A similar behavior exists in the all analyzed BC and BGC columns, as shown in Fig. 4.5(b-f). The comparison of buckling shapes for both BC1 and BGC1 columns is shown in Fig. 4.6. The BC1 column bulged outward near the base of the column as expected and formed an elephant-foot-budge buckling mode (see Fig. 4.6a), while the buckling in the BGC1 column is moved upward from the column base with less severity (see Fig. 4.6b). A similar buckling was noticed for the all analyzed BC and BGC columns.

### 4.6 Loading Path Effect

A comparison between unidirectional, presented in Chapter 2, and circular bidirectional cyclic lateral loading conditions is conducted to highlight the effect of the cyclic loading pattern on the hysteretic behavior of thin-walled steel tubular circular columns. Fig. 4.7 shows the hysteretic behavior of the uniform C and BC columns and graded-thickness GC and BGC columns under unidirectional and circular bidirectional cyclic lateral loading.

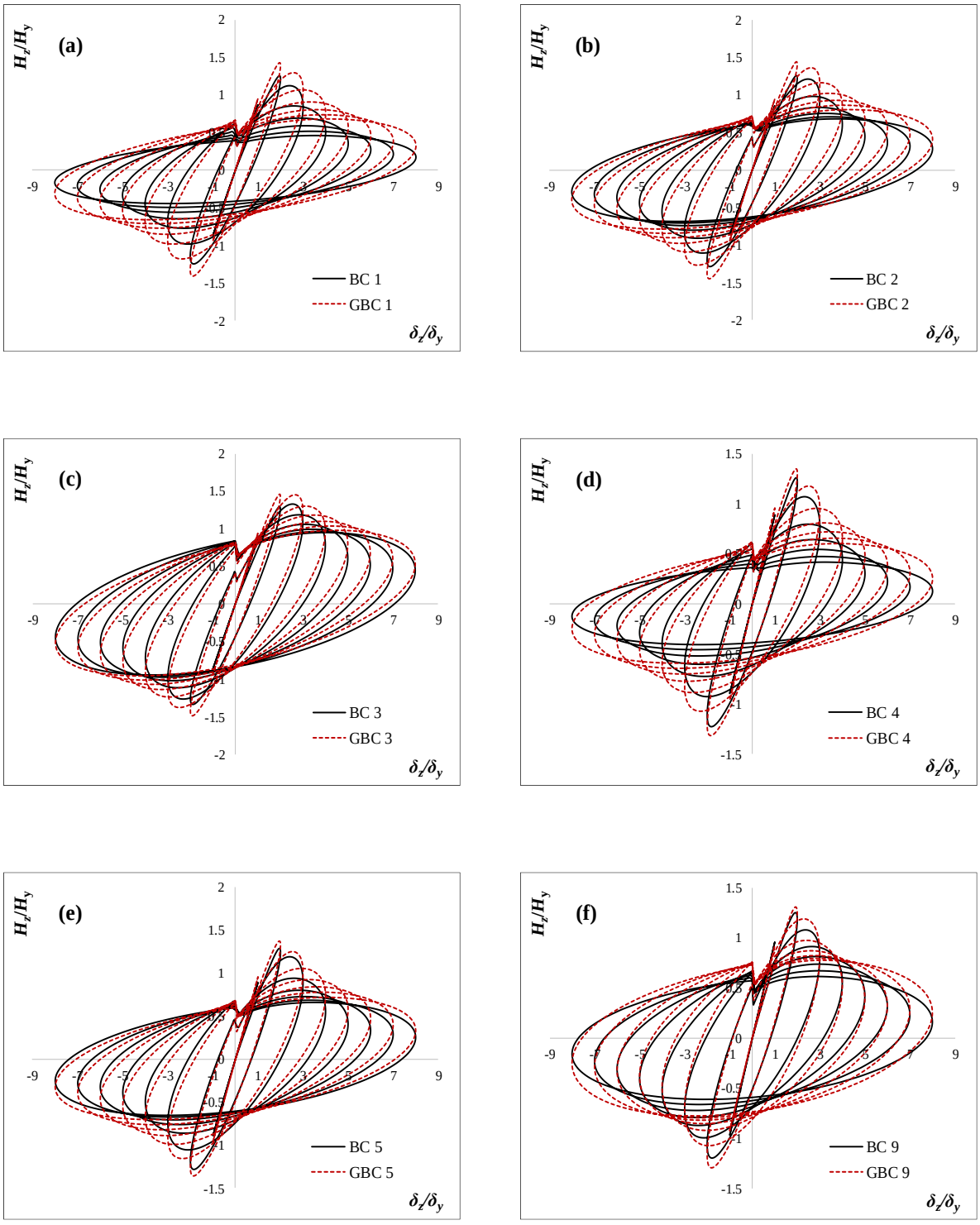


Fig. 4.5. Hysteretic Behavior in Z direction of: (a) BC1 & BGC1, (b) BC2 & BGC2, (c) BC3 & BGC3, (d) BC4 & BGC4, (e) BC5 & BGC5, and (f) BC9 & BGC9.

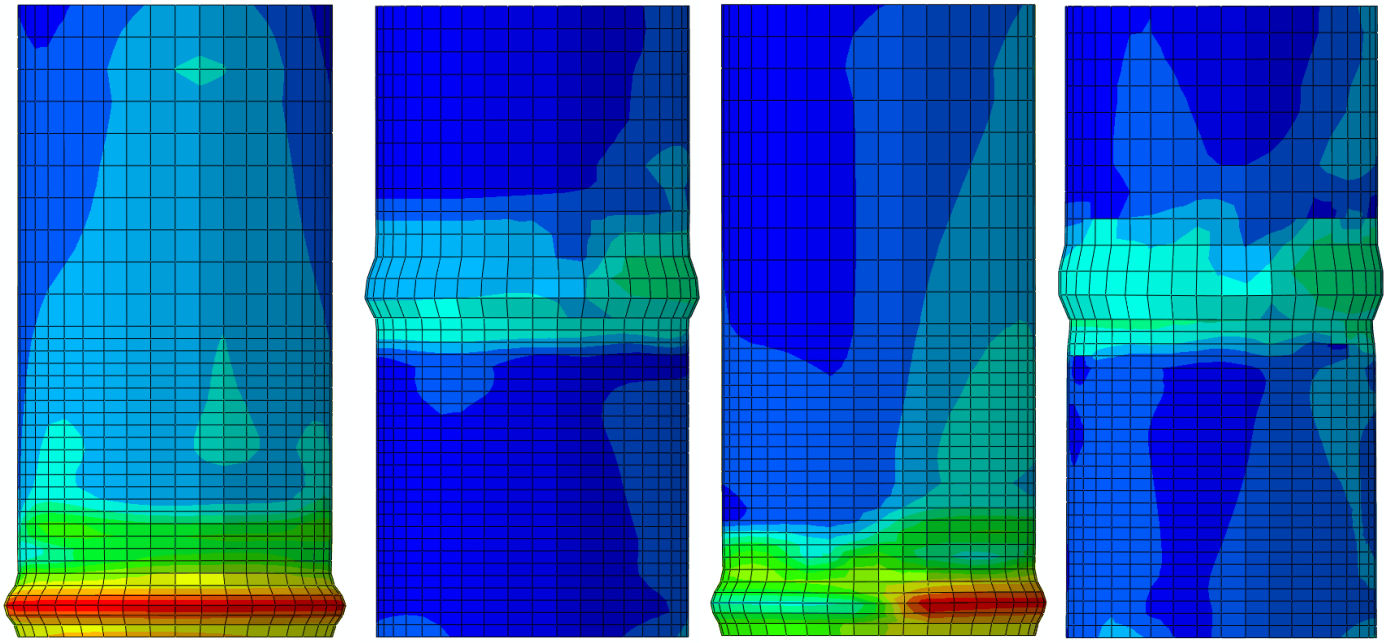

(a) BC1 Column (b) BGC1 Column (c) C1 Column (d) GC1 Column

Fig. 4.6. Buckling Deformation of BC1 and BGC1 Columns.

The comparison indicates that the hysteresis loops under circular bidirectional cyclic lateral loading is totally different from those under unidirectional cyclic lateral loading. At the same amplitude of applied displacement, bidirectional loading pattern significantly causes more degradation in the strength and ductility of the column with the same material and structural parameters than unidirectional loading pattern. The significant deterioration is due to the accelerated local buckling under circular bidirectional cyclic lateral loading. To make a quantitative comparison between of the hysteretic behavior of thin-walled steel tubular circular columns under unidirectional and circular bidirectional loading conditions, the normalized loading path (i.e., $H_x/H_y$-$H_z/H_y$ path for bidirectional loading) of BC and BGC columns are plotted as shown in Fig. 4.8. In addition, the ultimate strength of C column ($H_{max}/H_y$ = 1.403) and GC column ($H_{max}/H_y$ = 1.675) under one-cycle unidirectional cyclic lateral loading is also superimposed as a circular envelope on the Fig. 4.8 with a dashed and dash-dot lines, respectively. The ultimate

strength difference is 11% (C vs. BC) and 16% (GC vs. BGC) between unidirectional and circular bidirectional cyclic lateral loading. Therefore, the hysteretic behavior of thin-walled steel tubular circular columns under unidirectional loading is over-simplified and leads to over-estimated strength and ductility capacity.

#### 4.6.1.1 Buckling Deformations

Fig. 4.6 compares the buckling shapes of the columns at the end of the analysis. The comparison visually indicates that the BC column ($\delta_{zm}/\delta_y$ = 1.95) (see Fig. 4.6a) and BGC column ($\delta_{zm}/\delta_y$ = 1.95) (see Fig. 4.6b), under circular bidirectional cyclic lateral loading, buckled earlier than the C column ($\delta_m/\delta_y$ = 2.16) (see Fig. 4.6c) and GC column ($\delta_m/\delta_y$ = 2.71) (see Fig. 4.6d) under unidirectional cyclic lateral loading. Furthermore, the magnitude of the local buckling seems more critical under circular bidirectional loading. As opposed to the unidirectional cyclic lateral loading, it is believed that because all the plates of the column are subjected to loading all the time of the analysis under circular bidirectional cyclic lateral loading.

#### 4.6.1.2 Energy Absorption Capacity

In order to predict the strength degradation, the dissipated energy of the column is investigated and presented in Fig. 4.9. The cumulative dissipated energy is calculated as the sum of the enclosed area under the normalized hysteresis loops in X and Z direction for circular bidirectional loading and in X direction for unidirectional loading. As observed in Fig. 4.9, the columns with same material and geometrical properties, dissipate more energy under the circular bidirectional cyclic lateral loading than those under unidirectional cyclic lateral loading which, in turns, results in a degradation in the strength and ductility of the column.

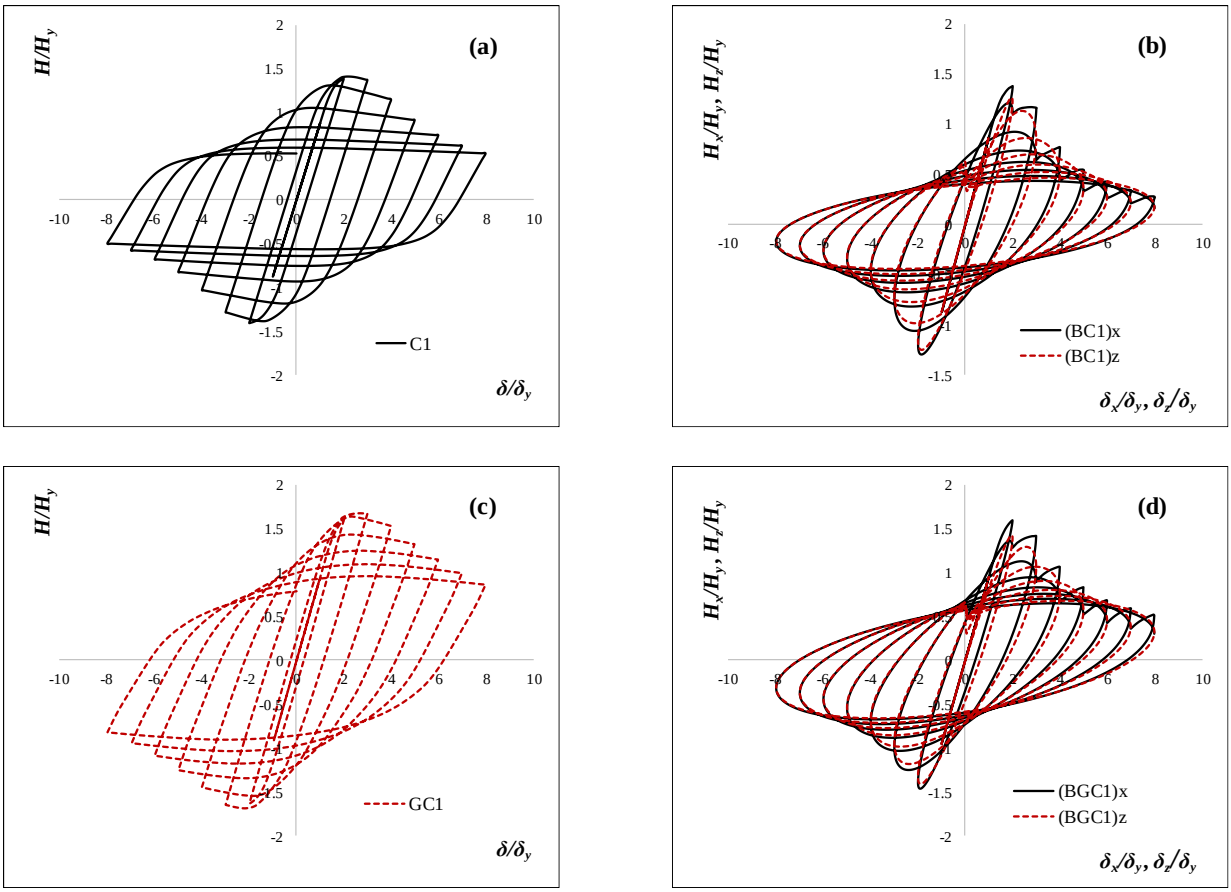


Fig. 4.7. Hysteretic Behavior of Uniform and Graded-thickness Columns.

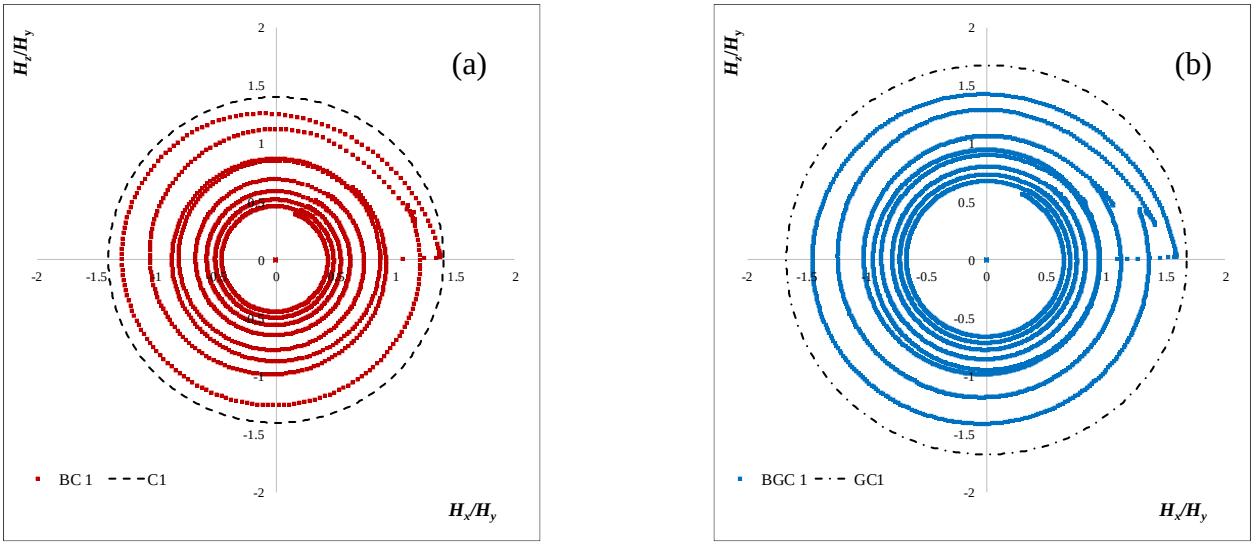


Fig. 4.8. Loading Paths of Columns: (a) BC1 vs. C1 Columns, and (b) BGC1 vs. GC1 Columns.

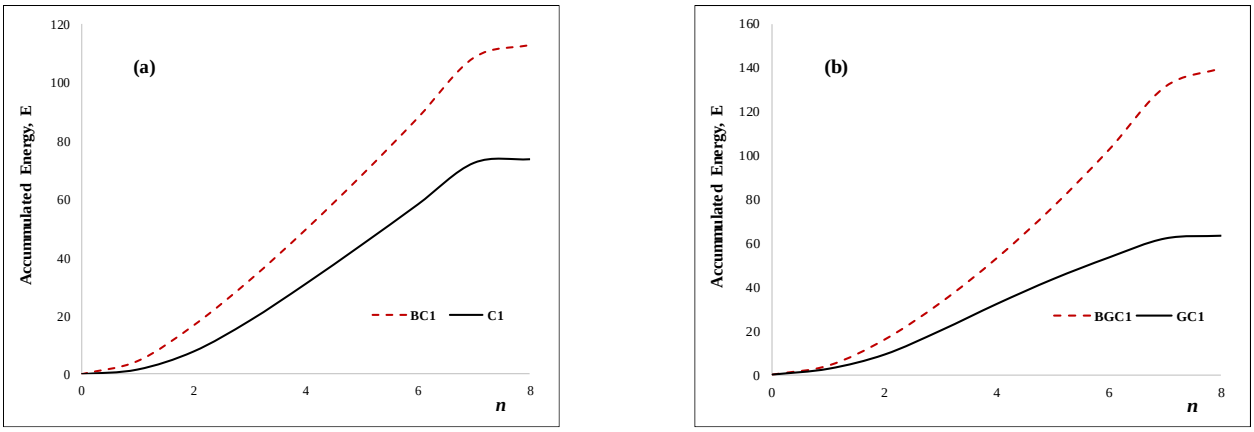


Fig. 4.9. Energy Absorption Capacity of Columns.

## 4.7 Parametric Study

A comprehensive parametric study was conducted to provide insight into the effect of key design parameters including: radius-to-thickness ratio parameter ($R_t$), column slenderness ratio parameter ($\lambda$), magnitude of axial load ($P/P_y$), and number of loading cycles ($N$), on the overall behavior of the BC and BGC columns. The practical range of these parameters in the design of circular bridge piers are: $0.03 \leq R_t \leq 0.08$ , $0.2 \leq \lambda \leq 0.4$ and $P/P_y \leq 0.2$ (Frangopol and Saydam, 2014; Usami, 1996). In this section, a total of 40 columns, listed in Table 4.1, is analyzed using the previously validated FEM in ABAQUS/Standard (Hibbit et al., 2014b). The main parameters are: $R_t$ varying from 0.04 to 0.116, $\lambda$ with a range of 0.26 - 0.5, the axial load ratio $P/P_y$, where five different ratios (i.e., $P/P_y$ = 0.1, 0.124, 0.15, 0.20, and, 0.3) are applied on BC6 and BGC6 columns, and the number of loading cycles at each displacement amplitude ($N$). To investigate the effect of $N$, the BC1 and BGC1 columns were analyzed under both one ($N = 1$), and three ($N = 3$) cycles at each displacement level.

### 4.7.1 Effect of Radius-to-Thickness Ratio Parameter ($R_t$)

The effect of the $R_t$ on the strength and ductility of the column was investigated. The increase in $R_t$ is either due to an increase in the column radius or a decrease in the thickness. In this study, the columns' diameter is kept constant and the thickness is changed for all the analyzed columns. The normalized lateral load vs. lateral displacement envelope curves for both BC and BGC columns with different values of $R_t$ are presented in Fig. 4.10. The normalized ultimate strength (i.e., $H_{zmax}/H_y$) and normalized maximum displacement (i.e., $\delta_{zm}/\delta_y$) of both BC and BGC columns are improved by decreasing $R_t$ and keeping the other column parameter unchanged. For an example, the $H_{zmax}/H_y$ and $\delta_{zm}/\delta_y$ are increased by 17% and 54%, respectively, as $R_t$ is decreased from 0.116 (BC1 column) to 0.04 (BC11 column) with $\lambda = 0.26$ (see Fig. 4.10a). In a similar way, as the $R_t$ decreases from 0.116 (column BGC1) to 0.04 (column BGC11), $H_{zmax}/H_y$ and $\delta_{zm}/\delta_y$ increase by 14% and 68%, respectively, as shown in Fig. 4.10c. After the peak point, the post-buckling curve is less steep as $R_t$ gets smaller and the column experiences higher ductile behavior.

### 4.7.2 Effect of Slenderness Ratio Parameter (λ)

The effect of the λ on the ultimate strength and ductility of both BC and BGC columns was studied. For both BC and BGC columns, the $H_{zmax}/H_y$ and $\delta_{zm}/\delta_y$ improve as λ gets smaller as illustrated in Fig. 4.11. For instance, the $H_{zmax}/H_y$ and $\delta_{zm}/\delta_y$ are increased by 6% and 32%, respectively, as λ decreases from 0.5 (BC9 column, $R_t = 0.08$) to 0.26 (BC3 column, $R_t = 0.08$) as shown in Fig. 4.11b. Similarly, the $H_{zmax}/H_y$ and $\delta_{zm}/\delta_y$ are improved by 11% and 37%, respectively, as λ decreases from 0.5 (BGC9 column, $R_t = 0.08$) to 0.26 (BGC3 column, $R_t = 0.08$) when $R_t = 0.08$ as shown in Fig. 4.11d.

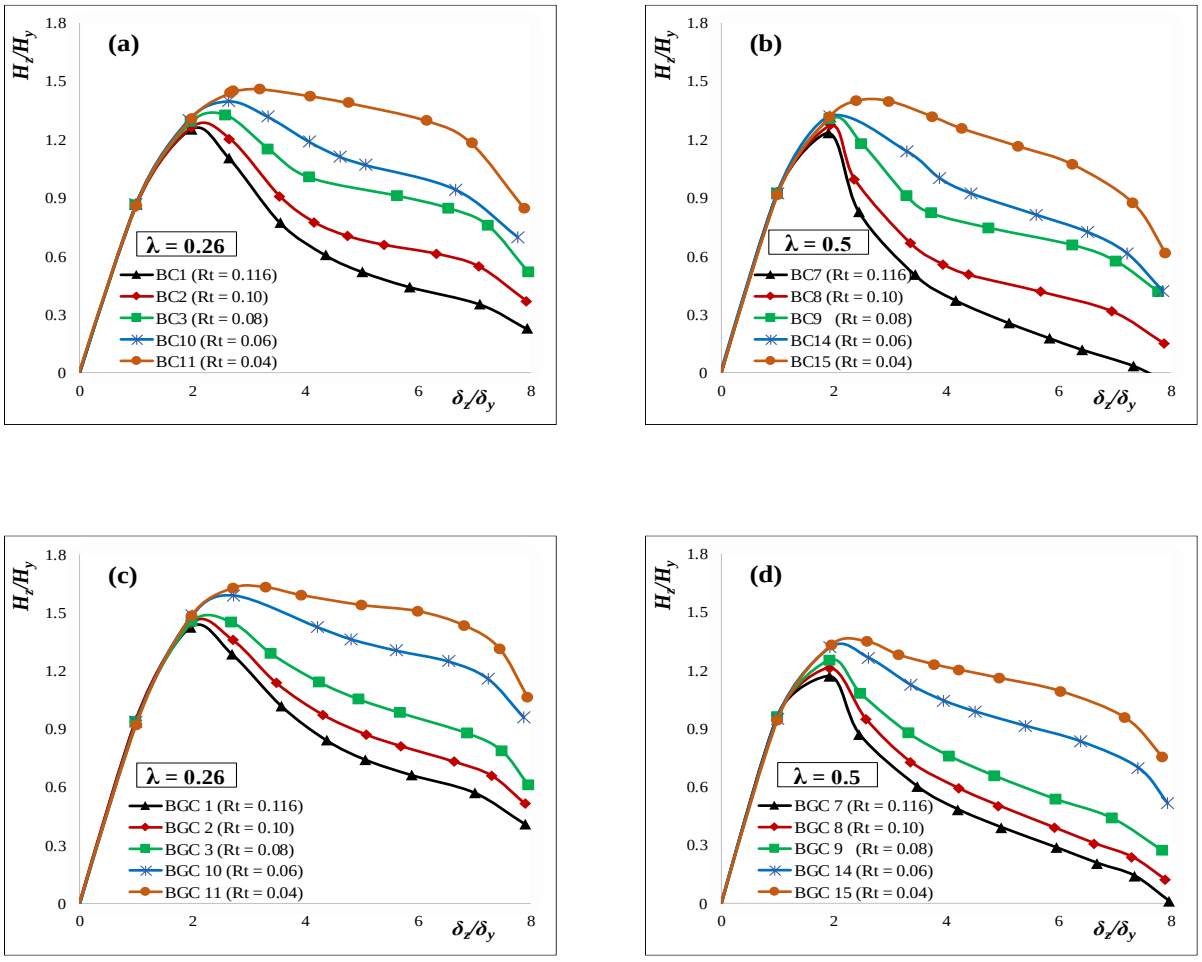


Fig. 4.10. Effect of $R_t$ parameter: (a) BC columns with λ = 0.26, (b) BC columns with λ = 0.5, (c) BGC columns with λ = 0.26, and (d) BGC columns with λ = 0.5.

After the peak point, the strength decreases in a faster rate for both BC7 (at an average of 74%) and BGC7 (at an average of 35%) columns when λ = 0.5 and $R_t$ = 0.116, while the strength drops less for both BC1 (at an average of 28%) and BGC1 (at an average of 20%) in the case of λ = 0.26, and $R_t$ = 0.116. In other words, the post-buckling curve slope gets steeper, and the area enclosed by the envelope curve decreases when λ is higher. The same trend exists in all other analyzed columns with different $R_t$ values.

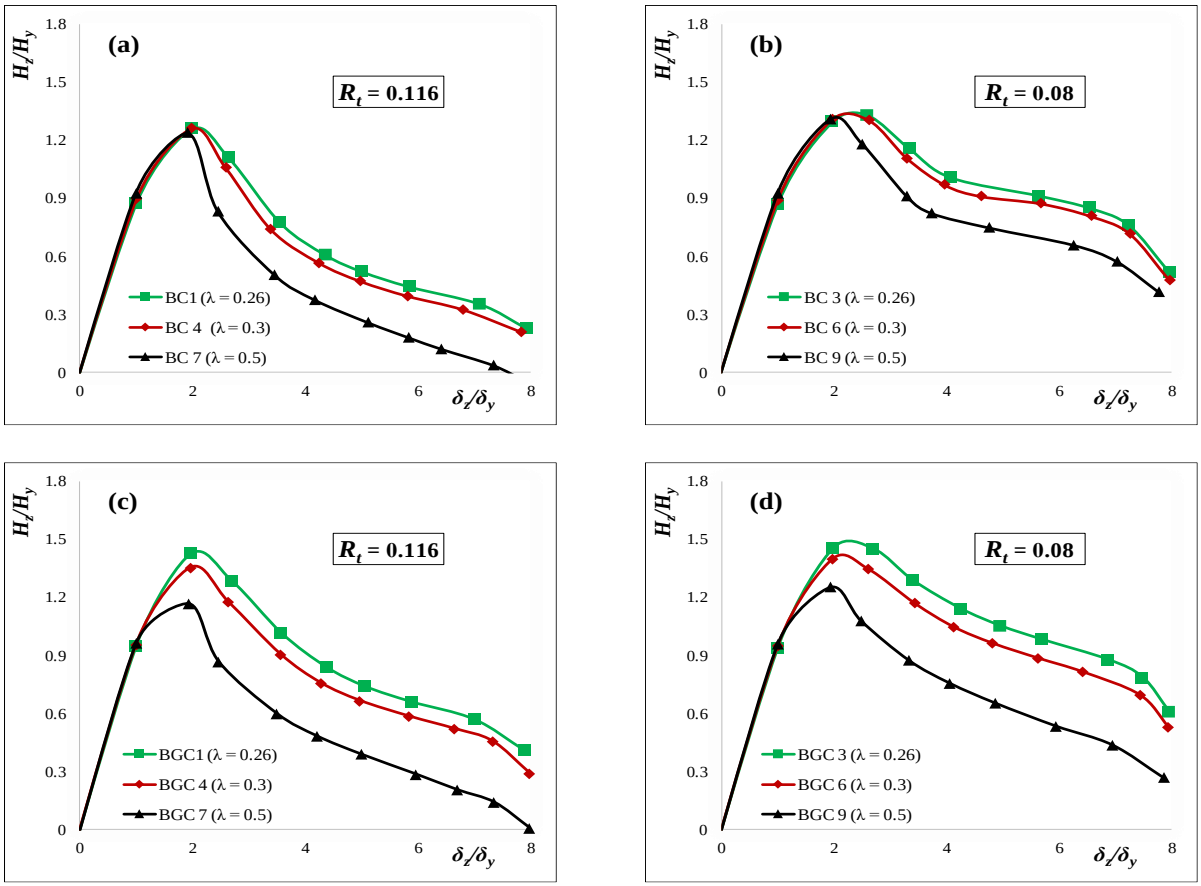


Fig. 4.11. Effect of λ (a) BC columns with $R_t$ = 0.116, (b) BC columns with $R_t$ = 0.08 (c) BGC columns with $R_t$ = 0.116, and (d) BGC columns with $R_t$ = 0.08.

### 4.7.3 Effect of Axial Load ($P/P_y$)

The ultimate strength and ductility of the BC and BGC columns were studied under different axial load ratios (i.e., $P/P_y$ = 0.1, 0.124, 0.15, 0.2, and 0.3). Five of BC6 columns (BC6-10, BC6-12.4, BC6-15, BC6-20, and BC6-30) and five of the BGC6 columns (BGC6-10, BGC6-12.4, BGC6-15, BGC6-20, and BGC6-30) are analyzed, where the number after the hyphen indicates the applied axial load ratio. As shown in Fig. 4.12, the envelope curves of the lateral load ($H_z/H_{y0}$) vs. lateral displacement ($\delta_z/\delta_{y0}$) are normalized by $H_{y0}$ (lateral yield load under zero axial load) and $\delta_{y0}$ (yield displacement under zero axial load) to highlight the axial load effect. For both BC6 and BGC6,

the ultimate strength (i.e., $H_{zmax}/H_{y0}$) decreases as the axial load ratio ($P/P_y$) increases due to the *P-Δ* effect in the case of large axial loads. For example, the $H_{zmax}/H_{y0}$ and $\delta_{zm}/\delta_{y0}$ are increased by 17% and 8%, respectively, when $P/P_y$ decreases from 30% (BC6-30 column) to 10% (BC6-10 column). In the case of BGC columns, the $H_{zmax}/H_{y0}$ and $\delta_{zm}/\delta_{y0}$ are increased by 30% and 28%, respectively, when $P/P_y$ decreases from 30% (BGC6-30 column) to 10% (BGC6-10 column). Furthermore, the post-buckling curve slope becomes steeper, which, in turn, dissipates less energy, as observed in the cases of BC6-30 and BGC6-30 columns, while more energy is dissipated in the cases of BC6-10 and BGC6-10 columns, respectively.

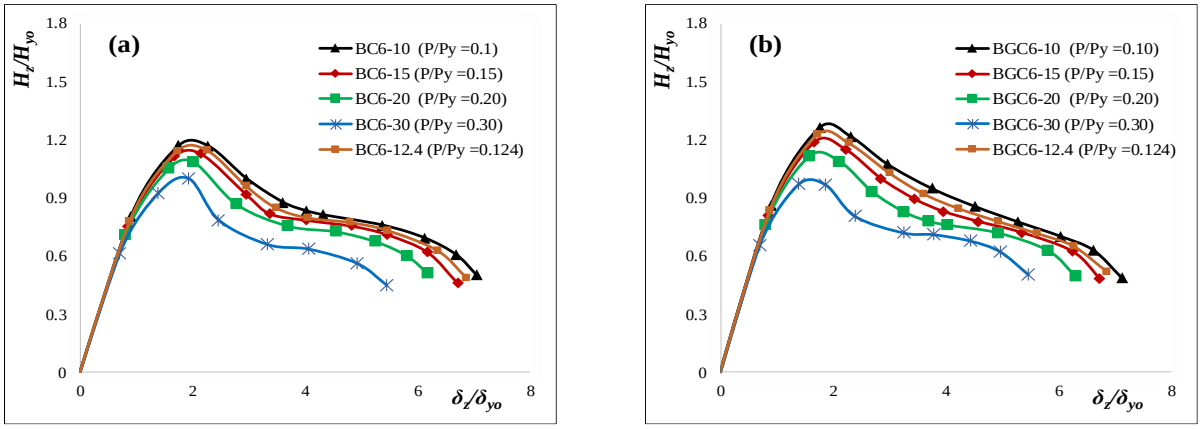


(a) BC6 Column (b) BGC6 Column

Fig. 4.12. Effect of Axial Load on Strength and Ductility.

### 4.7.4 Effect of Number of Loading Cycles (*N*)

The normalized lateral load vs. lateral displacement envelope curves of the BC1 (Fig. 4.13a) and BGC1 (Fig. 4.13b) columns in the cases of one ($N$ = 1) and three ($N$ = 3) loading cycles at each displacement level are presented in Fig. 4.13. After $\delta = 2\delta_y$, the column strength drops at a faster rate, and larger damage is noticed in the case of $N$ = 3 compared to $N$ = 1. For instance, the slopes of BC1 and BGC1 columns, respectively, decrease at an average of 28% and 20% in the case of $N$

= 1, while the slopes decrease at an average of 34% and 27% in the case of $N$ = 3. No remarkable effect is observed when $\delta$ is less than $2\delta_y$, which might be due to the small plastic deformation. It is worth noting that the deterioration in the BGC1 column is less than in the BC1 column under both $N$ = 1 and $N$ = 3.

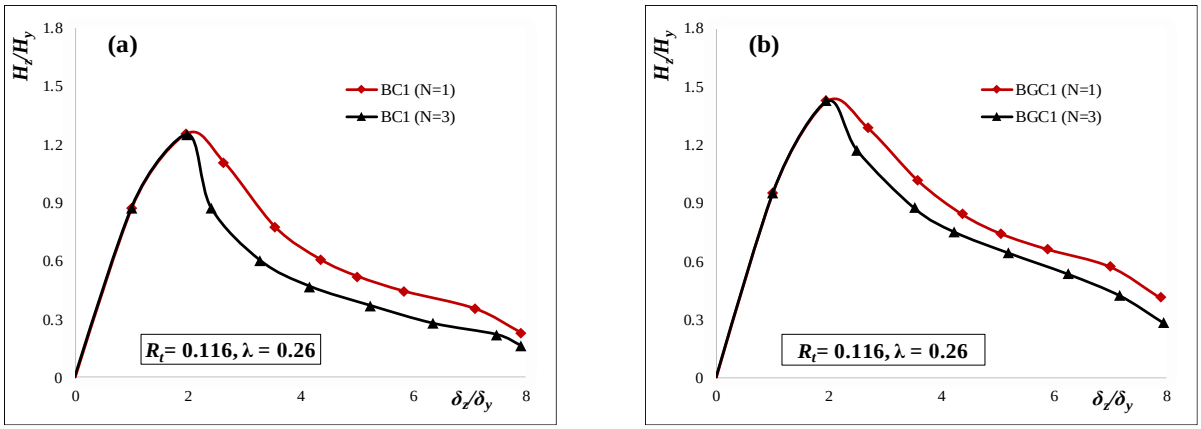


(a) BC1 column (b) BGC1 column

Fig. 4.13. Effect of $N$ on Ductility Capacity.

### 4.8 Strength and Ductility Evaluation of BC and BGC Columns

Table 4.2 lists the computed ultimate strength and ductility values of both BC and BGC columns. In Fig. 4.14, $H_{zmax}/H_y$ is plotted against integrated parameters $(1+P/P_y)\ R_t\ \lambda$ considering the interaction of $R_t$, λ, and $P/P_y$ on the strength of the column. The Equations 5 and 6 are proposed to fit the computed ultimate strength of BC and BGC columns, respectively:

$$\frac{H_{z\max}}{H_y} = \frac{0.841}{\left[(1+\frac{P}{P_y})R_t\lambda\right]^{0.126}} \qquad \text{BC Columns} \qquad (4.5)$$

$$\frac{H_{z\max}}{H_y} = \frac{0.734}{\left[(1+\frac{P}{P_y})R_t\lambda\right]^{0.18}} \qquad \text{BGC Columns} \qquad (4.6)$$

Table 4.2. Strength and Ductility Evaluation of BC and BGC Columns.

| BC Columns | | | | | | BGC Columns | | | | | |
|---|---|---|---|---|---|---|---|---|---|---|---|
| **Column** | $H_y$ **(KN)** | $\delta_y$ **(mm)** | $H_{zmax}/H_y$ | $\delta_{zm}/\delta_y$ | $\delta_{z0.9}/\delta_y$ | **Column** | $H_y$ **(KN)** | $\delta_y$ **(mm)** | $H_{zmax}/H_y$ | $\delta_{zm}/\delta_y$ | $\delta_{z0.9}/\delta_y$ |
| **BC1** | 414.2 | 10.6 | 1.26 | 1.95 | 2.53 | **BGC1** | 414.2 | 10.6 | 1.45 | 1.96 | 2.63 |
| **BC2** | 478.7 | 10.6 | 1.26 | 1.97 | 2.87 | **BGC2** | 478.7 | 10.6 | 1.46 | 1.97 | 2.87 |
| **BC3** | 593.2 | 10.6 | 1.33 | 2.54 | 3.16 | **BGC3** | 593.2 | 10.6 | 1.46 | 2.65 | 3.30 |
| **BC10** | 779.5 | 10.6 | 1.40 | 2.60 | 3.68 | **BGC10** | 779.5 | 10.6 | 1.61 | 2.74 | 4.02 |
| **BC11** | 1135.5 | 10.6 | 1.47 | 3.01 | 5.80 | **BGC11** | 1135.5 | 10.6 | 1.65 | 3.30 | 6.26 |
| **BC4** | 355.9 | 14.3 | 1.27 | 1.95 | 2.33 | **BGC4** | 355.9 | 14.3 | 1.38 | 1.95 | 2.39 |
| **BC5** | 411.4 | 14.3 | 1.29 | 1.96 | 2.59 | **BGC5** | 411.4 | 14.3 | 1.40 | 1.96 | 2.66 |
| **BC6** | 509.8 | 14.3 | 1.31 | 1.97 | 3.02 | **BGC6** | 509.8 | 14.3 | 1.40 | 1.97 | 3.07 |
| **BC6-10** | 523.7 | 14.3 | 1.30 | 1.95 | 3.05 | **BGC6-10** | 523.7 | 14.3 | 1.40 | 1.95 | 3.04 |
| **BC6-15** | 494.6 | 14.3 | 1.33 | 1.96 | 3.00 | **BGC6-15** | 494.6 | 14.3 | 1.40 | 1.96 | 3.00 |
| **BC6-20** | 465.5 | 14.3 | 1.36 | 1.96 | 2.97 | **BGC6-20** | 465.5 | 14.3 | 1.39 | 1.96 | 3.03 |
| **BC6-30** | 407.3 | 14.3 | 1.38 | 1.96 | 3.10 | **BGC6-30** | 407.3 | 14.3 | 1.39 | 1.96 | 3.13 |
| **BC12** | 669.8 | 14.3 | 1.39 | 2.53 | 3.54 | **BGC12** | 669.8 | 14.3 | 1.50 | 2.66 | 3.89 |
| **BC13** | 975.8 | 14.3 | 1.45 | 2.73 | 5.77 | **BGC13** | 975.8 | 14.3 | 1.56 | 2.74 | 6.00 |
| **BC7** | 213.6 | 39.7 | 1.17 | 1.90 | 2.02 | **BGC7** | 213.6 | 39.7 | 1.24 | 1.90 | 2.15 |
| **BC8** | 246.8 | 39.7 | 1.21 | 1.91 | 2.07 | **BGC8** | 246.8 | 39.7 | 1.28 | 1.92 | 2.23 |
| **BC9** | 305.9 | 39.7 | 1.25 | 1.93 | 2.17 | **BGC9** | 305.9 | 39.7 | 1.31 | 1.93 | 2.65 |
| **BC14** | 401.9 | 39.7 | 1.32 | 1.93 | 2.89 | **BGC14** | 401.9 | 39.7 | 1.35 | 2.31 | 2.95 |
| **BC15** | 585.5 | 39.7 | 1.35 | 2.45 | 3.38 | **BGC15** | 585.5 | 39.7 | 1.40 | 2.78 | 4.73 |

The ultimate strength of both BC and BGC columns is improved when integrated parameters $(1+P/P_y)$ $R_t$ $\lambda$ decrease as illustrated in Fig. 4.14. The failure of thin-walled steel columns is considered to have occurred when the displacement equals either $\delta_{zm}$ or $\delta_{z0.9}$. the $\delta_{zm}$ is the displacement corresponding to $H_{zmax}/H_y$, where the $\delta_{z0.9}$ is defined as the displacement where the post-peak strength drops to 90% of $H_{zmax}/H_y$ after the peak (Al-Kaseasbeh and Mamaghani, 2018; Mamaghani et al., 2015; Usami, 1996). The $\delta_{zm}/\delta_y$ and $\delta_{z0.9}/\delta_y$ are key parameters used to evaluate the ductility performance for both BC and BGC columns. Moreover, the strength of thin-walled steel columns decreases significantly after the peak due to the influence of local buckling. Therefore, it is more reasonable to use the $\delta_{z0.9}/\delta_y$ parameter to evaluate ductility (Gao et al., 1998a;

Usami, 1996; Usami et al., 2000b). Table 4.2 shows an increasing trend of the strength and ductility in both the BC and BGC columns as the $R_t$ and λ decrease. All $\delta_{zm}/\delta_y$ and $\delta_{z0.9}/\delta_y$ values of both BC and BGC columns are plotted vs. integrated $R_t$, λ and/or $P/P_y$, as shown in Fig. 4.15. The proposed formulae that fit the computed $\delta_{zm}/\delta_y$ and $\delta_{z0.9}/\delta_y$ values of the analyzed columns are as follows:

$$\frac{\delta_{zm}}{\delta_y} = \frac{0.713}{(R_t\lambda)^{0.303}} \tag{4.7}$$

$$\frac{\delta_{z0.9}}{\delta_y} = \frac{0.352}{\left[(1+\frac{P}{P_y})R_t\lambda\right]^{0.6}} \tag{4.8}$$

BC Columns

$$\frac{\delta_{zm}}{\delta_y} = \frac{0.649}{(R_t\lambda)^{0.337}} \tag{4.9}$$

$$\frac{\delta_{z0.9}}{\delta_y} = \frac{0.373}{\left[(1+\frac{P}{P_y})R_t\lambda\right]^{0.6}} \tag{4.10}$$

BGC Columns

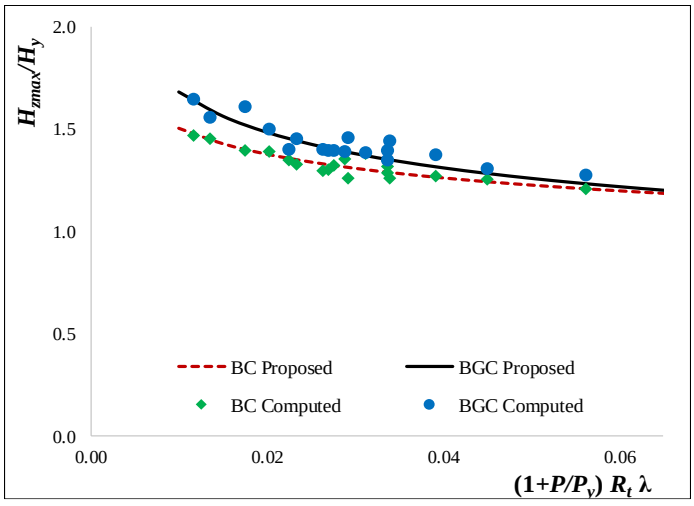


Fig. 4.14. Ultimate Strength of the BC and BGC Columns.

As can be seen from Fig. 4.12, the axial load magnitude has a significant effect on the post-buckling of the BC and BGC columns. Therefore, the axial load influence is considered in the fitting of the ductility parameter $\delta_{z0.9}/\delta_y$ as it appears in Eqs. (4.8) and (4.10). In contrast, the axial load has an insignificant effect on the maximum displacement of the BC and BGC columns. Thus, the axial load influence is not included in the fitting of the $\delta_{zm}/\delta_y$ parameter, as shown in Eqs. (4.7) and (4.9). The applicable restrictions of these formulae are $0.04 \leq R_t \leq 0.116$, $0.26 \leq \lambda \leq 0.5$, and $P/P_y \leq 0.3$. It is worth mentioning that nonlinear least-squares regression was used for the curve fitting.

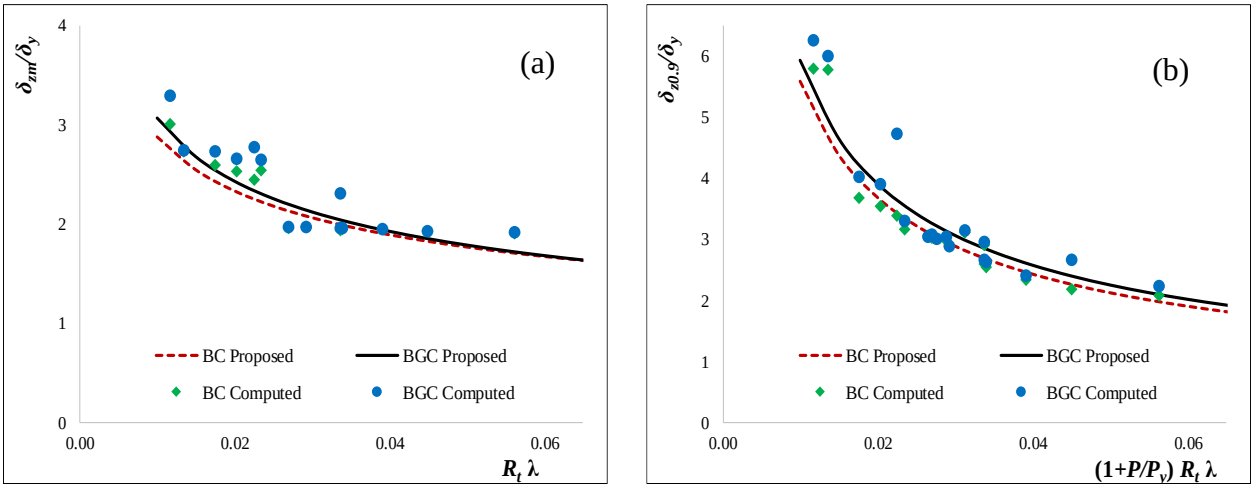


Fig. 4.15. Ductility of BC and BGC Columns: (a) $\delta_{zm}/\delta_y$, and (b) $\delta_{z0.9}/\delta_y$.

### 4.9 Summary

This chapter aims to evaluate the strength and ductility of thin-walled steel tubular circular columns with uniform thickness (BC) and graded thickness (BGC) under a constant axial load and circular bidirectional cyclic lateral loading. The effect of main design parameters including: radius-to-thickness ratio parameter ($R_t$), column slenderness ratio parameter ($\lambda$), magnitude of axial load ($P/P_y$), and number of loading cycles ($N$) on the strength and ductility of both BC and BGC

columns under circular bidirectional cyclic lateral loading was investigated. From this study, the following conclusions are drawn:

- The numerical results, obtained by using the adopted FEM, show a reasonable agreement with the experimental results confirming FEM ability to capture the column cyclic elastoplastic behavior under a constant axial load and circular bidirectional cyclic lateral loading.
- The proposed BGC column, with the same size and volume of material of counterpart of uniform BC column investigated under a constant axial force and circular bidirectional cyclic lateral loading. The results show a significant improvement in the overall hysteretic behavior of BGC column compared to the counterpart of BC column. In general, the ultimate strength of BGC columns was improved by 13% and 8% as $\lambda$ = 0.26 and 0.3, respectively. In the case of $\lambda$ = 0.5, the ultimate strength was improved by only 4% for the BGC columns compared to BC columns.
- The parametric study concluded that the ultimate strength, ductility, and post buckling of BC and BGC columns improve with the decrease of $R_t$ and $\lambda$, while deteriorate when the axial load increases. As the number of loading cycles ($N$) at each displacement level increases, more strength deterioration happens when $\delta > 2\delta_y$.
- Based on the extensive parametric study, design formulae in predicting the ultimate strength and ductility of the BC and BGC columns have been derived

# CHAPTER 5 Stiffened Square Box Columns under Bidirectional Cyclic Lateral Loading

## 5.1 Introduction

As main goal of this chapter, the proposed graded-thickness thin-walled steel square box columns (denoted as BGB in this chapter) is evaluated in regard to the strength and ductility under a a constant axial force and circular bidirectional cyclic lateral loading. In order to achieve this goal, a thin-walled steel square box column with uniform thickness reported in the literature (Aoki et al., 2007; Dang et al., 2017) was numerically analyzed under a constant axial force and circular bidirectional cyclic lateral loading to validate the accuracy of the adopted FEM. Then, the proposed BGB column with size and volume of material equivalent to a uniform thin-walled steel square box column (i.e., BB column) is investigated under the same loading amplitude and conditions. The study results indicate the proposed BGB columns are advantageous in achieving significant improvements in ultimate strength and ductility compared to their counterpart BB columns, emphasizing the effect of the plate thickness and sectional configuration in the proposed BGB column. The achieved improvements in the overall hysteretic behavior of the proposed BGB is due to their ability to inhibit the local buckling near the base of the column. Furthermore, the hysteretic behavior of BB and BGB columns is more severe and critical under circular bidirectional cyclic lateral loading compared to unidirectional cyclic lateral loading.

## 5.2 Numerical Model

In this study, a commercial finite element software ABAQUS 6.14 is employed for the FE analysis where material and geometric nonlinearities are taken into account during computational process (Hibbit et al., 2014a). The validity of the adopted FEM is substantiated with the experimental

results reported in the literature (Aoki et al., 2007; Dang et al., 2017). The main structural parameters in the practical design of thin-walled steel square box columns are $R_f$ and $\lambda$. The local buckling is influenced by $R_f$ and $\lambda$ affects the global buckling (Al-Kaseasbeh and Mamaghani, 2019) which are defined as follows:

$$R_f = \frac{D}{t}\sqrt{\frac{\sigma_y}{E}\frac{12(1-\nu^2)}{\pi^2 k_R}}, \quad k_R = 4n^2 \tag{5.1}$$

$$\lambda = \frac{2h}{r}\frac{1}{\pi}\sqrt{\frac{\sigma_y}{E}} \tag{5.2}$$

where $h$ = column height, $D$ = column diameter, $t$ = plate thickness, $r$ = radius of gyration of cross section, $\sigma_y$ = yield stress, $E$ = Young's modulus, and $\nu$ = Poisson's ratio. For the tested column, $h$ = 2420 mm, $D$ = 450 mm, $t$ =6 mm, $r$ = 175 mm, $\sigma_y$ = 325 MPa, $E$ = 206 GPa, and $\nu$ = 0.3 (Aoki et al., 2007). As shown in Fig. 5.1, the column is fixed at the bottom and subjected to constant axial force ($P$) and circular bidirectional cyclic lateral displacement at the top. The lower part of the column (3$D$), which accurately consider the local buckling, is modeled by reduced integration four-node shell elements (S4R), while the two-node beam element (B31) is employed for the upper part of the column ($h$-3$D$). All the employed elements are available in ABAQUS /Standard library. The interface between S4R and B31 elements is linked using multi-point constraint (MPC). For computational efficiency and accuracy, the upper part of the column, height of $h$-3$D$, is divided into B31 elements with size of 90 mm. The bottom and middle portions of the lower part of the column (equal to the side width, $D$) are, respectively, divided into 30, and 20 S4R elements, while the remaining height ($D$) is only divided into 15 elements. Finally, each longitudinal stiffeners and

subpanel between the stiffeners, respectively, have 3 and 6 columns of S4R. The above-stated mesh sizes are found to give more efficient and reasonable results.

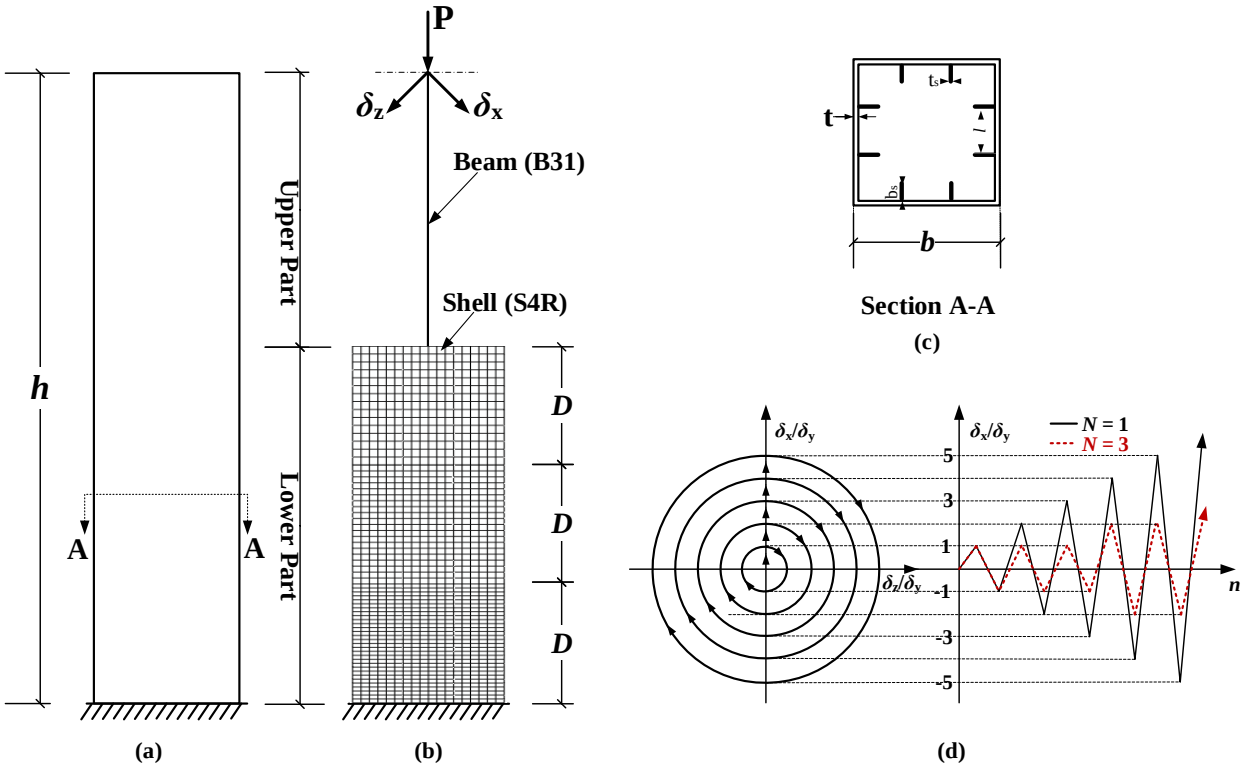


Fig. 5.1. Tested Column Model: (a) Column; (b) FE Meshing; (c) Cross Section; and (d) Loading Program.

A recent study by Chen et al. (2019) concluded that initial geometric and welding residual stress have insignificant impact on the hysteretic behavior of thin-walled steel columns under cyclic loading (Chen, S. et al., 2019). Also, similar findings have been reported by a number of researchers (Al-Kaseasbeh and Mamaghani, 2018, 2019; Banno et al., 1998; Hassan et al., 2018b; Ucak and Tsopelas, 2012). Accordingly, the initial imperfection and residual stress are not taken into account in this study.

### 5.2.1 Bidirectional Cyclic Loading Program

As illustrated in Fig. 5.1d, among several recorded earthquake ground motions, the displacement-controlled circular cyclic lateral loading is selected as the severest loading path (Goto et al., 2006; Ucak and Tsopelas, 2014; Watanabe et al., 2000). The adopted quasi-static bidirectional cyclic lateral loading is applied to the top of the column concurrently with a constant axial force ($P$). In each loading step, the amplitude of the cyclic displacement is increased as a multiple of the yield displacement ($\delta_y$), which is defined by:

$$\delta_y = \frac{H_y h^3}{3EI} \tag{5.3}$$

$$H_y = \left(\sigma_y - \frac{P}{A}\right)\frac{S}{h} \tag{5.4}$$

where $H_y$ is the lateral yield load and $A$, $I$, and $S$, respectively, are the cross-sectional area, moment of inertia, and elastic section modulus of the column, and other parameters are indicated in the earlier context (Al-Kaseasbeh and Mamaghani, 2019).

## 5.3 Numerical Model

As illustrated in Fig. 5.2, the hysteretic behavior of the tested column, in both lateral X and Z directions, obtained from the FE analysis is compared to the experimental results in the literature (Aoki et al., 2007; Dang et al., 2017). The FE analysis results in solid line and the experimental results depicted with dashed line. $H_y$ and $\delta_y$, respectively, are the lateral yield load and yield displacement. In both X and Z directions, the FE analysis results have a reasonable agreement with the experimental results. The ultimate strength of the column is predicted with 1% error in X

direction (FEM: $H_{xmax}/H_y$ = 1.167, Experiment: $H_{xmax}/H_y$ = 1.160, see Fig. 5.2a) and less than 5% in Z direction (FEM: $H_{zmax}/H_y$ = 1.123, Experiment: $H_{zmax}/H_y$ = 1.174, see Fig. 5.2b). In conclusion, the FE model, is able to capture the structural behavior of thin-walled steel square box columns with a reasonable accuracy considering the local buckling under constant axial force and circular bidirectional cyclic lateral loading. As shown in Fig. 5.3, buckling shape of the FE analysis at the end of analysis (Aoki et al., 2007; Dang et al., 2017) (see Fig. 5.3b) is captured relatively well compared to the experimental buckling deformation (see Fig. 5.3a). In both the experiment and analysis, the column buckled inward and outward at the column' base.

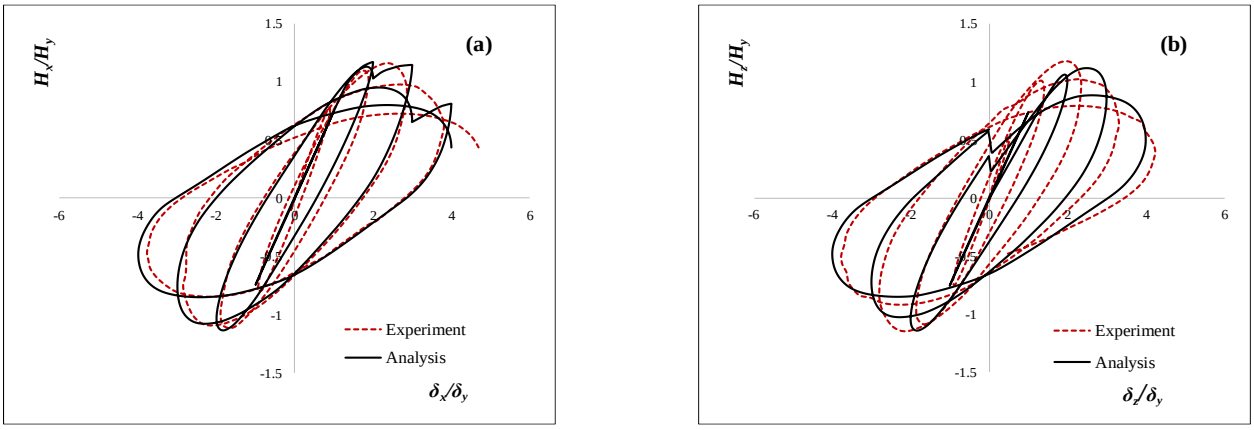


Fig. 5.2. Hysteretic Behavior of the Tested Column.

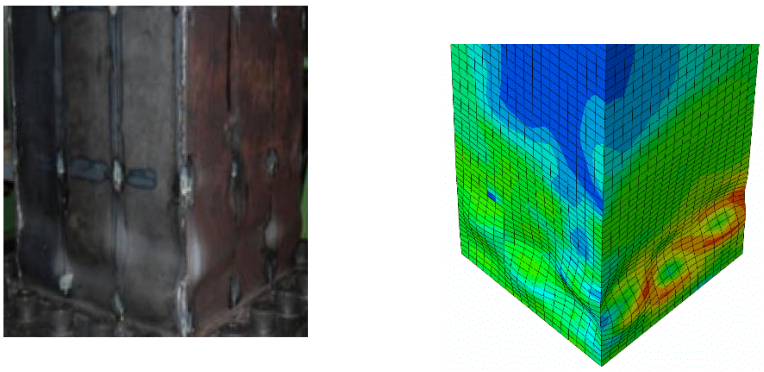

(a) Experiment (Dang and Aoki, 2013b)

(b) FE Analysis

Fig. 5.3. Buckling Deformation of Tested Column.

### 5.4 Review of Proposed Thin-Walled Steel Column with Graded Thickness

In Chapter 3, the graded-thickness thin-walled steel square box column has been introduced and examined, under constant axial force and unidirectional cyclic lateral loading, to inhibit the local buckling near the base of the column. The proposed BGB column has the same size and volume of material of the uniform BB column. As shown in Fig. 5.4c, the BGB column is divided into three segments of constant cross sections along its height. The first two segments from the base have the same height, which is equal to the side width ($D$) of BB column. The upper segment has a height of $h$-2$D$, where $h$ and $D$ are same for both BB and BGB columns. In the proposed BGB column (see Fig. 5.4d), the first and second segments, respectively, have a thickness of 1.25$t$, and $t$, where $t$ is the thickness of the BB column. The thickness of the upper segment, $t_3$, is calculated by equating the volume of material in both BB and BGB columns. The above configuration of the BGB column was chosen based on failure pattern of the tested columns in the literature (Al-Kaseasbeh and Mamaghani, 2019; Usami, 1996). As listed in Table 5.1, the same material and geometrical properties (except the plate thickness) are the same for both of the BB and BGB columns which are assumed to be made of the same carbon steel ASTM A242 (ASTM, 2018). For both BB and BGB columns, the same FEM details of the tested column, except the FE meshing, are used, as shown in Fig. 5.4b. For computational efficiency, the upper part of the column, height of $h$-2$D$, is divided into B31 elements with size of 90 mm. The bottom half of the lower part of the column (equal to the side width, $D$) is divided into 30 S4R elements, while the remaining height ($D$) is only divided into 18 elements. Finally, each longitudinal stiffeners and subpanel between the stiffeners, respectively, have 3 and 6 columns of S4R elements.

### 5.5 Hysteretic Behavior of BB and Proposed BGB Columns

In order to investigate the hysteretic behavior of BB and BGB columns under a constant axial force and circular bidirectional cyclic lateral loading, FE analyses were conducted using the substantiated FEM. Under the circular bidirectional cyclic lateral loading, the applied displacement is equal in both lateral X and Z directions. Consequently, the BB and BGB columns exhibit isotropic response in both X and Z directions (e.g., see the results in Fig. 5.2a and b).

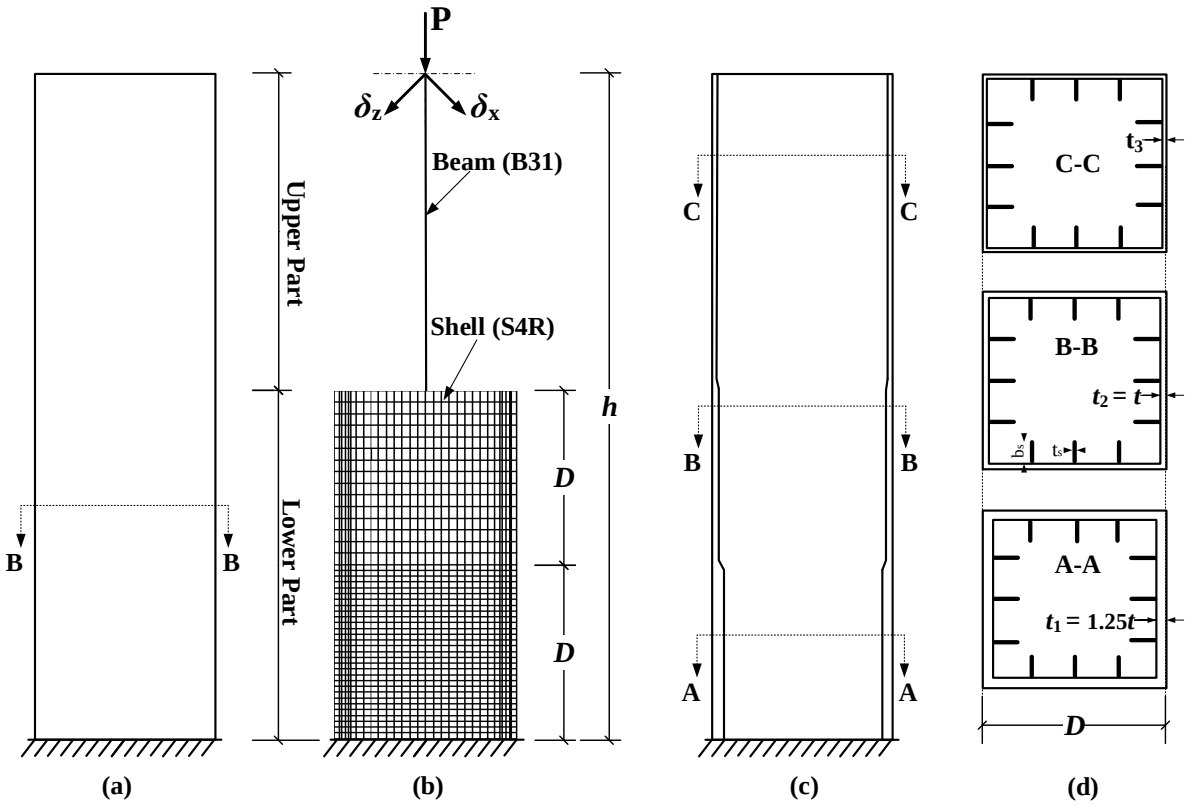


Fig. 5.4. (a) BB Column, (b) FE Meshing, (c) BGB Column, and (d) Graded-thickness Sections.

In this chapter, for brevity purpose, the results in the Z direction are presented in the further analysis. For both BB and BGB columns, the normalized lateral load vs. lateral displacement hysteresis loops are shown in Fig. 5.5. The plotted hysteresis loops indicate a remarkable strength and ductility improvement in the proposed BGB columns. As compared to their BB column counterparts, the post-buckling of the BGB columns is also improved. For instance, the normalized

ultimate strength (i.e., $H_{zmax}/H_y$ = 1.56) and the corresponding normalized maximum displacement (i.e. $\delta_{zm}/\delta_y$ = 2.64) of BGB1 column, respectively, are 32% and 36% greater than those of the BB1 column as shown in Fig. 5.5a. In the BB1 column, the buckling initiated earlier, where $\delta_{zm}/\delta_y$ = 1.93, than the BGB1 column. A similar behavior exists in the all analyzed BB and BGB columns, as shown in Fig. 5.5(b-j).

Table 5.1. Material and Geometrical Properties of Analyzed BB and BGB Columns.

| BB Columns | | | | | | BGB Columns | | | | | | | | |
|---|---|---|---|---|---|---|---|---|---|---|---|---|---|---|
| Column | *h(mm)* | *t(mm)* | $R_f$ | $\lambda$ | $P/P_y$ | Column | *h(mm)* | *t (mm)* | | | $R_f$ | $\lambda$ | $P/P_y$ |
| | | | | | | | | $t_1$ | $t_2$ | $t_3$ | | | |
| **BB1** | 3403 | 9.00 | 0.56 | 0.26 | 0.122 | **BGB1** | 3403 | 11.25 | 9.00 | 7.75 | 0.56 | 0.26 | 0.122 |
| **BB2** | 3403 | 11.00 | 0.46 | 0.26 | 0.122 | **BGB2** | 3403 | 13.75 | 11.00 | 9.46 | 0.46 | 0.26 | 0.122 |
| **BB3** | 3403 | 14.00 | 0.36 | 0.26 | 0.122 | **BGB3** | 3403 | 17.50 | 14.00 | 12.00 | 0.36 | 0.26 | 0.122 |
| **BB4** | 3403 | 16.90 | 0.30 | 0.26 | 0.122 | **BGB4** | 3403 | 21.14 | 16.90 | 14.55 | 0.30 | 0.26 | 0.122 |
| **BB5** | 3403 | 19.50 | 0.26 | 0.26 | 0.122 | **BGB5** | 3403 | 24.40 | 19.50 | 16.80 | 0.26 | 0.26 | 0.122 |
| **BB5-10** | 3403 | 19.50 | 0.26 | 0.26 | 0.100 | **BGB5-10** | 3403 | 24.40 | 19.50 | 16.80 | 0.26 | 0.26 | 0.100 |
| **BB5-15** | 3403 | 19.50 | 0.26 | 0.26 | 0.150 | **BGB5-15** | 3403 | 24.40 | 19.50 | 16.80 | 0.26 | 0.26 | 0.150 |
| **BB5-20** | 3403 | 19.50 | 0.26 | 0.26 | 0.200 | **BGB5-20** | 3403 | 24.40 | 19.50 | 16.80 | 0.26 | 0.26 | 0.200 |
| **BB5-30** | 3403 | 19.50 | 0.26 | 0.26 | 0.300 | **BGB5-30** | 3403 | 24.40 | 19.50 | 16.80 | 0.26 | 0.26 | 0.300 |
| **BB6** | 3920 | 9.00 | 0.56 | 0.30 | 0.122 | **BGB6** | 3920 | 11.25 | 9.00 | 8.00 | 0.56 | 0.30 | 0.122 |
| **BB7** | 3920 | 11.00 | 0.46 | 0.30 | 0.122 | **BGB7** | 3920 | 13.00 | 11.00 | 9.36 | 0.46 | 0.30 | 0.122 |
| **BB8** | 3920 | 14.00 | 0.36 | 0.30 | 0.122 | **BGB8** | 3920 | 16.25 | 14.00 | 11.65 | 0.36 | 0.30 | 0.122 |
| **BB9** | 3920 | 16.90 | 0.30 | 0.30 | 0.122 | **BGB9** | 3920 | 21.14 | 16.90 | 15.13 | 0.30 | 0.30 | 0.122 |
| **BB10** | 3920 | 19.50 | 0.26 | 0.30 | 0.122 | **BGB10** | 3920 | 16.25 | 19.50 | 11.65 | 0.26 | 0.30 | 0.122 |
| **BB11** | 6530 | 9.00 | 0.56 | 0.50 | 0.122 | **BGB11** | 6530 | 11.25 | 9.00 | 8.60 | 0.56 | 0.50 | 0.122 |
| **BB12** | 6530 | 11.00 | 0.46 | 0.50 | 0.122 | **BGB12** | 6530 | 13.00 | 11.00 | 9.96 | 0.46 | 0.50 | 0.122 |
| **BB13** | 6530 | 14.00 | 0.36 | 0.50 | 0.122 | **BGB13** | 6530 | 16.25 | 14.00 | 12.40 | 0.36 | 0.50 | 0.122 |
| **BB14** | 6530 | 16.90 | 0.30 | 0.50 | 0.122 | **BGB14** | 6530 | 21.14 | 16.90 | 16.11 | 0.30 | 0.50 | 0.122 |
| **BB15** | 6530 | 19.50 | 0.26 | 0.50 | 0.122 | **BGB15** | 6530 | 21.75 | 19.50 | 16.60 | 0.26 | 0.50 | 0.122 |

For all columns: Width side *(D)* = 900 mm, $t_s/b_s/l$ = *6/ 80/ 225 mm*. $\sigma_y$ = 378.6 MPa, $E$ = 206 GPa, and, $v$ = 0.3.
Columns BB3 and BGB3 are loaded with one-cycle ($N$ = 1) and three-cycle ($N$ = 3).
$P_y = \sigma_y * A$, $A = (D^2 - D_i^2)$, $D_i = D - 2t$, $t$ = thickness for the B column.
$I$ = moment of inertia = $(D^4 - D_i^4)/12$ (Include the stiffeners), $S$ = elastic section modulus = $(D^4 - D_i^4)/6D$.

As shown in Fig. 5.6, the buckling shape of the proposed BGB1 column (see Fig. 5.6b) suffered less severe damage in its both flange and web compared to the conventional BB1 column (see Fig.

5.6a), and similar buckling is observed in all other BB and BGB columns. The previous comparison indicated the superior behavior in the proposed BGB column configuration over the uniform BB columns.

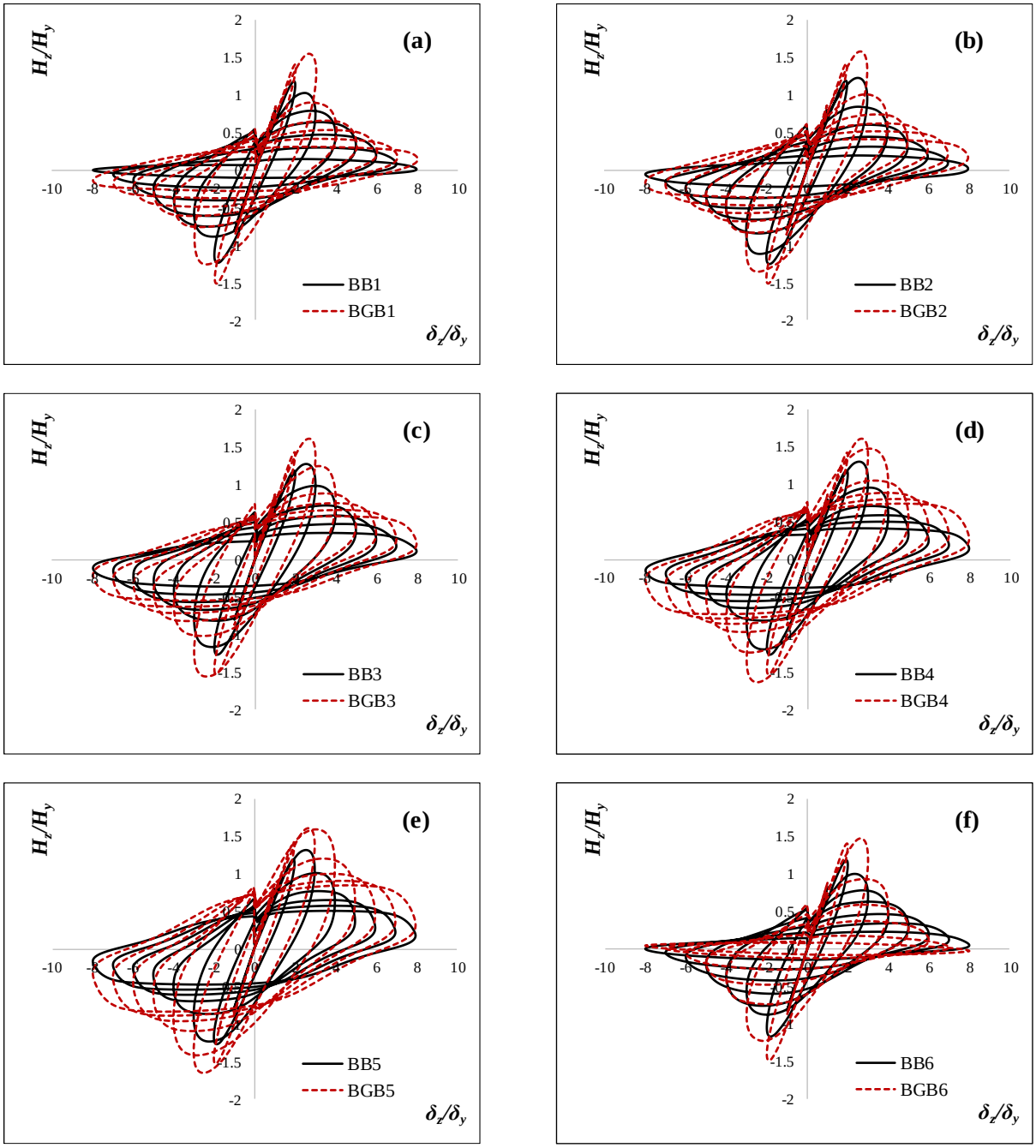


Fig. 5.5. Comparison of Hysteretic Loops in Z direction of: (a) BB1 & BGB1, (b) BB2 & BGB2, (c) BB3 & BGB3, (d) BB4 & BGB4, (e) BB5 & BGB5, (f) BB6 & BGB6, (g) BB7 & BGB7, (g) BB8 & BGB8, (g) BB9 & BGB9, and (g) BB10 & BGB10.

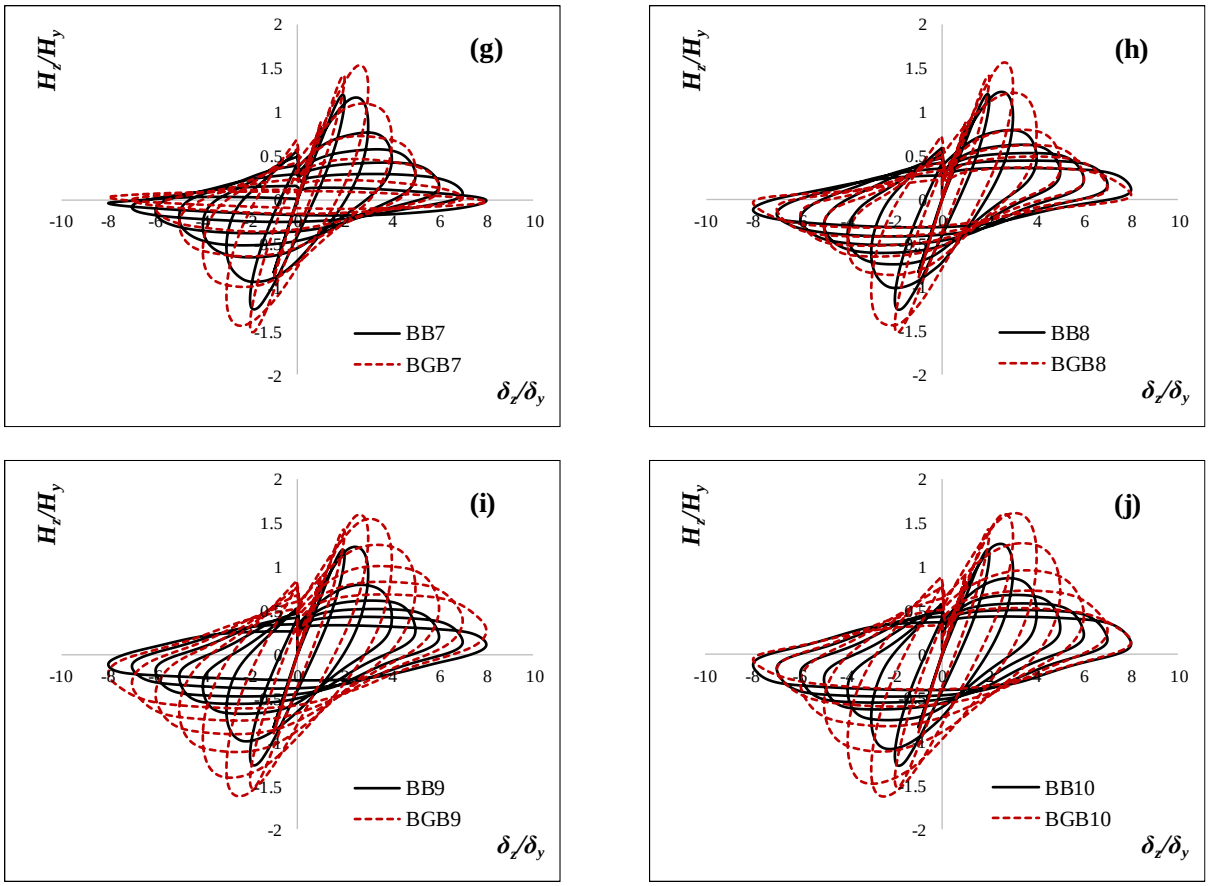


Fig. 6.5. Continued.

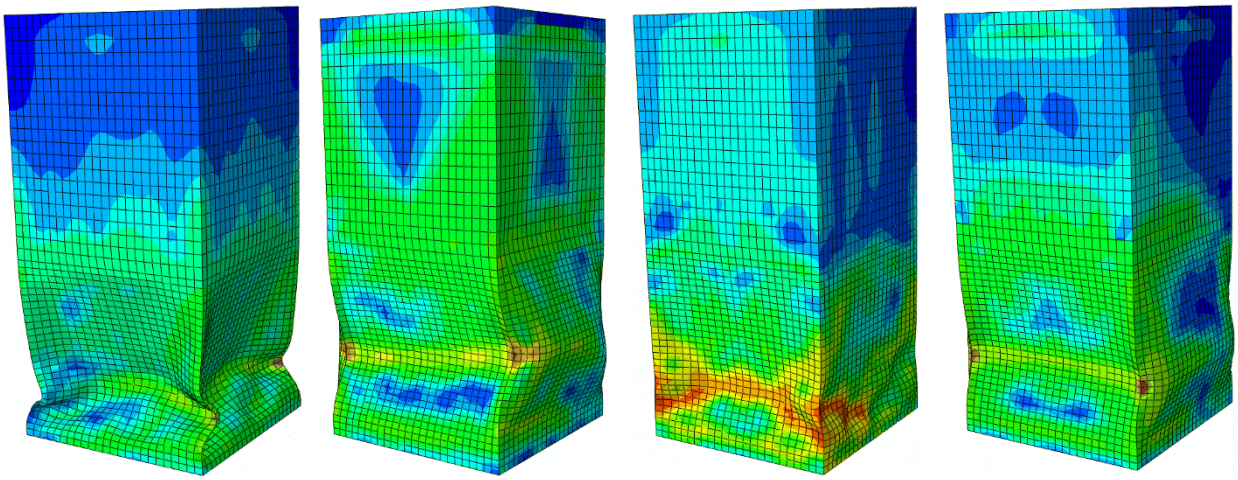

(a) BB Column (b) BGB1 Column (c) B1 Column (Al-Kaseasbeh and Mamaghani, 2019) (d) GB1 Column (Al-Kaseasbeh and Mamaghani, 2019)

Fig. 5.6. Buckling Deformation of Columns.

### 5.6 Loading Path Effect

A comparison between unidirectional, presented in Chapter 3, and bidirectional cyclic lateral loading conditions is conducted to highlight the effect of the cyclic loading pattern on the hysteretic behavior of thin-walled steel square box columns. Fig. 5.7 shows the hysteretic behavior of the uniform B and BB columns and graded-thickness GB and BGB columns under unidirectional and circular bidirectional cyclic lateral loading. The comparison indicates that the hysteresis loops under circular bidirectional cyclic lateral loading is totally different from those under unidirectional cyclic lateral loading. At the same amplitude of applied displacement, bidirectional loading pattern significantly causes more degradation in the strength and ductility of the column with the same material and structural parameters than unidirectional loading pattern. The significant deterioration is due to the accelerated local buckling under circular bidirectional cyclic lateral loading. To make a quantitative comparison between of the hysteretic behavior of the thin-walled steel square box columns under unidirectional and circular bidirectional loading conditions, the normalized loading path (i.e., $H_x/H_y$-$H_z/H_y$ path for bidirectional loading) of BB and BGB columns are plotted as shown in Fig. 5.8. In addition, the ultimate strength of B column ($H_{max}/H_y$ = 1.328) and GB column ($H_{max}/H_y$ = 1.644) under one-cycle unidirectional cyclic lateral loading is also superimposed as a circular envelope on the Fig. 5.8 with a dashed and dash-dot lines, respectively. The ultimate strength difference is 13% (B vs. BB) and 6% (GB vs. BGB) between unidirectional and circular bidirectional cyclic lateral loading. Therefore, the hysteretic behavior of thin-walled steel square box columns under unidirectional loading is over-simplified and leads to over-estimated strength and ductility capacity.

### 5.6.1.1 Buckling Deformations

Fig. 5.6 compares the buckling shapes of the columns at the end of the analysis. The comparison visually indicates that the BB column ($\delta_{zm}/\delta_y$ = 1.93) (see Fig. 5.6a) and BGB column ($\delta_{zm}/\delta_y$ = 2.64) (see Fig. 5.6b), under circular bidirectional cyclic lateral loading, buckled earlier than the B column ($\delta_m/\delta_y$ = 2.28) (see Fig. 5.6c) and GB column ($\delta_m/\delta_y$ = 3) (see Fig. 5.6d) under unidirectional cyclic lateral loading. Furthermore, the magnitude of the local buckling seems more critical under circular bidirectional loading. As opposed to the unidirectional cyclic lateral loading, it is believed that because all the plates of the column are subjected to loading all the time of the analysis under circular bidirectional cyclic lateral loading.

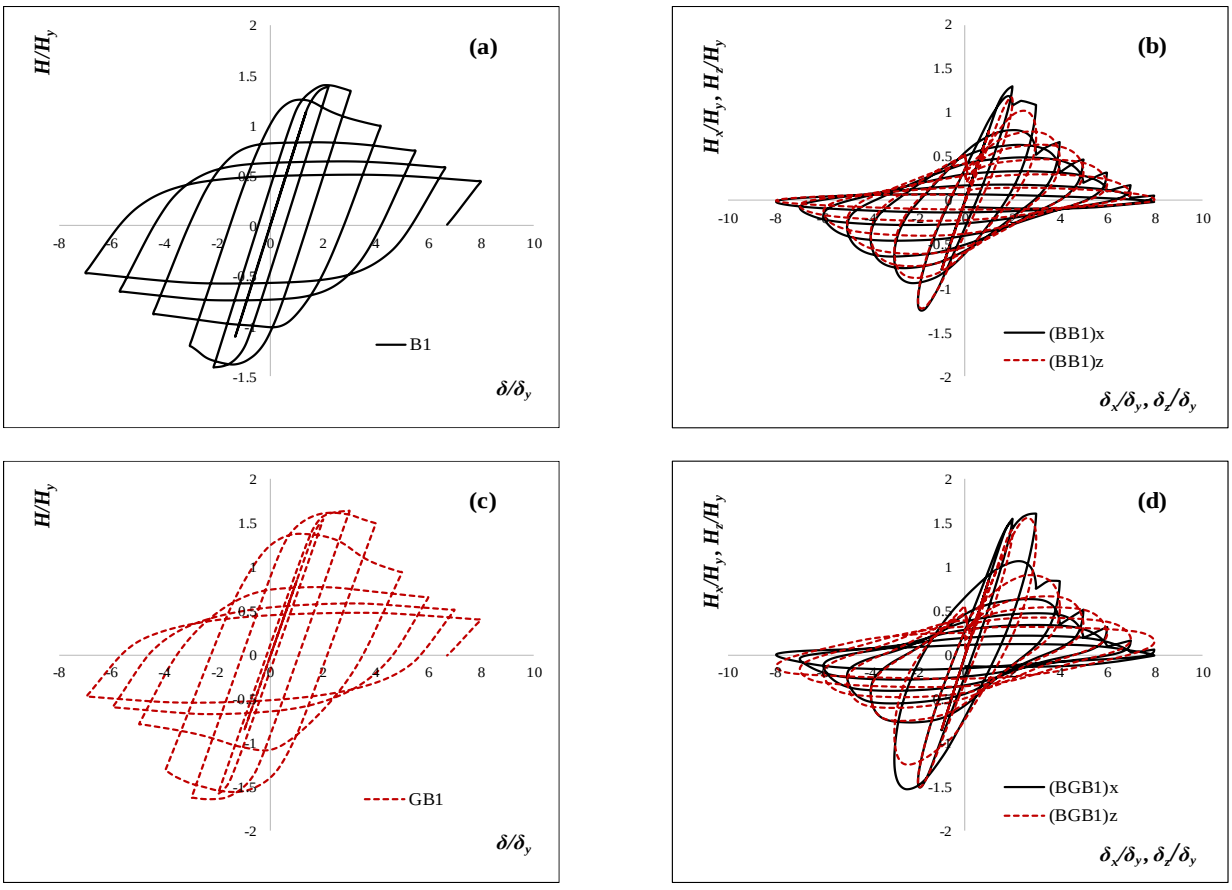


Fig. 5.7. Hysteretic Behavior of Uniform and Graded-thickness Columns.

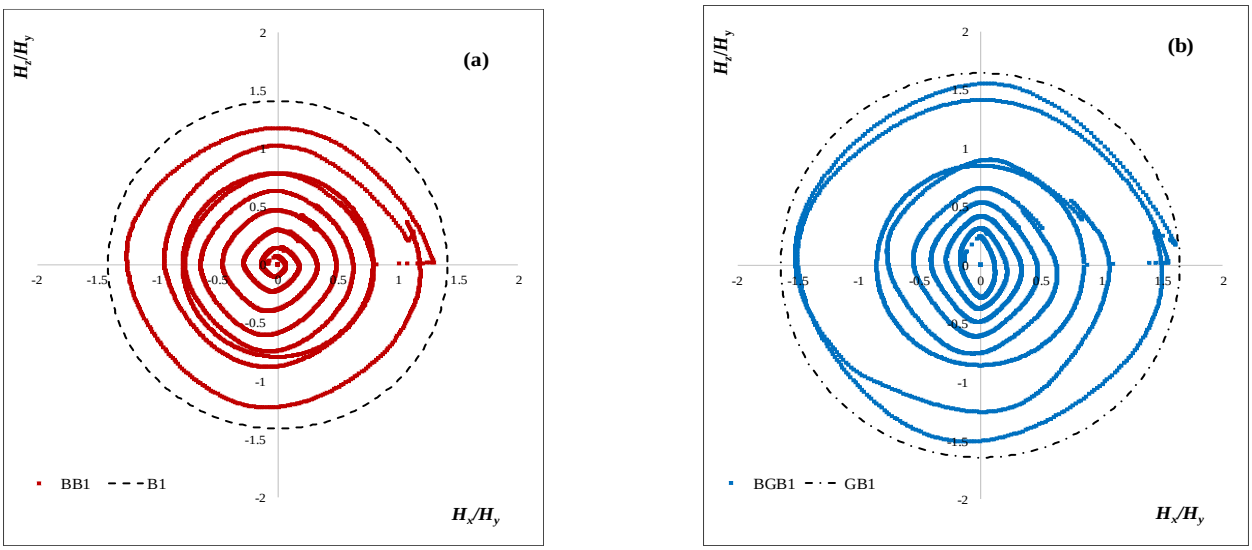


Fig. 5.8. Loading Paths of Columns: (a) BB1 vs. B1 Columns, and (b) BGB1 vs. BG1 Columns.

### 5.6.1.2 Energy Absorption Capacity

In order to predict the strength degradation, the dissipated energy of the column is investigated and presented in Fig. 5.9. The cumulative dissipated energy is calculated as the sum of the enclosed area under the normalized hysteretic loops in X and Z direction for circular bidirectional loading and in X direction for unidirectional loading. As observed in Fig. 5.9, the columns with same material and geometrical properties, dissipate more energy under the circular bidirectional cyclic lateral loading than those under unidirectional cyclic lateral loading which, in turns, results in a degradation in the strength and ductility of the column.

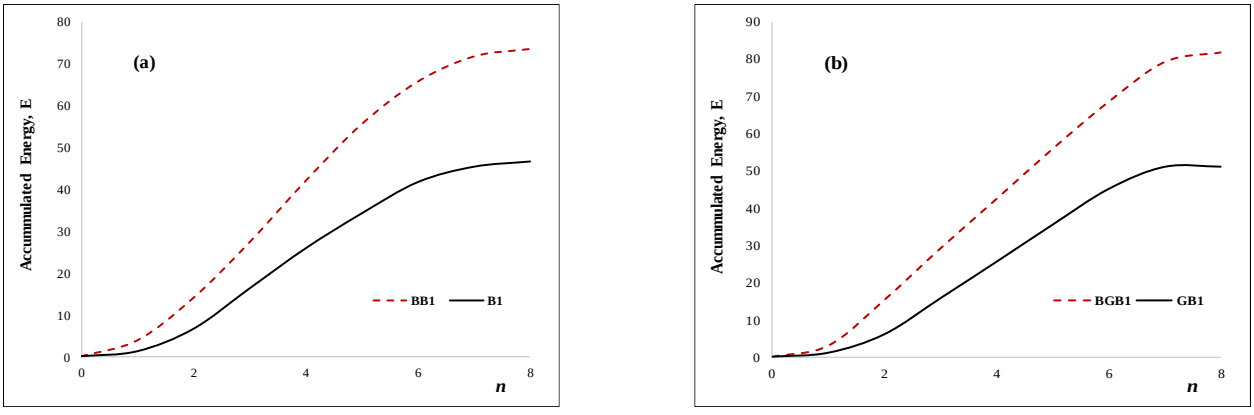


Fig. 5.9. Energy Absorption Capacity of Columns.

## 5.7 Parametric Study

A parametric study was carried out to provide insight into the effect of key design parameters including: width-to-thickness ratio parameter ($R_f$), column slenderness ratio parameter ($\lambda$), magnitude of axial load ($P/P_y$), and number of loading cycles ($N$), on the overall inelastic structural behavior of the BB and BGB columns. The practical range of these design parameters of thin-walled steel square box bridge piers are: $0.3 \leq R_f \leq 0.5$ , $0.2 \leq \lambda \leq 0.5$ (Chen, W. F. and Duan, 2014). For thin-walled steel stiffened square box columns, diaphragms are usually installed at an interval smaller than the pier width ($D$), $\alpha = a/D \leq 1.0$, where $a$ is the distance between diaphragms (Chen, W. F. and Duan, 2014). There is no limitation in $n$. However, $n$ = 4-6 is frequently used. As listed in Table 5.1, a total of 40 columns is analyzed using the adopted FEM in ABAQUS/Standard (Hibbit et al., 2014a). The studied range of these parameters are: $R_f$ varying from 0.26 to 0.56, $\lambda$ with a range of 0.26 - 0.5, the axial load ratio, $P/P_y$, where five different ratios (i.e., $P/P_y$ = 0.1, 0.122, 0.15, 0.20, and 0.3) are applied on BB5 and BGB5 columns. To investigate the effect of the number of loading cycles at each displacement amplitude ($N$), the BB1 and BGB1 columns were analyzed under both one ($N$ = 1), and three ($N$ = 3) loading cycles at each displacement level.

### 5.7.1 Effect of Width-to-Thickness Ratio Parameter ($R_f$)

The effect of the $R_f$ parameter on the hysteretic behavior of the column was investigated. The increase in $R_f$ parameter is either due to an increase in the side width of the column or a decrease in its thickness. In this study, the side width of the BB and BGB columns kept constant and the thickness is changed. As shown in Fig. 5.10, the envelope curves of the normalized lateral load vs. lateral displacement relation for both BB and BGB columns with different $R_f$ values are plotted.

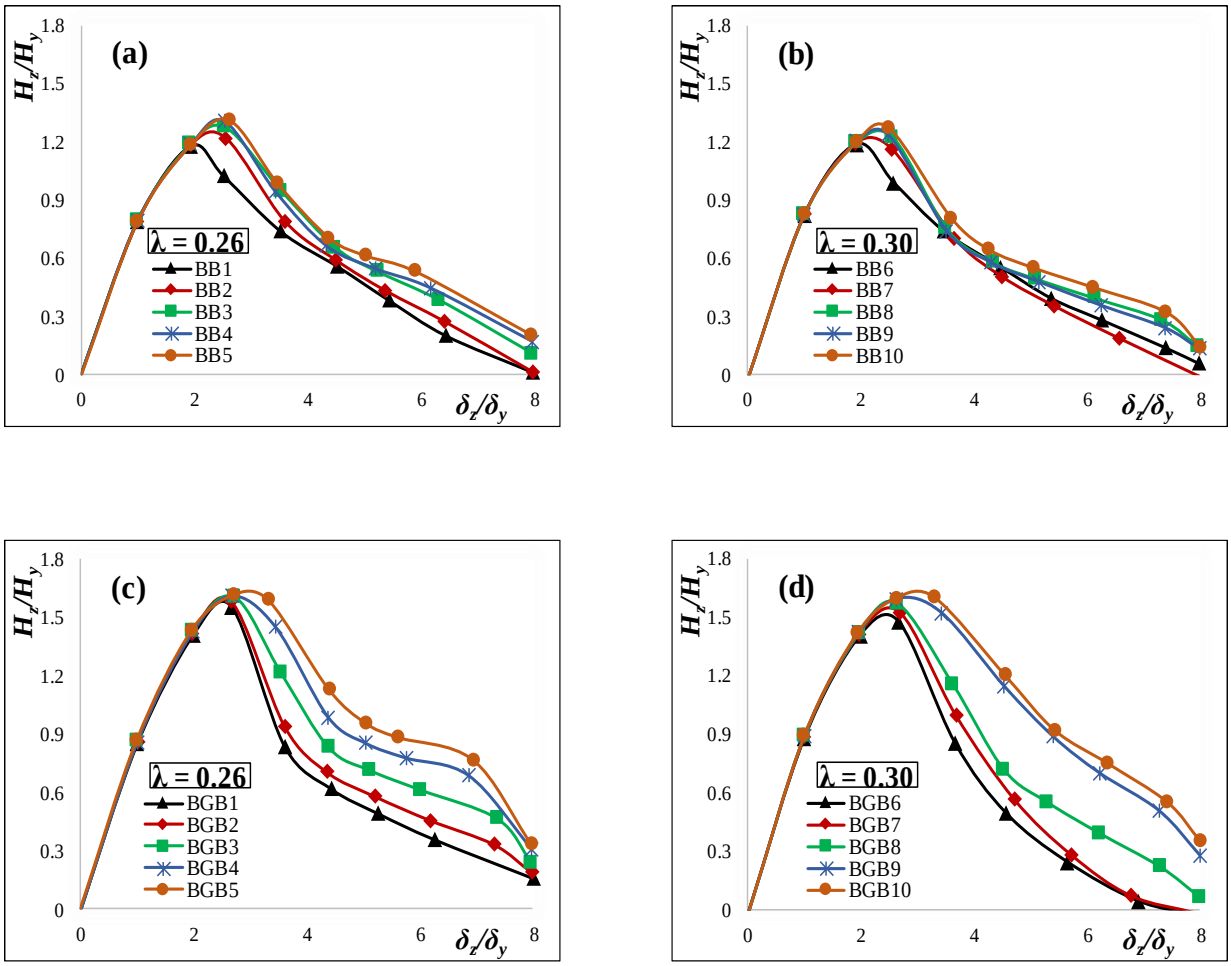


Fig. 5.10. Effect of $R_f$ parameter: (a) BB columns with λ = 0.26, (b) BB columns with λ = 0.3, (c) BGB columns with λ = 0.26, and (d) BGB columns with λ = 0.3.

The $H_{zmax}/H_y$ and $\delta_{zm}/\delta_y$ of both BB and BGB columns are improved by decreasing $R_f$ and keeping the other column's parameter unchanged. For instance, the $H_{zmax}/H_y$ and $\delta_{zm}/\delta_y$ , respectively, are increased by 11% and 33% as $R_f$ is decreased from 0.56 (BB1 column) to 0.26 (BB5 column) with λ = 0.26 (see Fig. 5.10a). In a similar way, as shown in Fig. 5.10c, $H_{zmax}/H_y$ and $\delta_{zm}/\delta_y$ are increased by 4% and 2%, respectively, as the $R_f$ decreases from 0.56 (BGB1 column) to 0.26 (BGB5 column). After the peak point, the post-buckling curve is less steep as $R_f$ gets smaller and the column experiences higher ductile behavior.

### 5.7.2 Effect of Slenderness Ratio Parameter (λ)

The λ parameter effect on the hysteretic behavior of both BB and BGB columns was studied. The $H_{zmax}/H_y$ and $\delta_{zm}/\delta_y$ of both BB and BGB columns improve as λ gets smaller as shown in Fig. 5.11. For example, the $H_{zmax}/H_y$ and $\delta_{zm}/\delta_y$, with $R_f$ = 0.26, are increased by 10% and 36%, respectively, as decreases from 0.5 (BB15 column) to 0.26 (BB5 column) as shown in Fig. 5.11b. In the BGB columns, the $H_{zmax}/H_y$ and $\delta_{zm}/\delta_y$ are improved by 21% and 40%, respectively, as λ decreases from 0.5 (BGB15 column) to 0.26 (BGB5 column) as shown in Fig. 5.11d. After the peak point, the post-buckling curve slope gets steeper, and the area enclosed by the envelope curve decreases when λ is higher. The same behavior exists in all other analyzed columns with different $R_f$ values.

### 5.7.3 Effect of Axial Load ($P/P_y$)

The hysteretic behavior of the BB5 and BGB5 columns were investigated under different axial load ratios (i.e., $P/P_y$ = 0.1, 0.122, 0.15, 0.2, and 0.3). As shown in Fig. 5.12, the envelope curves of the lateral load ($H_z/H_{y0}$) vs. lateral displacement ($\delta_z/\delta_{y0}$) are normalized by $H_{y0}$ (lateral yield load under zero axial load) and $\delta_{y0}$ (yield displacement under zero axial load) to highlight the axial load effect. The $H_{zmax}/H_{y0}$ of both BB5 and BGB5 columns decreases as the $P/P_y$ increases. For instance, the $H_{zmax}/H_{y0}$ and $\delta_{zm}/\delta_{y0}$ are, respectively, increased by 35% and 30% when $P/P_y$ decreases from 30% (BB5-30 column) to 10% (BB5-10 column). Similarly, the $H_{zmax}/H_{y0}$ and $\delta_{zm}/\delta_{y0}$ are increased by 15% and 14%, respectively, when $P/P_y$ decreases from 30% (BGB5-30 column) to 10% (BGB5-10 column). Furthermore, the post-buckling curve slope becomes steeper, the dissipated energy is way less in the case of BB5-30 and BGB5-30 columns compared to the ones of 10% axial load.

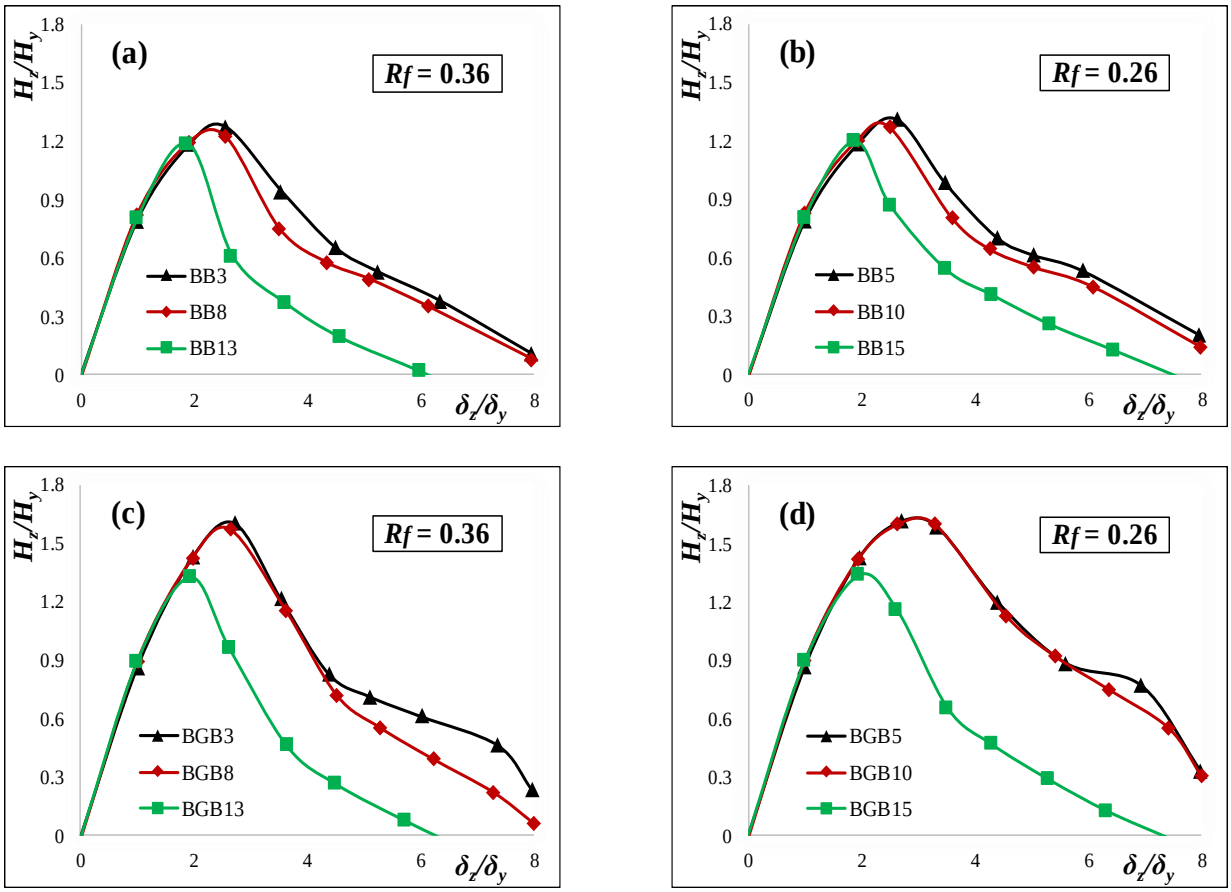


Fig. 5.11. Effect of λ parameter: (a) BB columns with $R_f$ = 0.36, (b) BB columns with $R_f$ = 0.26 (c) BGB columns with $R_f$ = 0.36, and (d) BGB columns with $R_f$ = 0.26.

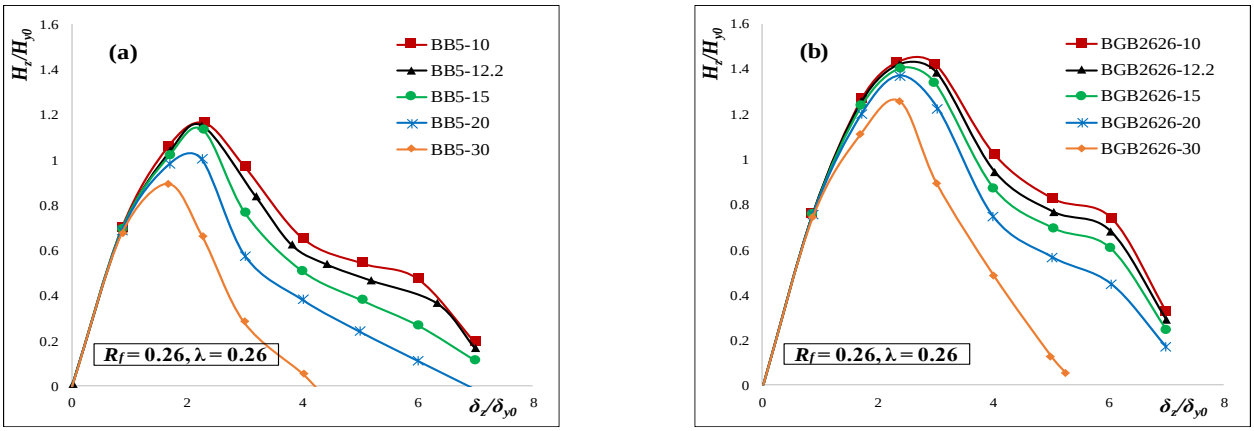


(a) BB5 Column (b) BGB5 Column

Fig. 5.12. Effect of Axial Load on Hysteretic Behavior.

### 5.7.4 Effect of Number of Loading Cycles (*N*)

As illustrated in Fig. 5.13, the envelope curves of the normalized lateral load vs. lateral displacement relations of both BB1 and BGB1 columns under one ($N = 1$) and three ($N = 3$) loading cycles at each displacement level are plotted. Under the case of $N = 3$, the strength deterioration of the BB1 (approximately, starts at $\delta = 1.5\delta y$) and BGB1 (at $\delta = 2\delta y$) columns starts earlier compared to $N = 1$. On contrast, no significant influence is noticed when $\delta$ is less than $1.5\delta_y$ (BB1 column), $2\delta_y$ (BGB1 column) which might be due to the small plastic deformation. It is worth noting that the deterioration in the BGB1 column is less than in the BB1 column under both $N = 1$ and $N = 3$ loading conditions.

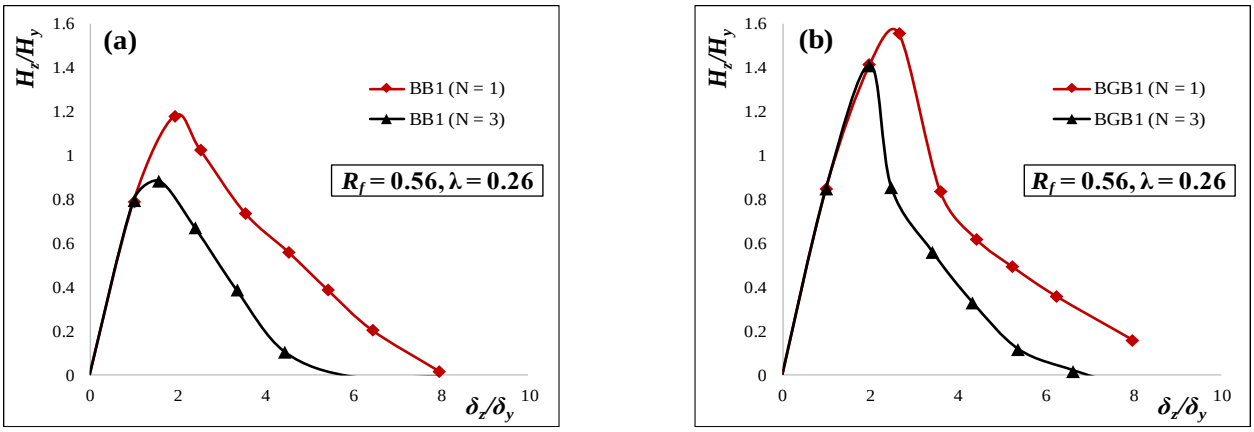


(a) BB1 Column (b) BGB1 Column

Fig. 5.13. Effect of *N* on Hysteretic Behavior.

### 5.8 Strength and Ductility Evaluation of BB and BGB Columns

The computed ultimate strength and ductility of both BB and BGB columns are listed in Table 5.2. In Fig. 5.14, $H_{zmax}/H_y$ is plotted vs. integrated parameters $(1+P/P_y)\ R_f\ \lambda$ considering the interaction of $R_f$, $\lambda$, and $P/P_y$ on the strength of the column. The Eqs. (5.5) and (5.6), respectively, are the best fitting equations to the computed ultimate strength of BB and BGB columns.

$$\frac{H_{z\max}}{H_y} = \frac{1.017}{\left[\left(1+\frac{P}{P_y}\right)R_f\lambda\right]^{0.092}} \quad \text{BB Columns} \tag{5.5}$$

$$\frac{H_{z\max}}{H_y} = \frac{1.002}{\left[\left(1+\frac{P}{P_y}\right)R_f\lambda\right]^{0.201}} \quad \text{BGB Columns} \tag{5.6}$$

As shown in Fig. 5.14, for both BB and BGB columns, an improvement in the ultimate strength is observed when integrated parameters $(1+P/P_y)\ R_f\ \lambda$ decrease. In this study, the failure criterion of thin-walled steel columns is set to occur when the displacement equals either $\delta_{zm}$ or $\delta_{z0.9}$. The $\delta_{zm}$ is the displacement corresponding to $H_{zmax}/H_y$ while the $\delta_{z0.9}$ is defined as the displacement where the post-peak strength drops to 90% of $H_{zmax}/H_y$ after the peak (Al-Kaseasbeh and Mamaghani, 2018, 2019; Mamaghani et al., 2015; Usami, 1996). The ductility factors (i.e., $\delta_{zm}/\delta_y$ and $\delta_{z0.9}/\delta_y$) are key parameters in the evaluation of the ductile behavior of both BB and BGB columns. As the strength significantly deteriorates after the peak point due to the local buckling, it is reasonable to use the $\delta_{z0.9}/\delta_y$ parameter to evaluate ductility of the columns (Al-Kaseasbeh and Mamaghani, 2018, 2019; Gao et al., 1998a; Usami, 1996; Usami et al., 2000b). The $\delta_{zm}/\delta_y$ and $\delta_{z0.9}/\delta_y$ of both BB and BGB columns are reported in Table 5.2 and plotted vs. integrated $R_f$, $\lambda$ and/or $P/P_y$ in Fig. 5.15. For both BB and BGB columns, the axial load effect was not  for the fitting equations of $\delta_{zm}/\delta_y$ parameter as shown in Eqs. (5.7) and (5.9), while it is included in the equations of $\delta_{z0.9}/\delta_y$ parameter as presented in Eqs. (5.8) and (5.10). The applicable restrictions of these formulae are $0.26 \le R_f \le 0.56$, $0.26 \le \lambda \le 0.5$, and $P/P_y \le 0.3$. It is worth mentioning that nonlinear least-squares regression was used for the curve fitting.

Table 5.2. Strength and Ductility Evaluation of BB and BGB Columns.

| BB Columns | | | | | | BGB Columns | | | | | |
|---|---|---|---|---|---|---|---|---|---|---|---|
| **Column** | $H_y$ **(KN)** | $\delta_y$ **(mm)** | $H_{zmax}/H_y$ | $\delta_{zm}/\delta_y$ | $\delta_{z0.9}/\delta_y$ | **Column** | $H_y$ **(KN)** | $\delta_y$ **(mm)** | $H_{zmax}/H_y$ | $\delta_{zm}/\delta_y$ | $\delta_{z0.9}/\delta_y$ |
| **BB1** | 1039 | 13.80 | 1.178 | 1.93 | 2.38 | **BGB1** | 1039 | 13.80 | 1.555 | 2.64 | 2.86 |
| **BB2** | 1240 | 13.80 | 1.219 | 2.52 | 2.85 | **BGB2** | 1240 | 13.80 | 1.580 | 2.66 | 2.89 |
| **BB3** | 1529 | 13.80 | 1.273 | 2.55 | 2.93 | **BGB3** | 1529 | 13.80 | 1.605 | 2.69 | 3.05 |
| **BB4** | 1804 | 13.8 | 1.303 | 2.56 | 2.86 | **BGB4** | 1804 | 13.8 | 1.614 | 2.68 | 3.44 |
| **BB5** | 2044 | 13.80 | 1.312 | 2.57 | 2.96 | **BGB5** | 2044 | 13.80 | 1.617 | 2.68 | 3.64 |
| **BB5-10** | 2095 | 14.19 | 1.292 | 2.50 | 3.01 | **BGB5-10** | 2095 | 14.19 | 1.599 | 3.00 | 3.61 |
| **BB5-15** | 1979 | 13.40 | 1.331 | 2.66 | 2.96 | **BGB5-15** | 1979 | 13.40 | 1.652 | 2.77 | 3.70 |
| **BB5-20** | 1862 | 12.61 | 1.253 | 2.79 | 3.08 | **BGB5-20** | 1862 | 12.61 | 1.710 | 2.97 | 3.76 |
| **BB5-30** | 1630 | 11.00 | 1.276 | 2.38 | 2.75 | **BGB5-30** | 1630 | 11.00 | 1.797 | 3.36 | 3.79 |
| **BB6** | 906 | 18.37 | 1.177 | 1.93 | 2.33 | **BGB6** | 906 | 18.37 | 1.476 | 2.63 | 2.89 |
| **BB7** | 1076 | 18.37 | 1.190 | 1.92 | 2.76 | **BGB7** | 1076 | 18.37 | 1.528 | 2.63 | 2.97 |
| **BB8** | 1327 | 18.37 | 1.223 | 2.51 | 2.81 | **BGB8** | 1327 | 18.37 | 1.569 | 2.63 | 3.00 |
| **BB9** | 1566 | 18.37 | 1.233 | 2.43 | 2.75 | **BGB9** | 1566 | 18.37 | 1.593 | 2.63 | 3.68 |
| **BB10** | 1774 | 18.37 | 1.268 | 2.46 | 2.79 | **BGB10** | 1774 | 18.37 | 1.610 | 2.63 | 3.77 |
| **BB11** | 544 | 50.97 | 1.165 | 1.90 | 2.09 | **BGB11** | 544 | 50.97 | 1.282 | 1.92 | 2.15 |
| **BB12** | 646 | 50.97 | 1.165 | 1.88 | 2.01 | **BGB12** | 646 | 50.97 | 1.301 | 1.93 | 2.25 |
| **BB13** | 797 | 50.97 | 1.181 | 1.88 | 2.05 | **BGB13** | 797 | 50.97 | 1.321 | 1.93 | 2.18 |
| **BB14** | 940 | 50.97 | 1.191 | 1.89 | 2.07 | **BGB14** | 940 | 50.97 | 1.331 | 1.92 | 2.29 |
| **BB15** | 1065 | 50.97 | 1.196 | 1.89 | 2.11 | **BGB15** | 1065 | 50.97 | 1.333 | 1.92 | 2.46 |

The proposed formulae that fit the computed $\delta_{zm}/\delta_y$ and $\delta_{z0.9}/\delta_y$ values of the analyzed columns are as follows:

$$\frac{\delta_{zm}}{\delta_y} = \frac{1.183}{\left[R_f \lambda\right]^{0.306}} \qquad \text{BB Columns} \qquad (5.7)$$

$$\frac{\delta_{z0.9}}{\delta_y} = \frac{1.332}{\left[\left(1+\frac{P}{P_y}\right) R_f \lambda\right]^{0.315}} \qquad \text{BB Columns} \qquad (5.8)$$

$$\frac{\delta_{zm}}{\delta_y} = \frac{1.257}{\left[R_f \lambda\right]^{0.325}} \qquad \text{BGB Columns} \qquad (5.9)$$

$$\frac{\delta_{z0.9}}{\delta_y} = \frac{1.185}{\left[\left(1+\frac{P}{P_y}\right)R_f\lambda\right]^{0.447}} \tag{5.10}$$

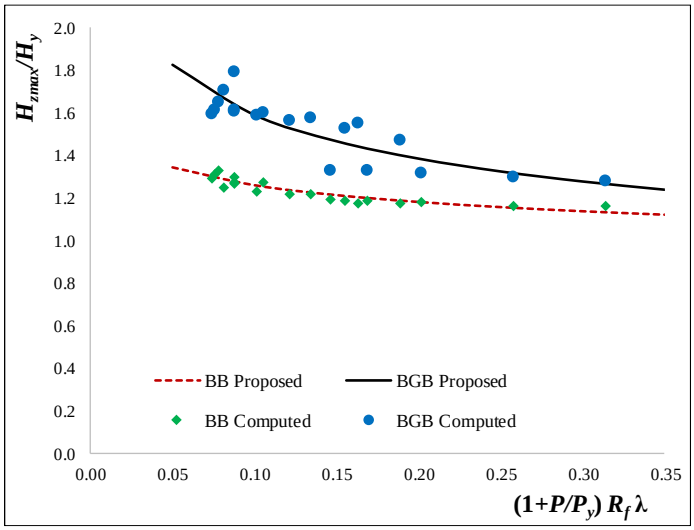


Fig. 5.14. Ultimate Strength of the BB and BGB Columns.

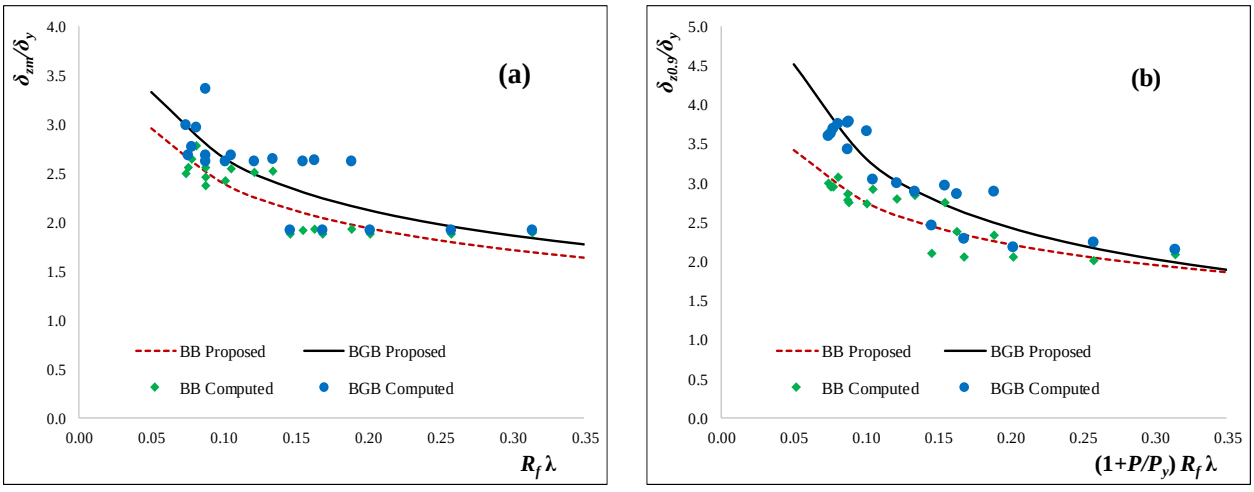


Fig. 5.15. Ductility of BB and BGB Columns: (a) $\delta_{zm}/\delta_y$, and (b) $\delta_{z0.9}/\delta_y$.

## 5.9 Summary

The main objective of this chapter is evaluating the hysteretic behavior of the uniform (BB) and proposed graded-thickness (BGB) thin-walled steel square box columns under a constant axial force and circular bidirectional cyclic lateral loading. The loading path effect is investigated to highlight the influence of the circular bidirectional loading over the unidirectional loading pattern. Finally, a comprehensive parametric study is conducted to investigate the effect of main design parameters (i.e., $R_f$, $\lambda$, $P/P_y$, and $N$) on the hysteretic behavior of BB and BGB columns. The following conclusions are summarized:

- The validity of adopted FEM in capturing the cyclic elastoplastic behavior of the column, under a constant axial force and circular bidirectional cyclic lateral loading, is verified with experimental results reported in the literature.
- The proposed BGB column, with size and volume of material equivalent to the uniform BB column, under constant axial force and circular bidirectional cyclic lateral loading, is proved to have a superior overall hysteretic behavior and significant improvement compared to counterpart of the BB column. In overall, the ultimate strength of BGB column was increased at an average of 28% when $\lambda$ , respectively, equals 0.26 and 0.3. In the case of $\lambda = 0.5$, the ultimate strength was improved by only 11% in comparison with BB columns.
- For BB and BGB columns with the same material and geometrical properties, bidirectional cyclic lateral loading significantly leads to degradation in strength and ductility at the same amplitude of displacement. In addition, more damage and dissipated energy were reported under bidirectional loading. Therefore, the hysteretic behavior of thin-walled steel square

box columns under unidirectional loading is over-simplified and leads to over-estimated strength and ductility capacity.

- The strength and ductility of BB and BGB column were improved by decreasing $R_f$ and $\lambda$ parameters. Furthermore, increasing of the $P/P_y$ and $N$ at each displacement level causes more deterioration in the overall hysteretic behavior of the column after the peak point.
- In order to predict the ultimate strength and ductility of BB and BGB columns, design formulae have been derived based on a conducted parametric study.

# CHAPTER 6 Summary and Future Work

Thin-walled steel tubular columns either with circular or stiffened square box sections are employed diversely in a variety of structural applications for their remarkable architectural, structural and constructional advantages. Under earthquake motions, the thin-walled steel tubular columns are exposed to the risk of local buckling which leads to a significant strength and ductility degradation, and causes a premature full collapse. Up to date, researchers have made effort to investigate thin-walled steel tubular columns either with circular or square box sections with uniform thickness under uni/multidirectional cyclic lateral loading. All these studies indicate that thin-walled steel columns suffer local buckling near the base in a range that is equal to the diameter or side width of the circular and square box columns, respectively. In order to overcome this deficiency and ensure an adequate strength and ductile behavior of thin-walled steel columns, a graded-thickness thin-walled steel tubular column ,with size and volume of material equivalent to a uniform thin-walled steel tubular column, has been proposed and investigated under constant axial force and uni/bidirectional cyclic lateral loading.

The main objective of this study is evaluating the inelastic structural behavior of the uniform and newly proposed graded-thickness thin-walled steel tubular columns under a constant axial force and uni/bidirectional cyclic lateral loading. The characteristics of the loading path are studied to highlight the influence of the bidirectional loading over the unidirectional loading pattern. Finally, a comprehensive parametric study is carried out to investigate the effect of key design parameters including: radius-to-thickness ratio parameter ($R_t$), the width-to-thickness ratio parameter ($R_f$), the column slenderness ratio parameter ($\lambda$), the magnitude of the axial load ($P/P_y$), and the number of loading cycles ($N$) on overall hysteretic behavior of thin-walled steel tubular columns under

uni/bidirectional cyclic lateral loading. The following conclusions are summarized within the scope of this study:

- The validity of adopted FEM in capturing the cyclic elastoplastic behavior of the thin-walled steel tubular column, under a constant axial force and uni/bidirectional cyclic lateral loading, is verified with experimental results reported in the literature. Also, the satisfactory agreement between the FE analysis and experimental results confirms the ability of the FEM in considering the local buckling of the column under a constant axial force and uni/bidirectional cyclic lateral loading.
- Newly proposed graded-thickness thin-walled steel tubular column, with size and volume of material equivalent to the uniform column, was introduced and evaluated under constant axial force and uni/bidirectional cyclic lateral loading. In general, the newly proposed graded-thickness columns are advantageous in achieving significant improvements in the hysteretic behavior compared to their counterpart of the uniform columns, emphasizing the effect of the plate thickness and sectional configuration in the proposed graded-thickness columns. The achieved improvements in the overall hysteretic behavior of the proposed columns is due to their ability to inhibit and/or eliminate the local buckling near the base of the column, where the local buckling usually occurs.
- For both uniform and proposed graded-thickness columns with the same material and geometrical properties, bidirectional cyclic lateral loading significantly leads to degradation in strength and ductility at the same amplitude of displacement. Furthermore, more accumulated damage and dissipated energy were reported under bidirectional cylic lateral loading. Therefore, the hysteretic behavior of thin-walled steel tubular columns

under unidirectional cyclic lateral loading is over-simplified and tends to over-estimated strength and ductility capacity.

- Based on the comprehensive study, the ultimate strength and ductility of uniform and proposed graded-thickness columns were improved by decreasing $R_t$, $R_f$, and $\lambda$ parameters. Furthermore, increasing of the $P/P_y$ and $N$ at each displacement level causes more deterioration in the overall hysteretic behavior of the column after the peak point.
- In predicting the ultimate strength and ductility of uniform and proposed graded-thickness columns, design formulae have been derived.
- The proposed formulae are expected to be useful for the practical design of the thin-walled steel tubular columns with uniform and graded thickness.

The further step of this study to set up experimentation on thin-walled steel tubular columns to validate the analysis results and introduce the design formula to the practical code. Furthermore, hysteretic behavior of graded-thickness thin-walled steel tubular columns with concrete infilling is recommended to be investigated under constant axial force and uni/bidirectional cyclic lateral loading.

# REFERENCES


AISC. (2010). "Specification for Structural Steel Buildings". *AISC 360*, 610.

Al-Kaseasbeh, Q., and Mamaghani, I. H. P. (2018). "Buckling Strength and Ductility Evaluation of Thin-Walled Steel Tubular Columns with Uniform and Graded Thickness under Cyclic Loading". *Journal of Bridge Engineering*, *24*(1), 04018105.

Al-Kaseasbeh, Q., and Mamaghani, I. H. P. (2019). "Buckling strength and ductility evaluation of thin-walled steel stiffened square box columns with uniform and graded thickness under cyclic loading". *Engineering Structures*, *186*, 498–507.

Anderson, E. L., and Mahin, S. A. (2004). "An Evaluation of Bi-Directional Earthquake Shaking on the Provisions of the AASHTO Guide Specifications for Seismic Isolation Design". In *Proc. 13th World Conf. on Eq. Eng*.

Aoki, T., Ohnishi, A., and Suzuki, M. (2007). "Experimental Study on the Seismic Resistance Performance of Rectangular Cross Section Steel Bridge Piers Subjected to Bi-Directional Horizontal Loads". *Doboku Gakkai Ronbunshuu A*, *63*(4), 716–726.

Aoki, T., and Susantha, K. A. S. (2005a). "Seismic Performance of Rectangular-Shaped Steel Piers under Cyclic Loading". *Journal of Structural Engineering*, *131*(2), 240–249.

Aoki, T., and Susantha, K. A. S. (2005b). "Seismic Performance of Rectangular-Shaped Steel Piers under Cyclic Loading". *Journal of Structural Engineering*, *131*(2), 240–249.

ASTM. (2014). "ASTM A36 / A36M - 14 Standard Specification for Carbon Structural Steel". *ASTM International, West Conshohocken, PA*, 12–14.

ASTM. (2018). "ASTM A242 / A242M-13(2018), Standard Specification for High-Strength Low-Alloy Structural Steel". *ASTM International, West Conshohocken, PA.*

Banno, S., Mamaghani, I. H. P., Usami, T., and Mizuno, E. (1998). "Cyclic Elastoplastic Large Deflection Analysis of Thin Steel Plates". *Journal of Engineering Mechanics*, *124*(4), 363–370.

Bedair, O. (2015). "Novel Design Procedures for Rectangular Hollow Steel Sections Subject to Compression and Major and Minor Axis Bending". *Practice Periodical on Structural Design and Construction*, *20*(4), 04014051.

Bruneau, M. (1998). "Performance of steel bridges during the 1995 Hyogoken–Nanbu (Kobe, Japan) earthquake—a North American perspective". *Engineering Structures*, *20*(12), 1063–1078.

Chaboche, J. L. (1986). "Time-independent constitutive theories for cyclic plasticity". *International Journal of Plasticity*, *2*(2), 149–188.

Chen, S., Xie, X., and Zhuge, H. (2019). "Hysteretic model for steel piers considering the local buckling of steel plates". *Engineering Structures*, *183*, 303–318.

Chen, W. F., and Duan, L. (2014). *Bridge Engineering Handbook, 2nd Edition, Seismic Design*. CRC Press.

Dang, J., and Aoki, T. (2013a). "Bidirectional loading hybrid tests of square cross-sections of steel bridge piers". *Earthquake Engineering & Structural Dynamics*, *42*(8), 1111–1130.

Dang, J., and Aoki, T. (2013b). "Bidirectional loading hybrid tests of square cross-sections of steel bridge piers". *Earthquake Engineering and Structural Dynamics*, *42*(8), 1111–1130.

Dang, J., Yuan, H., Igarashi, A., and Aoki, T. (2017). "Multiple-Spring Model for Square-Section Steel Bridge Columns under Bidirectional Seismic Load". *Journal of Structural Engineering*, *143*(5), 04017005.

Frangopol, D. M., and Saydam, D. (2014). "Structural performance indicators for bridges". In

*Bridge Engineering Handbook: Fundamentals, Second Edition* (pp. 185–206). CRC Press.

Fukumoto, Y., Uenoya, M., Nakamura, M., and Saya, H. (2003). "Cyclic performance of stiffened square box columns with thickness tapered plates". *Int. J. Steel and Structures*, *3*(2).

Gao, S., Usami, T., and Ge, H. . (1998a). "Ductility Evaluation of Steel Bridge Piers with Pipe Sections". *Journal of Engineering Mechanics*, *124*(3), 260.

Gao, S., Usami, T., and Ge, H. . (1998b). "Ductility of Steel Short Cylinders in Compression and Bending". *Journal of Engineering Mechanics*, *124*(2), 176–183.

Ge, H., Gao, S., and Usami, T. (2000a). "Stiffened steel box columns. Part 1: Cyclic behaviour". *Earthquake Engineering and Structural Dynamics*, *29*(11), 1691–1706.

Ge, H., Gao, S., and Usami, T. (2000b). "Stiffened steel box columns. Part 1: Cyclic behaviour". *Earthquake Engineering and Structural Dynamics*, *29*(11), 1691–1706.

Goto, Jiang, K., and Obata, M. (2006). "Stability and Ductility of Thin-Walled Circular Steel Columns under Cyclic Bidirectional Loading". *Journal of Structural Engineering*, *132*(10), 1621–1631.

Goto, Mizuno, K., and Prosenjit Kumar, G. (2012). "Nonlinear Finite Element Analysis for Cyclic Behavior of Thin-Walled Stiffened Rectangular Steel Columns with In-Filled Concrete". *Journal of Structural Engineering*, *138*(5), 571–584.

Goto, Wang, Q., and Obata, M. (1998). "FEM Analysis for Hysteretic Behavior of Thin-Walled Columns". *Journal of Structural Engineering*, *124*(11), 1290–1301.

Goto, Y., Koyama, R., Fujll, Y., and OBATA, M. (2009). "Ultimate State of Thin-Walled Stiffened Rectangular Steel Columns under Bi-Directional Seismic Excitations". *Doboku Gakkai Ronbunshuu A*, *65*(1), 61–80.

Goto, Y., Kumar, G., and Kawanishi, N. (2010). "Nonlinear Finite-Element Analysis for

Hysteretic Behavior of Thin-Walled Circular Steel Columns with In-Filled Concrete". *Journal of Structural Engineering*, *136*(11), 1413–1422.

Guo, L., Yang, S., and Jiao, H. (2013a). "Behavior of thin-walled circular hollow section tubes subjected to bending". *Thin-Walled Structures*, *73*, 281–289.

Guo, L., Yang, S., and Jiao, H. (2013b). "Behavior of thin-walled circular hollow section tubes subjected to bending". *Thin-Walled Structures*, *73*, 281–289.

Hassan, M. S., Salawdeh, S., and Goggins, J. (2018a). "Determination of geometrical imperfection models in finite element analysis of structural steel hollow sections under cyclic axial loading". *Journal of Constructional Steel Research*, *141*, 189–203.

Hassan, M. S., Salawdeh, S., and Goggins, J. (2018b). "Determination of geometrical imperfection models in finite element analysis of structural steel hollow sections under cyclic axial loading". *Journal of Constructional Steel Research*, *141*, 189–203.

Hibbit, Karlsson, and Sorensen. (2014a). "Abaqus 2014 Documentation". Dassault.

Hibbit, Karlsson, and Sorensen. (2014b). "ABAQUS 2014 Documnetation". Dassault Systèmes, Providence, RI, USA.

Jaiswal, K., Bausch, D., Rozelle, J., Holub, J., and McGowan, S. (2017). *Hazus® estimated annualized earthquake losses for the United States (No. FEMA P-366).*

Jiang, L., Goto, Y., and Obata, M. (2002). "Hysteretic modeling of thin-walled circular steel columns under biaxial bending". *ASCE J. Struct. Engng*, *128*(March), 319–327.

JIS. (2012). *JIS handbook: Ferrous Materials & Metallurgy*. Japanese Standards Association.

Kulkarni, N. G. (2012). *Seismic Design Methodology for Circular Steel Bridge Piers Subjected to Multi-Directional Earthquake Motions*. NAGOYA UNIVERSITY.

Kwon, Y. B., Kim, N. G., and Hancock, G. J. (2007). "Compression tests of welded section

columns undergoing buckling interaction". *Journal of Constructional Steel Research*, *63*(12), 1590–1602.

Li, H., Gao, X., Liu, Y., and Luo, Y. (2017). "Seismic performance of new-type box steel bridge piers with embedded energy-dissipating shell plates under tri-directional seismic coupling action". *International Journal of Steel Structures*, *17*(1), 105–125.

Liu, Y., and Young, B. (2003). "Buckling of stainless steel square hollow section compression members". *Journal of Constructional Steel Research*, *59*(2), 165–177.

Mahin, S. A. (1998). "Lessons from damage to steel buildings during the Northridge earthquake". *Engineering Structures*, *20*(4–6), 261–270.

Mamaghani, I. H. P. (1996). *Cyclic Elastoplastic Behavior of steel structures: Theory and Experiment*. Nagoya University. https://doi.org/10.11501/3111155

Mamaghani, I. H. P. (2004). "Seismic design and retrofit of thin-walled steel tubular columns". In *13th World Conference on Earthquake Engineering*.

Mamaghani, I. H. P. (2005). "Assessment of Earthquake Resistance Capacity and Retrofit of Steel Tubular Bridge Piers.". *Structural Engineers Association of California (SEAOC)*, 357–370.

Mamaghani, I. H. P. (2008). "Seismic Design and Ductility Evaluation of Thin-Walled Steel Bridge Piers of Box Sections". *Transportation Research Record: Journal of the Transportation Research Board*, *2050*(1), 137–142.

Mamaghani, I. H. P., Ahmad, F., and Dorose, B. (2015). "Strength and Ductility Evaluation of Steel Tubular Columns under Cyclic Multiaxial Loading". In *ISTS15 - 15th International Symposium on Tubular Structures*. Rio, Brasil.

Mamaghani, I. H. P., and Packer, J. A. (2002). "Inelastic behaviour of partially concrete-filled steel hollow sections". In *4th Structural Specialty Conference* (pp. 1–10).

Mamaghani, I. H. P., Shen, C., Mizuno, E., and Usami, T. (1995). "Cyclic Behavior of Structural Steels. I: Experiments". *Journal of Engineering Mechanics, 121*(11), 1158–1164.

Mamaghani, I. H. P., Usami, T., and Mizuno, E. (1996a). "Cyclic elastoplastic large displacement behaviour of steel compression members". *Journal Of Structural Engineering*, *42*, 135–145.

Mamaghani, I. H. P., Usami, T., and Mizuno, E. (1996b). "Inelastic large deflection analysis of structural steel members under cyclic loading". *Engineering Structures*, *18*(9), 659–668.

Mamaghani, I. H. P., Usami, T., and Mizuno, E. (1997). "Hysteretic behavior of compact steel box beam-columns". *Journal of Structural Engineering, JSCE, Japan*, *43A*, 187–194.

Miller, D. K. (1998). "Lessons learned from the Northridge earthquake". *Engineering Structures*, *20*(4–6), 249–260.

Mustafa, S. A. A., Elhussieny, O. M., Matar, E. B., and Alaaser, A. G. (2016, December 20). "Experimental and FE analysis of stiffened steel I-column with slender sections". *Ain Shams Engineering Journal*.

Nakashima, M., Inoue, K., and Tada, M. (1998). "Classification of damage to steel buildings observed in the 1995 Hyogoken-Nanbu earthquake". *Engineering Structures*, *20*(6), 271–281.

Nishikawa, K., Yamamoto, S., Natori, T., Terao, K., Yasunami, H., and Terada, M. (1998a). "Retrofitting for seismic upgrading of steel bridge columns". *Engineering Structures*, *20*(4–6), 540–551.

Nishikawa, K., Yamamoto, S., Natori, T., Terao, K., Yasunami, H., and Terada, M. (1998b). "Retrofitting for seismic upgrading of steel bridge columns". *Engineering Structures*, *20*(4–6), 540–551.

Nishikawa, K., Yamamoto, S., Natori, T., Terao, K., Yasunarni, H., and Terada, M. (1996). "An experimental study on improvement of seismic performance of existing steel bridge piers". *J.*

*Struct. Engrg*, *42A*, 975–986.

Okazaki, T., U., and A., and K. (2003). "Elasto-plastic dynamic analysis of steel bridge piers subjected to bi-directional earthquakes.". *J. Struct. and Eq. Eng., JSCE*, *27*, 1–8.

Onishi, A., Aoki, T., and Suzuki, M. (2005). "Experimental study on the seismic resistance performance of steel bridge subjected to bi-directional horizontal loads". *Bulletin of Aichi Institute of Tech*, *40*, 121–129.

Oyawa, W., Watanabe, E., and Sugiura, K. (2004). "Finite element studies on hollow steel columns under multi-directional cyclic loads". *J. Civil Eng. Research and Practice*, *1*(1), 33–49.

Shen, C., Mamaghani, I. H. P., Mizuno, E., and Usami, T. (1995). "Cyclic Behavior of Structural Steels. II: Theory". *Journal of Engineering Mechanics*, *121*(11), 1165–1172.

Susantha, K. A. S., Aoki, T., Kumano, T., and Yamamoto, K. (2005). "Applicability of low-yield-strength steel for ductility improvement of steel bridge piers". *Engineering Structures*, *27*(7), 1064–1073.

Takaku, T., Fukumoto, Y., and Aoki, T. (2004). "Seismic design of bridge piers with stiffened box sections using LP plates". In *iProceeding of the thirteenth world conference on earthquake engineering (on CD)*.

Tang, Z., Xie, X., and Wang, T. (2016a). "Residual seismic performance of steel bridges under earthquake sequence". *Earthquakes and Structures*, *11*(4), 649–664.

Tang, Z., Xie, X., and Wang, T. (2016b). "Residual seismic performance of steel bridges under earthquake sequence". *Earthquakes and Structures*, *11*(4), 649–664.

Tao, Z., Han, L. H., and Wang, Z. Bin. (2005). "Experimental behaviour of stiffened concrete-filled thin-walled hollow steel structural (HSS) stub columns". *Journal of Constructional Steel Research*, *61*(7), 962–983.

Ucak, A., and Tsopelas, P. (2006). "Cellular and corrugated cross-sectioned thin-walled steel bridge-piers/columns". *Structural Engineering and Mechanics*, *24*(3), 355–374.

Ucak, A., and Tsopelas, P. (2012). "Accurate modeling of the cyclic response of structural components constructed of steel with yield plateau". *Engineering Structures*, *35*, 272–280.

Ucak, A., and Tsopelas, P. (2014). "Load Path Effects in Circular Steel Columns under Bidirectional Lateral Cyclic Loading". *Journal of Structural Engineering*, *141*(2009), 1–11.

Usami, T. (1996). "Interim guidelines and new technologies for seismic design of steel structures". In *Committee on New Technology for Steel Structures, JSCE, Tokyo (in Japanes).*

Usami, T., Gao, S., and Ge, H. (2000a). "Elastoplastic analysis of steel members and frames subjected to cyclic loading". *Engineering Structures*, *22*(2), 135–145.

Usami, T., Gao, S., and Ge, H. (2000b). "Stiffened steel box columns. Part 2: Ductility evaluation". *Earthquake Engineering and Structural Dynamics*, *29*(11), 1707–1722.

Usami, T., and Ge, H. (1998). *Cyclic behavior of thin-walled steel structures—numerical analysis*. *Thin-Walled Structures* (Vol. 32). Elsevier.

Usami, T., Suzuki, M., Ge, H., and Mamaghani, I. H. P. (1995). "A Proposal for Check of Ultimate Earthquake Resistance of Partially Concrete Filled Steel Bridge Piers.". *Journal of Structural Mechanics and Earthquake Engineering*, (525), 69–82.

Wang, T., Xie, X., Shen, C., and Tang, Z. (2016). "Effect of hysteretic constitutive models on elasto-plastic seismic performance evaluation of steel arch bridges". *Earthquakes and Structures*, *10*(5), 1089–1109.

Watanabe, E., Sugiura, K., of JSCE, F., of JSCE, M., and Professor, A. (2000). *Effects of Multi-Directional Displacement Paths on the Cyclic Behaviour of Rectangular Hollow Steel Columns*. *J. Struct. Mech. Earthquake Eng* (Vol. 17).

Watanabe, E., Sugiura, K., of JSCE, F., of JSCE, M., and Professor, A. (2011). "Effects of multi-directional displacement paths on the cyclic behaviour of rectangular hollow steel columns.". *Doboku Gakkai Ronbunshu*, *2000*(647), 79–95.

Yang, C., Zhao, H., Sun, Y., and Zhao, S. (2017a). "Compressive stress-strain model of cold-formed circular hollow section stub columns considering local buckling". *Thin-Walled Structures*, *120*, 495–505.

Yang, C., Zhao, H., Sun, Y., and Zhao, S. (2017b). "Compressive stress-strain model of cold-formed circular hollow section stub columns considering local buckling". *Thin-Walled Structures*, *120*, 495–505.

Zhao, O., Rossi, B., Gardner, L., and Young, B. (2015). "Behaviour of structural stainless steel cross-sections under combined loading - Part I: Experimental study". *Engineering Structures*, *89*, 236–246.